Doctoral Dissertation

SHEAR BEHAVIOR OF REINFORCED CONCRETE BEAMS STRENGTHENED WITH CFRP GRID

Vu Ngoc Linh

2018

SHEAR BEHAVIOR OF REINFORCED CONCRETE BEAMS STRENGTHENED WITH CFRP GRID

by

Vu Ngoc Linh

Supervisor

Professor Kimitaka Uji

A thesis submitted to the Department of Civil and Environmental
Engineering - Tokyo Metropolitan University - Japan

in partial fulfillment of the requirements for the degree of

Doctor of Philosophy

Civil Engineering

2018

This dissertation is dedicated to my family for their endless love, continuous encouragement, and unreserved support all the time that keep me going ahead and especially to my lovely son Pichiu that I hope to meet soon.

ACKNOWLEDGEMENT

Table of Contents

List of Figures

List of Table

Chapter 1:

INTRODUCTION

1.1. STATEMENT OF THE PROBLEM

On over the world, FRP technology has been used for repairing and retrofitting concrete structures for a long time. First applying for civil engineering in the 1980's, up to now material technology has been developing f and obtaining significant progress. Many big constructions have been strengthened using FRP materials. Japan is one of the leading countries in researching and applying FRP to strengthening concrete structures. The peak of the booming era of construction happened in the middle of the 70s of the 20th century. In 1964, Olympic Games was held in Tokyo, a number of expressway system had been constructed serving for this event. After decades of rapidly establishing the infrastructure, in Japan, many constructions have become aging and decreasing quality. According to the published data by Ministry of Land, Infrastructure Transport and Tourism (MLIT) in 2013, the portion of highway bridge by is a high rate comparing to other countries (Fig. 1-2). Concrete bridge comprises 57% in quantity and 46% in length. The proportion of those facilities that have been aged for 50 years or older since initial construction for 20 years to come (Table 1-1).

Table 1-1: Percentage Ratios of Social Infrastructures over 50 years old

(Source: White paper on Land, Infrastructure, Transport and Tourism in Japan 2014)

	Year 2013	Year 2023	Year 2033
Highway bridges (Approx. 400,000 bridges)	18%	43%	67%
Tunnels (Approx. 10,000 tunnels)	20%	34%	50%
River management facilities (Approx. 10,000 facilities)	25%	43%	64%
Sewerage pipes (Approx. 450,000 km)	2%	9%	24%
Harbor quays (Approx. 5,000 facilities)	8%	32%	58%

Table 1-2: Comparisons of the Proportions of Structures by Country

(MLIT - Ministry of Land Infrastructure Transport and Tourism in Japan 2013)

Japan	26.4%	National expressway mean (2005)
U.S.	7.0%	Interstate highway mean (2003)
U.K.	4.4%	Superhighway and general highway mean (2001, England)
France	2.6%	Directly managed expressway and highway mean (2005)
Germany	10.1%	Federal Autobahn mean (2005)

Note: Proportion of structures = (Bridge beam length + Tunnel length/Total length Source) Infrastructure Development Institute

Besides, with such characteristic Japanese land and harsh natural conditions, it is sought to build a high level of disaster preparedness facilities, such as advanced earth quake resistance and soft-ground improvement, into the social infrastructures it develops, (Table 1-2). Also, bridges, tunnels and other structures command a higher proportion of the nation's networks of roads, railways and so on to address its steep topographical features than other nations. Therefore, The Japanese infrastructure system is aging speedily. These social infrastructures are considered to cost more to maintain, manage and upgrade.

Another example is Vietnam, a developing country, being independent in 1975, after more than 40 years of establishing the infrastructure, many constructions have become aging and decreasing quality. According to Atlas of Transportation- 2008, currently, the infrastructure system of Vietnam in transportation field has 93 national highways, with a total length of 17,202 km. There are 4,239 road bridges, total length of 144,539 m. Among them, 148 weak bridges have been repaired, 111 bridges are in poor condition requiring replacement, 307 bridges need to be repaired and upgraded (Report on weak bridge and traffic black spots – April 2012). In Vietnam, the first application for civil engineering in 1980's, up to now material technology has been developed for decadees and the construction industry has made considerable progress. Consequently, there is no doubt that the requirement for repairing and strengthening the concrete structure is a high and urgent demand. Vietnamese engineers have positively and proactively applied new materials and advanced technologies in building new constructions and repairing aging structures also. Fiber Reinforced Polymer (FRP) was first used for civil engineering in 1990's but widespread applying for concrete structures in recent years. Recently, numerous huge concrete structures have been strengthened using FRP material.

Applying FRP to reinforced concrete structures have their advantages when comparing to the others. And there are many options for CFRP reinforcement, whichever option to choose depends on the particular conditions of the project, the specific situation.

In Japan, various types of FRP have been used for maintaining and upgrading the infrastructure system. They are in the shape of rod, strand, braid, sheet and grid. Together with CFRP sheet, CFRP grid has been developed and widely applied to many concrete structures for decades. CFRP sheet is much more popular in repairing the concrete structures, but under some specific circumstances, CFRP grid proves its advantage when comparing to others. The study on CFRP grid and its application are still limited and in a restraint number of researches. There have been more recent extensive studies on CFRP grid, but not many researches have yet been conducted intensively on its application to reinforce concrete (RC) beams, especially on shear strengthening.

Considering the situation mentioned above, this dissertation focus on the *"shear behavior of reinforced concrete beams strengthened with CFRP grid"*. In the field of this study, both experiments in specimen scale and large scale have been conducted to gather the data on the performance of the CFRP grid. The collected results from test have been processed, then analyzed to conclude comments about the efficiency of the CFRP grid and its behavior in strengthening works also.

1.2.   OBJECTIVES

Researching the problem about CFRP grid is such a quite new area. In the scope of this thesis, these following objectives are covered:

The first objective is to examine the basic properties of composit specimens: concrete, steel, CFRP grid, and mortar, acting together in reinforcing the prismatic specimens. These concrete prisms are tested to investigate the effect of strengthening by the CFRP grid, the behavior of reinforcing materials and the capability of CFRP grid influenced by the bonding interface between concrete and mortar.

The second one is to evaluate the effectiveness of CFRP grid and sprayed mortar and the behavior of stirrups and CFRP grid in reinforcing the RC beams, to analyze the difference in behaviors between stirrups and CFRP grid. It also studies the cracking behavior of shear-strengthened RC beam based on the Acoustic Emission (AE) technique and clarifies the role of horizontal and vertical components of CFRP grid in strengthening work.

The third purpose is to generate the formula for estimating the shear strength of the RC beam reinforced with CFRP grid and sprayed mortar. These equations are derived from the mechanical analysis.

1.3.   URGENCY AND POSSIBILITY SIGNIFICANT OF THE STUDY

In general, the service lifetime of concrete structures is 50-100 years. Because of series of reasons, such as the impact of time, the corrosion of steel bars, or the lack of understanding about the structure and material in the past, these concrete structures expose the serious damage after a long period of serving. Especially, Japan is a country well known for natural disasters such as earthquakes and tsunamis. There is a list of earthquakes in Japan either a magnitude equal or greater than 7.0 which caused significant damage. A numerous of concrete structures were built several decades ago, their service quality is going to decrease significantly and shortly.

Consequently, the demand for retrofitting and maintaining the aging concrete structures is an enormous number. Adequate awareness of the repair method as well as the influenced parameter support for useful retrofit work. The goal of environmental and eco-nomical design for repairing is apparent.

Furthermore, the estimate of the efficiency of the strengthening method using CFRP grid is critical and valuable.

1.4. SCOPE OF PROJECT

1.4.1. Initial tests

This test aims to investigate the capability of four materials: concrete, steel, Carbon Fibre Reinforced Polymer (CFRP) grid, and mortar, acting together in a strengthened structure. In this experimental program, three concrete prisms reinforced by different schemes of steel bars and/or CFRP grid in the axial direction. Specimen 1, as the control, with a square section of concrete, axially reinforced by rebars. Specimen 2 was reinforced by CFRP grid and Specimen 3 , was reinforced by both rebars and CFRP grid. CFRP grid and sprayed mortar were applied on two sides of concrete prisms 2 and 3. The strengthened specimen 2 and 3 have the same dimensions as specimen 1, they were applied the axial tensile force until fail. Though specimens 2 and 3 the concrete surface is well-treated for the good adhesion between concrete and mortar, the failure still occurs at the bonding interface. The result of the test shows the effect of strengthening by CFRP grid, the behavior of reinforcing materials and the capability of CFRP grid influenced by the bonding interface between concrete and mortar.

1.4.2. Beam tests

This section examined the effect of CFRP grid and sprayed mortar in enhancing the shear capacity of RC beams. Three RC beams were fabricated and two of them were strengthened by CFRP grid and sprayed mortar. Then the four-points bending test was carried out to collect the data on the behavior of CFRP grid and stirrups in the three beams. The results are presented and discussed in this paper. This study evaluated the strengthening effectiveness of CFRP grid and sprayed mortar and the behavior of stirrups and CFRP grid. The difference in behaviors between stirrups and CFRP grid was analyzed.

1.4.3. Analytical approach

This dissertation presents the generated theoretical equations to estimate the shear strength of strengthened RC beams base on the mechanical model. The problems are solved in two cases, RC beam shear-strengthened by CFRP grid and/without stirrups. The contribution to the shear strength is assumed to be the sum of the shear transferred by un-crack concrete compression zone, by stirrups, by CFRP grid, by residual tensile and frictional stresses of the critical crack. These equations have been checked with experimental results and examined with other author's formulas.

1.5.   ORGANIZATION OF THESIS

This dissertation has been arranged in 7 chapters, with the main content is summarized as below:

Chapter 1 introduces the statement of the problem, the objectives, the significance as well as the organization of thesis.

Chapter 2 reviews the related studies and backgrounds of the issues will be presented in the dissertation.

Chapter 3 is about the investigation of the capability of four materials: concrete, steel, Carbon Fibre Reinforced Polymer (CFRP) grid, and mortar, acting together in composite specimens. In the experiment, three concrete prisms (500 mm in length) are reinforced by different schemes of steel bars and/or CFRP grid in the axial direction. Specimen 1, the control one, with a square section (100 x 100 mm) of concrete, axially reinforced by rebars. Specimen 2 is reinforced by CFRP grid, and Specimen 3 is reinforced by both rebars and CFRP grid. The strengthened specimen 2 and 3 have the same dimensions (100 x 100 mm) as specimen 1, they were applied the axial tensile force until fail. The result of the test shows the effect of CFRP CR5 grid in strengthening, good combination of four materials has been proved. Both strengthened specimens perform the very high bearing capacity comparing to the control one – specimen 1. The behavior of reinforcing materials and the capability of CFRP grid strongly influenced by the bonding interface between concrete and mortar. In this study, although the bonding surfaces are repaired by an appropriate method such as sandblasting (the roughness of surface after sandblasting is 0.158mm), epoxy primer applying. Both specimens the fracture still occurs at the bonding surface, (the average shear stresses is 1.1 MPa) and CFRP grid only performs 76% of tensile strength. To make use of the full capacity of CFRP grid, a better condition of surface roughness (of more than 0.3 mm) is necessary.

Chapter 4 shows the effectiveness of CFRP grid in enhancing the shear capacity of RC beams under four-point bending test. Three large beams (200 x 500 x 2750 mm) were fabricated, same in the longitudinal reinforcement but different in transverse reinforcement. RC beam 1, the reference one, shear-strengthened by stirrup D10, with RC beam 2 is Stirrup D6 and CFRP CR8, and with RC beam 3 is CFRP CR8 only. The cross-sectional area of reinforcing materials in RC beam 2 and RC beam 3 is equivalent to 119% and 74%, respectively, of the cross-sectional area of stirrups in RC beam 1. The result shows that CFRP grid and sprayed mortar could significantly improve the shear strengthening. RC beam 2 and RC beam 3 attains 10% higher and 10% lower of ultimate load comparing to RC beam 1. In general, the stiffness, ductility characteristic, and the cracking load of the strengthened RC beams are upgraded. When the load increased, variations of the stirrup strains and the CFRP grid strains at the same position in a

strengthened RC beam have similar tendencies. After stirrups yielded and cracks developed, the behavior of CFRP grid and stirrups was considerably affected. In this application, CFRP grid did not work at full capacity. The maximum stress of CFRP grid was 85.3% of the tensile strength. When calculating the shear strength of RC beam, the material factor for CFRP sheet in JSCE's guideline is 1.3, to apply this formula for CFRP grid, this factor of 1.5 is proposed.

Chapter 5 studies the crack propagation of strengthened beams using CFRP grid. Acoustic emission (AE) sensors were attached on the two beams to monitor the development of cracks from the starting point to the ultimate state. The actual observed fact is combined with AE result to conclude the better understanding of the formation and propagation of diagonal cracks. According to the test data, micro-cracks occur and develop so early, even when the load is low and in the compressed area also. Chapter 5 also discusses the contribution of the horizontal and vertical bar of CFRP grid to the shear strength. The analysis indicates that the vertical component of CFRP grid plays the key role for shear strength contribution when compared with the horizontal part. And horizontal CFRP bars work as anchors supporting the vertical movement between CFRP grid and spray mortar, especially, at the tip of the critical crack.

Chapter 6 presents the generated formula to estimate the shear strength of strengthened RC beams base on the mechanical model. The problems are solved in two cases, RC beam shear-strengthened by CFRP grid and/without stirrups. The contribution to the shear strength is assumed to be the sum of the shear transferred by un-crack concrete compression zone, by stirrups, by CFRP grid, by residual tensile and frictional stresses of the critical crack. These equations have been checked with cases of beams in chapter 4. In both cases of applying CFRP grid, the un-crack concrete chord plays a vital role in the shear strength contribution (nearly 50%). Moreover, the estimated value of shear strength is consistent with the experiment results very well.

Chapter 7 summarizes all results and conclusions of the overall dissertation.

Chapter 2:

BACKGROUND & LITERATURE REVIEW

2.1.   INTRODUCTION

When applying the bending load to RC beams, the maximum principal stress is at the extreme tension fiber around the mid-span, and its direction is parallel to the member axis. As the principal tensile stress rises and exceeds the tensile strength of concrete, the first flexural crack appears in the perpendicular direction with the member axis. After the flexural crack is formed, and the applied load increases, the bending crack propagates toward the compression zone of the cross-section and the other cracks occur parallel to the first one. In both side spans, there are also diagonal cracks starting with manner of flexural crack (perpendicular to member axis) then incline with respect to the member axis. The element along the diagonal crack is in different stages of stress.

This thesis focus on the behavior of CFRP grid in the application for shear-strengthening. Extracting these representative elements in 3 locations along the inclined crack (shown in Fig. 2-1). These elements are: Element A, element B and element C. The reinforcing scheme of these elements are displayed in Fig. 2-2

- Element A represents the tension area. The element A has the longitudinal reinforcing bars and both types of transverse reinforcement; stirrups and CFRP grid. The stage of stress is biaxial, see Fig. 2-3.

- Element B represents the neutral axis area. It locates at the middle of beam height. The stage of stress is pure shear.

- Element C represents the compression area. It locates at the top of the beam. The stage of stress is biaxial.
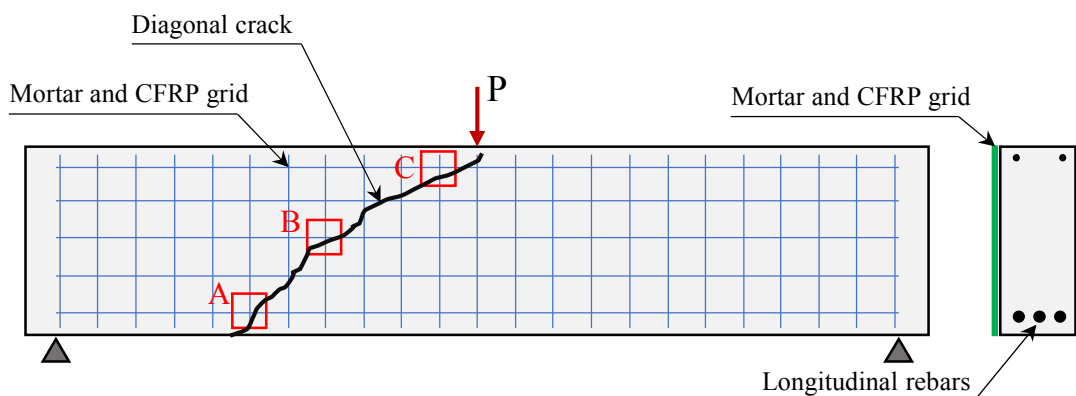
Figure 2-1: Locations of representative elements on strengthened beams
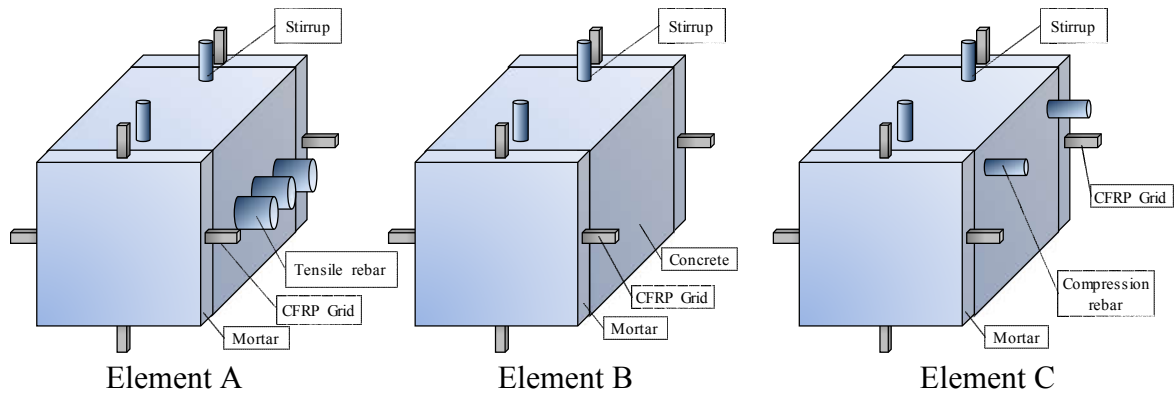
Figure 2-2 Extracted elements from the strengthened beam

a) Biaxial stage of stress   b) Pure shear stage of stress   c) Biaxial stage of stress
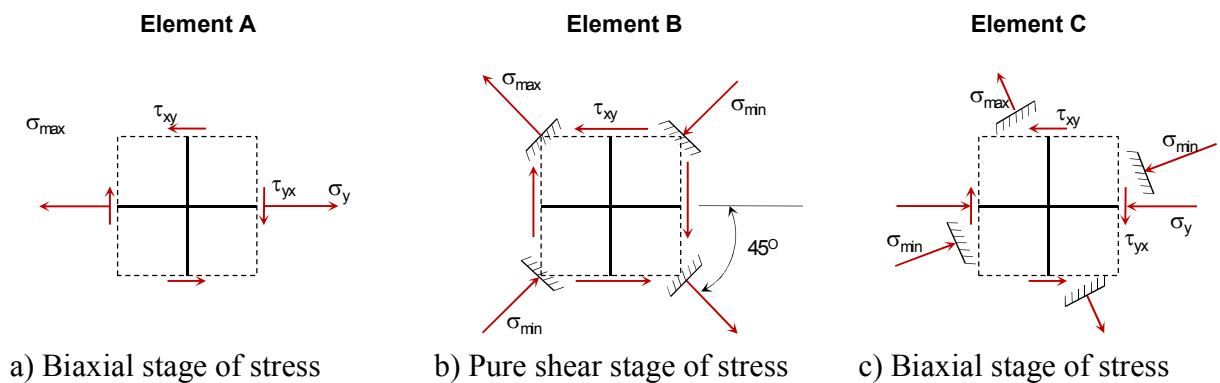
Figure 2-3: Stage of stress of elements

The location of element A is mainly suffered from the tension force, and longitudinal bars are in charge of it. The element C mostly carries the compression force; concrete chord is able to bear the high compression force. The working of the element B is essential for the shear strength of RC beams. Along the member axis of the beam, there are horizontal bars of CFRP grid (see Fig. 2-2), while in the beam height direction, there are stirrups and vertical bars.

When the applying load is still at low level, materials at this location is still elastic. As the load increases, cracks occur, the behavior of reinforcing material is complicated. Experiment models the behavior of materials is a vital point to clarify the work of CFRP grid in strengthening. The propagation of cracks also affects on the stress and strain in CFRP grid. All these points will be discussed and intensively studied in next sections of this dissertation.

2.2.   REPAIR AND REINFORCE CONCRETE STRUCTURE WITH FRP

2.2.1.   Introduction

Japan is one of the most consuming FRP product for strengthening concrete structure on over the world. Since the late 80's the application of FRP for concrete structures has been considerably rising. Especially after late 90's the FRP sheet has been widely used for seismic retrofitting, upgrading and durability retrofitting. The Great Hanshin Earthquake caused numerous damages to the concrete structure in large scale.
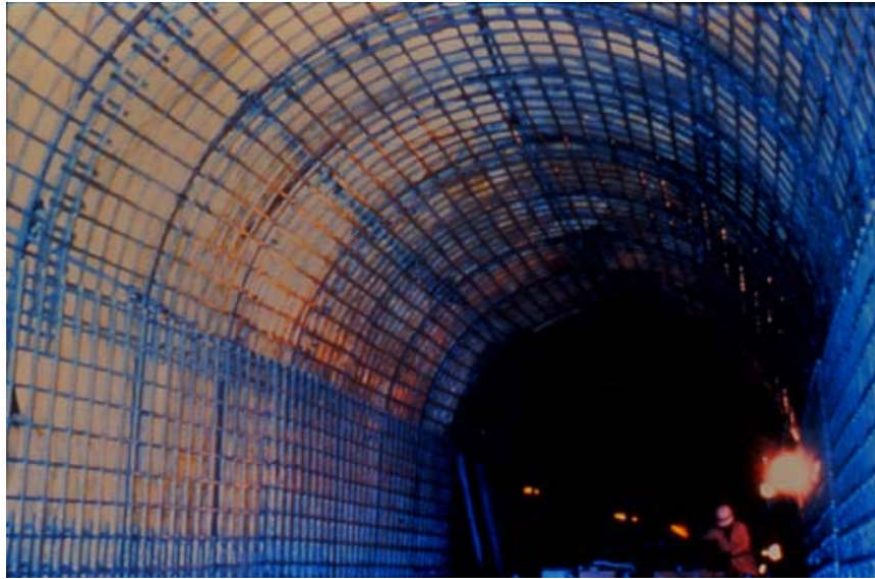
Figure 2-4: FRP grid as Reinforcement for Tunnel Lining Before shotcreting
(Banthia 2002)
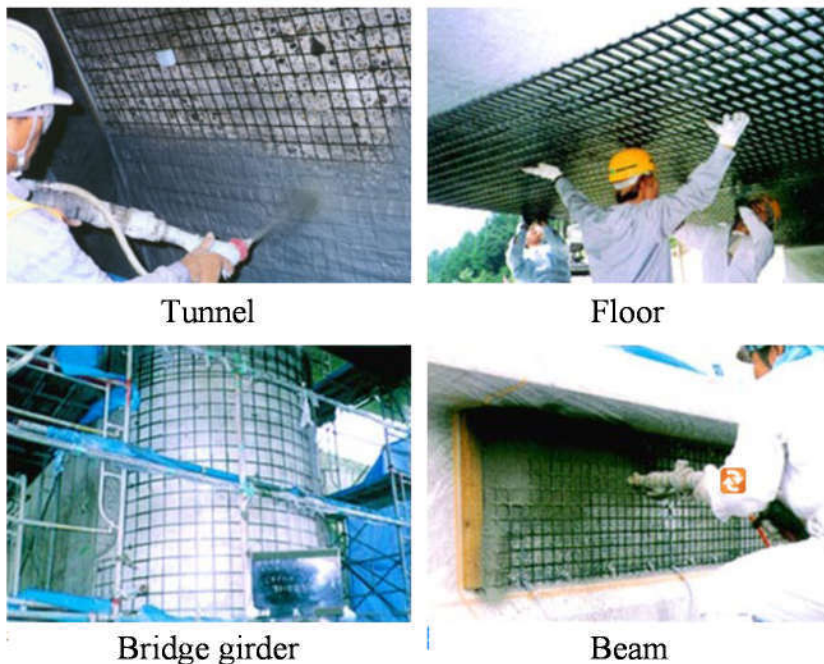
Figure 2-5: Strengthening applications of CFRP grid
Source: https://www.nck.nsmat.co.jp/construstion/towgrid/example/index.html

12
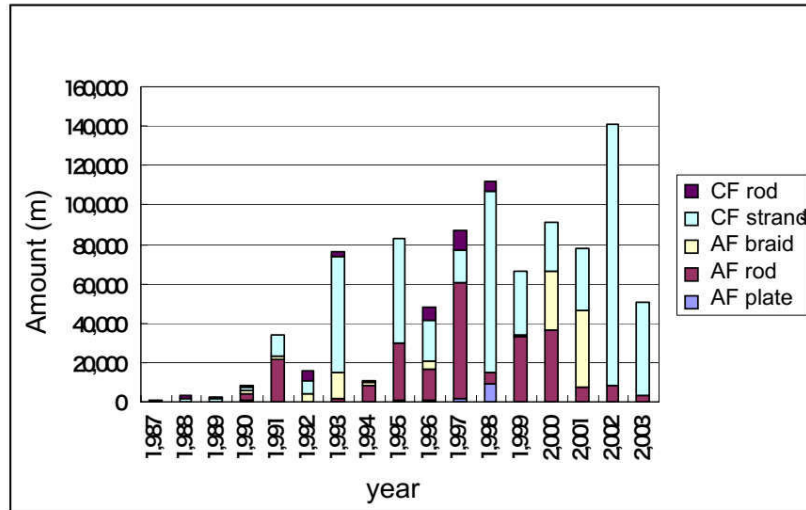
a) FRP reinforcement (excluding grid)
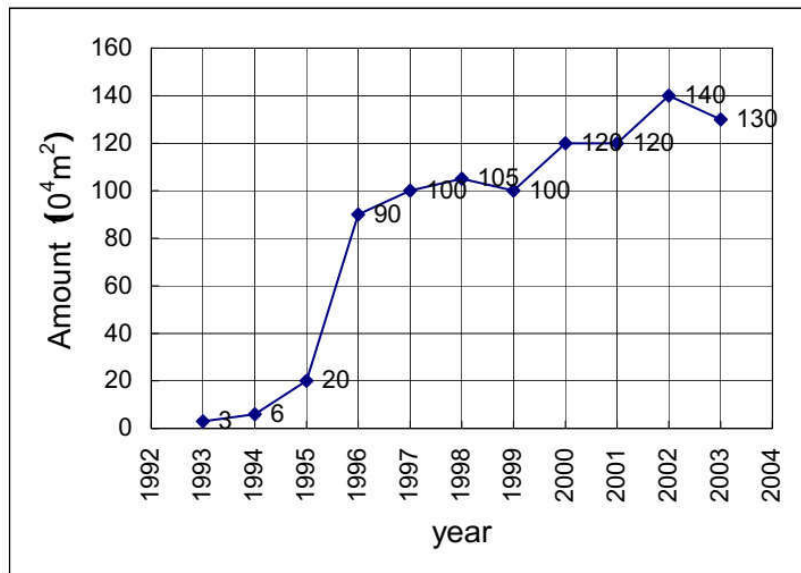
b) Carbon fiber sheet
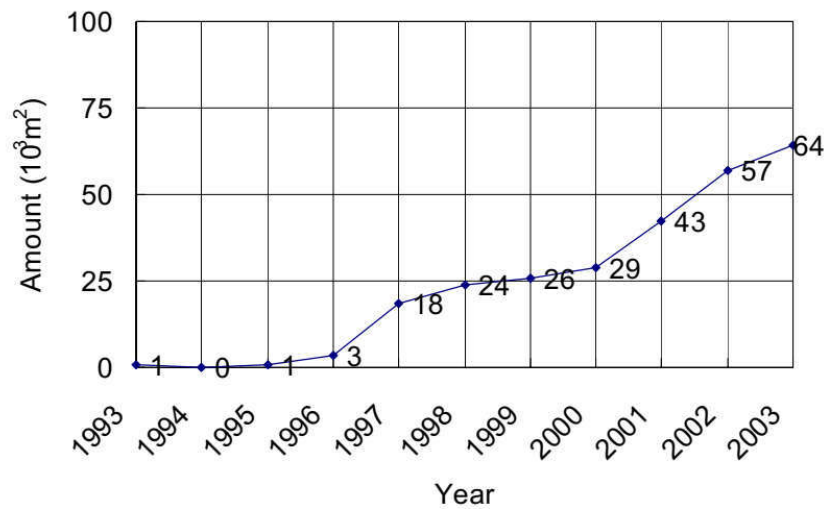
c) Aramid fiber sheet

Figure 2-6: Amount of FRP reinforcement use in Japan, (Tamon 2005)

In Japan, there are various types of FRP reinforcement at present. In Japan, various types of FRP reinforcement are available at present. Types of configuration are rod (round and rectangular), strand, braid, and grid. Fibers for each type are carbon and aramid (rod), carbon (strand), aramid (braid) and carbon, aramid and glass (grid). Table 2-1 and Fig. 2-4; 2-5 show examples of the FRP reinforcement. Major producers in Japan are Teijin for aramid rod, Tokyo Rope for carbon rod and strand, Nittetsu Composite for carbon strand and rod and carbon, aramid and glass grid, Fibex for aramid rod, and Mitsubishi Chemical for carbon rod.

Table 2-1: Configuration of FRP reinforcement for concrete in Japan

Type	Rod (round)	Rod (rectangular)	Strand	Braid	Grid
Symbol	R,D	P	S	B	L
Configuration					
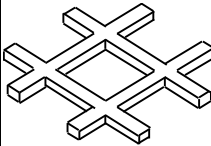
The continuous fiber reinforcing materials

The continuous fiber reinforcing materials (CFRM) introduced are composite materials made from the combination of the high strength, elasticity and heat resistance of carbon fiber, aramid fiber and glass fiber with epoxy resin and vinyl ester resin. CFRM have high corrosion resistance and show promise as materials that will be able to reduce the maintenance and repair costs of concrete structures. Their use is expected to increase along with the broader acceptance of the lifecycle cost (LCC). CFRM, as shown in the below photo, can be formed freely into rods, braids, strands, and grids, according to their intended application (Association for Advanced composite Technology on Construction 2018).

Table 2-2: Properties of CFRM compare to others

		Carbon (CFRP)	Aramid (AFRP)	Glass (GFRP)	Steel strand	Steel rebar
Specific gravity	-	1.5	1.3	1.7-1.9	7.85	7.85
Tensile strength	N/mm^2	1,900-2,300	1,400-1,800	600-900	1,700-1,900	490
Young's modulus	kN/mm^2	130-150	50-70	30	200	210
Elongation	%	0.6-1.9	2-4	2	6	10
Relaxation ratio	%	1.5-3	5-15	10	1-2	-
Coefficient of thermal expansion	$10^{-6}/^0C$	0.9	-2 -:- -5	9	12	12
Durability	-	good	good	good	poor	Poor
Non-Magnetism	-	yes	yes	yes	No	no

The main advantages of CFRP are listed as follow:
- CFRP is high tensile strength material. It is exceptional durability. Its tensile strength is higher than normal steel 4 or 5 times. With a small amount of CFRP, it works as much higher amount of other materials. Its modulus of elasticity is only about a haft of typical reinforcing steel. And comparing to steel, CFRP is a brittle material. The elongation of CFRP is around 1.7% before failure (Grace et al. 2012) compared to 4-5% of steel after yielding (H. Nilson 2018)
- CFRP is a lightweight material. The most widely known benefit of carbon fiber reinforced polymer is its strength-to-weight ratio. This property is of importance in cases when the weight of the object produced has a significant influence on its performance. It can be applied to strengthening concrete structures without increasing their weight considerably.
- Next benefit of CFRP is its resistance to corrosion. This process affects the surface and structure of metal and resub in a loss of weight of metal. All alleys deteriorate and corrode; however, the low rate of corrosion ensures more extended exploitation period. Moreover, low price of corrosion leads to the safe use. Depending on the type of resin used for production, CFRP can work well in a high-temperature environment. While made of the proper fiber and resins carbon fiber reinforced polymer is one of the most resistant to corrosion materials.
- CFRP grid is nonmagnetic material, it is characterized by radiolucence. Although carbon is fragile and it is hard to form it into small details; it also possesses excellent enhancing qualities. Since it is transparent to X-rays, it gradually replaces metallic alloys in medical devices Outstanding fatigue performance of the material allows medical specialists to

make implants with extended service life period.

2.2.2. FRP composite sheets

CFRP sheet is made of carbon, aramid or glass. Sheets with fiber in one direction are used for strengthening, while sheet with fiber in two directions are for repairing to improve/restore durability and to avoid concrete pieces from falling from the structure surface. FRP composite plates or sheets: this method has become popular because of the advantages of FRP composites such as their high strength-to-weight ratio, high corrosion resistance, and versatility in coping with different sectional shapes and corners (Chen and Teng 2003). The use of FRP materials in shear strengthening of reinforced concrete shallow beams has been investigated quite extensively in the past (Uji, 1992; Dolan et al., 1992, Al-Sulaimani et al., 1994; Chajes et al., 1995; Malvar et al., 1995; Sato et al., 1996; Triantafillou, 1998, Chaallal et al., 1998; Malek and Saadatmanesh, 1998; Colotti and Spadea, 2001; Li et al., 2001a, 2001b). The results of these investigations demonstrated the effectiveness of FRP to achieve the desired effects in shallow beams.

2.3. CFRP GRID FOR SHEAR REINFORCING

2.3.1. Application using CFRP grid –NEFMAC for strengthening

a) Wall reinforcement b) Floor Reinforcement
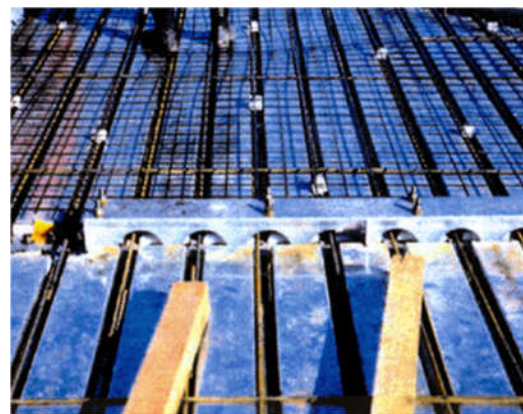
Figure 2-7: Use of NEFMAC grid
Source http://www.wtec.org/loyola/compce/03_07.htm

NEFMAC, or New Fiber Composite Material for Reinforcing Concrete, is made from glass, aramid, or carbon fibers (or combinations of each) impregnated with an appropriate resin system, such as polyester, vinyl ester or epoxy to form a grid.

NEFMAC grids have been used in tunnels, runways and aprons for airstrips/tarmacs, roads, buildings, channels, rehabilitation, and for general architectural elements. They are

regularly used as lightweight strengthening in building fascia and curtain walls, where the lower requirements for cover applications result in thinner and lighter panels. The use of NEFMAC grids is shown in the Fig. 2-4, 2-5, 2-7. Due to their non-magnetic properties, NEFMAC grids have been used as reinforcement in hospitals and free-access floors, as well as insensitive structures such as scientific laboratories and observatories. In coastal areas and regions where rapid corrosion of steel reinforcement is a concern, NEFMAC elements can be applied by themselves or in combination with conventional reinforcing bars.
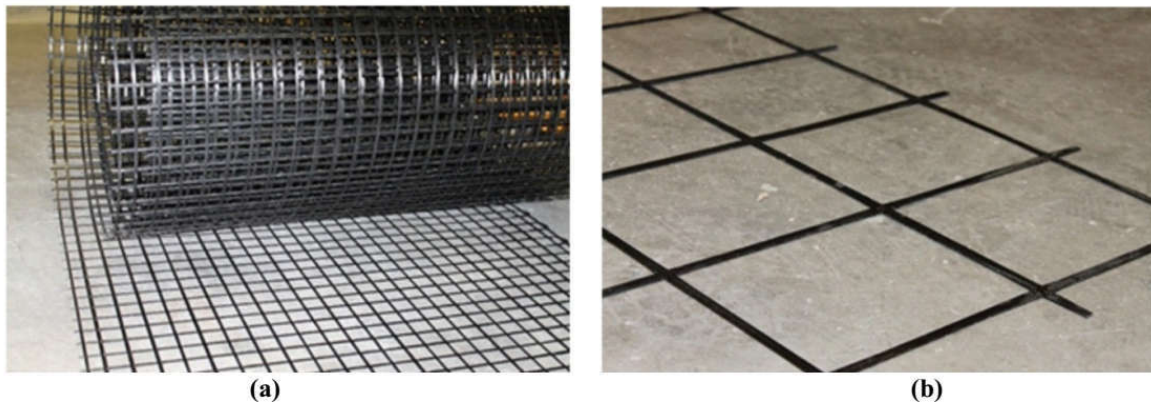
Figure 2-8: CFRP grid (a) and NEFMAC (b)
(Ward et al. 2018)
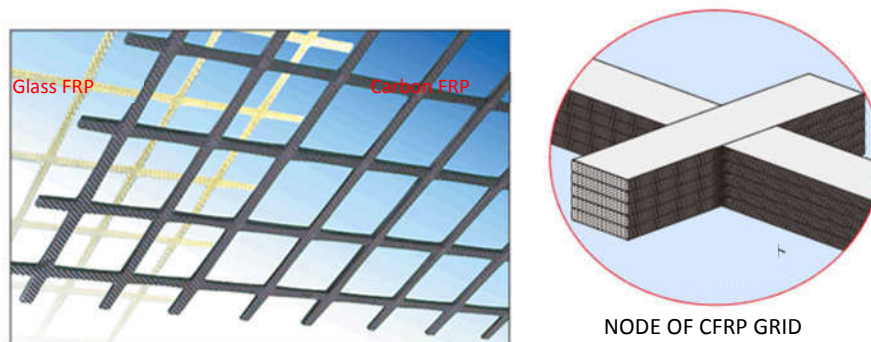
Figure 2-9: Carbon FRP grid, glass FRP grid and CFRP node

CFRP grid is made from carbon fibers (or combinations of each) impregnated with an appropriate resin system, such as polyester, vinyl ester or epoxy to form a grid. Figure 2-9 shows the images of carbon FRP grid, glass FRP grid and the component of CFRP node. The fiber grid is protected by the polymer mortar which is used in conjunction with FRP grid, and to improve the durability, the performance of fire resistance. Base on the dimension of grid, CFRP grid could be classified into two main types: 50mm x 50 mm and 100mm x 100 mm. The frame of CFRP grid is produced with the size of 2000x3000 mm or 2000x1500 mm or 2000x1000 mm.

Polymer-modified or polymer cement mortar (PCM) and concrete (PCC) are a category of concrete-polymer composites which are made by partially replacing the cement

hydrate binders of conventional cement mortar or concrete with polymers, i.e., polymeric admixtures or cement modifiers, thereby strengthening the binders with the polymers. Polymer- modified or polymer cement paste, which is prepared without any aggregate, is sometimes used.

Epoxy Primer is used to spray to old concrete surface before applying the PCM. Epoxy Primer is a clear, single-component epoxy primer/sealer. It incorporates state of the art water-based technology to produce an extremely versatile product that penetrates and seals porous substrates. Epoxy Primer is constructed to penetrate and seal porous substrates and to improve the adhesion of high-performance top coats. It develops a tenacious bond to concrete, asphalt, wood, fiberglass, steel, galvanized and aluminum surfaces.

FRP grid construction method is attached to a concrete precursor the FRP grid at anchor, is a method to be integrated by spraying or the like of the special polymer cement mortar (PCM).

2.3.2. Advantage of CFRP grid compared to CFRP sheet:

CFRP sheet is usually applied for strengthening or repair the aging or downing quality concrete structures, while CFRP grid is mainly used for substitute of reinforcing bars in the new contructions. CFRP grid takes the full advantages of FRP. Its light weight facilitates ease and speed in construction, without loss of performance. Also they can be applied as lightweight reinforcement in building fascia and curtain walls, which show the lower requirements for cover applications such as thinner and lighter panels. Due to its resistance to corrosion and excellent resistance to alkalis, acids and chemicals, it does not require a substantial cover and may instead of steel stirrups to solve the problems of the steel corrosion in harsh environments. Furthermore, due to the non-magnetic properties, CFRP grids are the excellent reinforcement material for hospitals and free-access floors, as well as sensitive structures such as scientific laboratories and observatories. Since the grating intersections are on the same plane, it is possible to reduce the cross-section in comparison with the case of using the rebar.

Under some specific circumstances, when comparing between CFRP grid and CFRP sheet, CFRP grid shows the advantages. Especially, when the surface of old concrete is damaged, using CFRP grid to repair the structure save the time and reduce the cost. Applying CFRP sheet, firstly, the damaged concrete has to be removed, then the surface of concrete needs to be repaired by patching mortar and grinding to create a smooth surface. While, applying CFRP grid, the patching procedure is already included in the shotcrete step. According to quotes of one of the biggest FRP manufacturer (Sumikin n.d.) in Japan, for the purpose bridge deck strengthening, the costs of two methods are same, but with the bridge deck in bad surface condition or waterway tunnel the cost for construction of method using CFRP sheet is 20% higher because of installing an inner repairing mortar layer. General comparison between CFRP sheet and CFRP grid is summarized in Table 2-3.

Table 2-3: Comparison of strengthening methods for the concrete structure using CFRP sheet and CRFP grid

	Strengthening method using CFRP sheet	Strengthening method using CFRP grid combined with polymer-mortar
Typical cross section	Figure 2-10: Typical cross section of using CFRP sheet	Figure 2-11: Typical cross section of using CFRP grid and sprayed mortar
Overview of the strengthening method	FRP sheet is pasted on the surface of concrete structure by epoxy	The grid of CFRP is fixed on the concrete surface by anchor bolts. After that, the special polymer-cement mortar is sprayed on the surface.
Feature of method	- Improvement strength of structures. - There is almost no increase of structure dimension - Preventing spalling and falling of concrete slab - Not increase the permanent load - Suppressing the propagation of the existing crack at the bottom surface of slab	- Improvement strength of the bridge deck. Thickness of the slab increase leading to the resistance cross section is expanded - Preventing spalling and falling of concrete slab - The permanent load is not much increased
Construc-tability	- Can keep traffic operations while doing repair work. There is no traffic restriction.	- Can keep traffic operations while doing repair work. There is no traffic restriction.
Usability and Maintenance	- It is necessary to combine with waterproof - It is difficult to determine damage at the surface after strengthening - The durability is long owing to non-corroded material	- It is necessary to combine with waterproof - Can determine damage at the surface after strengthening - The durability is long due to non-corroded materials
Installation step	(with the damaged surface condition) -Remove the bad concrete on the substrate concrete - Patch mortar and grind to make smooth surface - Apply the CFRP sheet to the concrete surface. - Cover layer (with the harsh environment)	(with the damaged surface condition) - Remove the damaged concrete on the substrate concrete - Clean the surface by the high-pressure water pump - Fix CFRP grid to old concrete surface by bolt anchor, spray epoxy primer then shotcrete.

Pictures	a) Pre-Construction b) Construction situation Completion Figure 2-12: Application of CFRP sheet	a) Floor slab reinforcement b) Shear reinforcement Completion Figure 2-13: Application of CFRP grid and sprayed mortar

Required equipment serving for the construction process is simple, easy to transport, set up and disassemble. It does not require the high qualifications of construction workers, a short period of training. Equipment needed for installing includes: high-pressure water pump machine, machine for shotcrete (electric generator, compressor, mixing machine, pump).

2.3.3. Codes for CFRP grid

While the use of CFRP as flexural reinforcing has been studied and used widely in Japan, the use of CFRP as transverse reinforcing in RC beams has not been studied extensively. In a RC beam, stirrups often have the least cover, they have the most exposure to chlorides that accelerate corrosion. Applying CFRP could prevent spalling of the beam's outer layer caused by corrosion of the shear reinforcement, thus helping keep the bridge in better condition and mitigating the need for routine maintenance. Beam sections with CFRP transverse reinforcement have been studied, but not to the extent of longitudinal CFRP products. Reinforced sections do not have the additional benefit of additional shear resistance from the longitudinal reinforcement. Additionally, the codes specify a minimum amount of transverse reinforcement to ensure the beam does not fail in shear prematurely.

Using CFRP as transverse reinforcing helps to ensure a longer design life for beams and bridges. Transverse CFRP reinforcing research has mainly consisted of the use of CFRP stirrups. As more CFRP products continue to come to market, the cost will be driven down allowing the CFRP has more competitive price with reinforcing steel, especially requires less maintenance.

There are a number of existing shear design equations for FRP RC beams with FRP stirrups published by some countries. Some of them are listed as below:

- ACI440.1R-06, Guide for the Design and Construction of Structural Concrete Reinforced with FRP Bars, Reported by ACI Committee 440- USA (Bank, Campbell, and Dolan 2006)
- Fib, 2005, FRP Reinforcement for reinforced concrete Structures, Task Group 9.3, Reinforcement for Concrete Structures, Lausanne, Switzerland.
- CSA S6-09-Addendum, The CANADIAN highway bridge design code (S6-09-Addendum and BRUNEAU 2018)
- CSA S806-12, Design and construction of Building components with FRP, reported by Canadian Standards Association, Rexdale, Canada (Can/Csa 2012)
- CNR DT-203/2006, Guidelines for the design, construction and production control of fiber reinforced concrete structures, Italian National Research Council (Advisory Committee on Technical Recommendations for Construction 2006).

Code for FRP reinforcement in Japan (Tamon 2005):

There are two specifications for applying FRP reinforcement for new concrete structures (Research Committee on Continuous Fiber Reinforcing Materials 1997; Editorial Committee on Concrete Reinforced with Continuous Fiber Reinforcement 1995) and the upgrading of existing concrete structures (Research Committee on Upgrading of Concrete Structures with Use of Continuous Fiber Sheet 2001). The following two codes are briefly introduced:

Recommendation for design and construction of concrete structures using continuous fiber reinforcing materials (Research Committee on Continuous Fiber Reinforcing Materials 1997). The Recommendation for design and construction of concrete structures using continuous fiber reinforcing materials can be applied to most of the FRP reinforcing bars available in Japan, which are carbon and aramid bars (round/rectangular rods, strands and braids) and Carbon, aramid and glass grids. The Recommendation is prepared by JSCE's Standard Specifications for Concrete Structures and introduces new design formulas, such as those for shear strength of linear members and anchorage length. At the same time-related standards were published by JSCE. They are quality Specifications for Continuous Fiber Reinforcing Materials, which specify the material properties of FRP reinforcement and the following test methods:

• Test method for flexural tensile properties of continuous fiber reinforcing materials

• Test method for creep failure of continuous fiber reinforcing materials

• Test method for long-term relaxation of continuous fiber reinforcing materials

• Test method for tensile fatigue of continuous fiber reinforcing materials

• Test method for the coefficient of thermal expansion of continuous fiber reinforcing materials by thermo-mechanical analysis

• Test method for performance of anchorages and couplers in prestressed concrete using

continuous fiber reinforcing materials

• Test method for alkali resistance of continuous fiber reinforcing materials

• Test method for the bond strength of continuous fiber reinforcing materials by pull-out

testing

• Test method for shear properties of continuous fiber reinforcing materials by double plane shear

Recommendations for upgrading of concrete structures with the use of continuous fiber sheets (Research Committee on Upgrading of Concrete Structures with Use of Continuous Fiber Sheet 2001). The Recommendations for upgrading of concrete structures with the use of continuous fiber sheets are applied to both column and beam retrofit with use of carbon and aramid fiber sheets. Column retrofit means seismic retrofit. The Recommendations were prepared based on Guidelines for Retrofit of Concrete Structures – Draft – (JSCE Working Group on Retrofit Design of Concrete Structures in Specification Revision Committee 2001) in which performance-based concept is accepted. In the Recommendations verification methods for safety are provided by newly proposed prediction methods of flexural strength, shear strength and ductility. In the flexural strength prediction, interfacial fracture energy concept is applied, while debonding is considered in the shear strength prediction.

As above, the approved code applying for FRP material is mainly focused on the continuous fiber sheets and FRP bars, there is no specification for CFRP grid. The application of these codes for CFRP grid faces many difficulties and sometimes is unreasonable. So more studies need to be conducted researching on CFRP grid for the further code for CFRP grid.

2.4. ACOUSTIC EMISSION
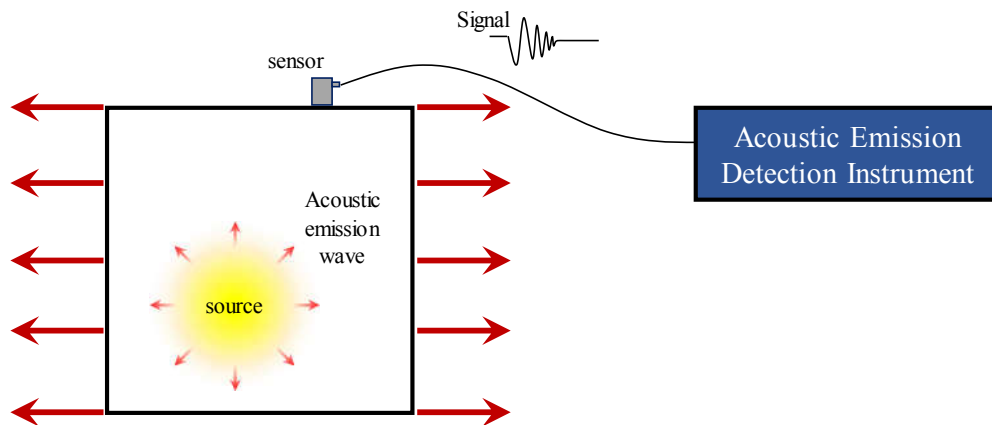
Figure 2-14: Principle diagram of the AE system

Acoustic Emission Testing (AET) is a nondestructive testing method that is based on the generation of waves produced by a sudden redistribution of stress in a material. It is a powerful method for examining behavior of materials deforming under stress. The Acoustic Emission NDT technique is based on the detection and conversion of high-frequency elastic waves into electrical signals. This is accomplished by directly coupling piezoelectric transducers on the surface of the structure under test and loading the structure. Sensors are coupled to the structure, and the output of each sensor (during structure loading) is amplified through a low-noise preamplifier, filtered to remove any extraneous noise and further processed by suitable electronic equipment. When a structure is subjected to an external stimulus, such as a change in pressure, load, or temperature, this triggers the release of energy in the form of stress waves, which propagate to the surface and are recorded by sensors. With the right equipment and setup, motions on the order of picometers (10 -12 m) can be identified. Sources of AE vary from natural events like earthquakes and rockbursts to the initiation and growth of cracks, slip and dislocation movements, melting, twinning, and phase transformations in metals. In composites, matrix cracking and fiber breakage and debonding contribute to acoustic emissions. AE's have also been measured and recorded in polymers, wood, and concrete, among other materials. Fig. 2-14 shows the principle diagram of AE system.

Detection and analysis of AE signals can supply valuable information regarding the origin and importance of a discontinuity in a material. Small-scale damage is detectable long before failure, so AE can be used as a non-destructive technique to find defects during structural proof tests and plant operation. AE also offers unique capabilities for materials research and development in the laboratory. Finally, AE equipment is adaptable to many forms of production testing, including weld monitoring and leak detection. Because of the versatility of Acoustic Emission Testing (AET), it has many industrial applications (e.g., assessing structural integrity, detecting flaws, testing for leaks, or monitoring weld quality) and is used extensively as a research tool.

Acoustic Emission is unlike most other nondestructive testing (NDT) techniques in two regards: The first difference pertains to the origin of the signal. Instead of supplying energy to the object under examination, AET simply listens for the energy released by the object. AE tests are often performed on structures while in operation, as this provides adequate loading for propagating defects and triggering acoustic emissions. The second difference is that AET deals with dynamic processes, or changes, in a material. This is particularly meaningful because only active features (e.g. crack growth) are highlighted. The ability to discern between developing and stagnant defects is significant. However, it is possible for flaws to go undetected altogether if the loading is not high enough to cause an acoustic event. Furthermore, AE testing usually provides an immediate indication relating to the strength or risk of failure of a component. Other advantages of AET include fast and complete volumetric inspection using multiple sensors, permanent sensor mounting for process control, and no need to disassemble and clean a specimen.

A system of AE comprises of Physical Acoustics' sensors, preamplifiers and PC. Physical Acoustics' sensors are built to "listen" to high frequency signals. Much like a highly-sensitive "ear," Acoustic Emission sensors interpret the material's "voice" into usable AE waveforms. Additionally, AE sensors help understand how materials behave in their natural setting. AE sensors are a vital link in defining how to apply remedial solutions and repairs to resolve structural issues. AE sensors are used to examine storage tanks, heat exchangers, piping, reactors, aerial lift devices, as well as gas, petro-chemical and nuclear power plants. Physical Acoustics' sensors can be built with particular features to meet project or application specific needs.

Preamplifiers recognize the extremely low amplitude AE signal produced from AE sensors, and convert the signals into amplified and usable forms. As applications and testing conditions vary, project needs may change as well. Physical Acoustics offers an entire line of preamplifiers for a variety of testing requirements. Operating in conjunction with our specialized AE software, preamplifiers also moderate signal size during the data collection process, helping to produce accurate results. This is achieved through transducers which

convert mechanical movement into an electrical voltage signal. The majority of AE equipment responds to movement in a range of 30 kHz to 1 MHz. For materials with high attenuation, such as plastic composites, lower frequencies may be used to better distinguish AE signals. The inverse is true as well.

In this study, AE system is applied to the three beams shear-strengthened by CFRP grid to locate the fracture of materials and monitor the propagation of the crack also.

2.5. DIAGONAL CRACK IN RC BEAMS

These inclined shear cracks can begin as a flexural crack or inside the web area (Zakaria et al. 2009). And the shear failure mechanism in RC beams is strongly affected by the appearance of the diagonal cracks. A number of studies (Adebar and Van Leeuwen 1999; HASSAN, FARGHALY, and UEDA 1991; Piyamahant and Shima 2008; Saravanakumar and Govindaraj 2016; De Silva et al. 2018) for decades focused on shear cracking mechanism and diagonal shear failure in RC member.

In ordinary beams, under four-point bending loading, the crack leading to collapse, the critical crack comprises typically of two branches (Fig. 2-15). Generally, these two branches are formed at different time instants and are due to different causes. The first branch is an inclined shear crack, which either develops after the onset of nearby flexural crack or begins like a flexural crack. While this first branch is usually formed at the end of the flexural cracks (close to the support), often it is formed between flexural cracks. The height of the first branch is similar to that of the flexural cracks. The failure is caused by the formation of the second branch of the critical crack, which initiates from the tip of the first branch and propagates, abruptly or gradually, toward the loading point crossing the compression zone. (Zararis and Papadakis 2001).

When applying at least two layers of CFRP grid for strengthening RC beam, the shear crack is controlled to a similar width as in beams using stirrups (Ward et al. 2018). And it is supposed that shear strengthening RC beams with CFRP grid to restraint the crack is no an economical method.
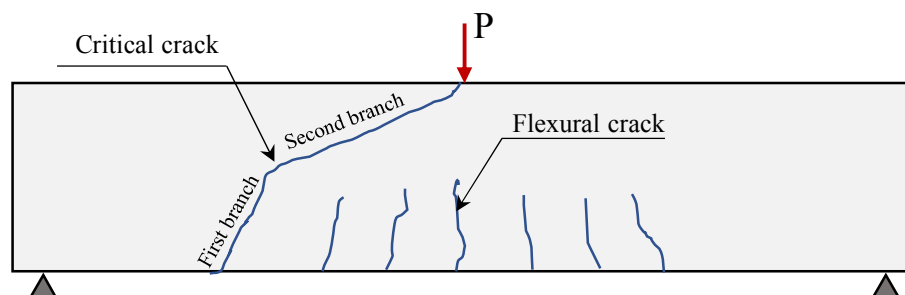
Figure 2-15: Two branches of critical crack

2.6. DIRECT RELATIVE RESEARCHES

There are two studies – dissertations – which have the same objects and studying contents are very close to this thesis. They are Dung Tran Vu's and Bo Wang's theses, fulfilled in 2016. The main contents of their dissertations are briefly summarized as follow:

2.6.1. Bo Wang's thesis

The related content in Bo Wang's thesis is concisely condensed as below;

This thesis investigates the interaction behavior between the CFRP grid and mortar. The tensile behavior of the CFRP grid-sprayed mortar in strengthened concrete structures was selected as the research object.

The result from investigating the tensile behavior of the crossing point in CFRP grid showed that; (1) Two mechanical models (Elastic Layer Model (ELM) and Spring Model (SM)) of the crossing point in CFRP grid were proposed. Based on the proposed models, the tensile behavior and failure mechanism of the crossing point can be clarified clearly. (2) The influencing mechanism of the mortar on the tensile stress transfer mode of multiple crossing points along the vertical bar in CFRP grid was revealed. (3) The failure mechanisms corresponding to different failure modes of pull-out specimens with multiple crossing points were publicized.

This study also implements the test to study the anchorage mechanism of CFRP grid in mortar based on pull-out tests. Types of CFRP grids, grid interval, number of nodes and anchorage conditions were selected as changing parameters to conduct pull-out tests. The maximum loads, failure modes, load-displacement curves were obtained. The tensile strength utilization of CFRP grid, growth gradient of maximum load, characteristics of bond action and resistant, tensile bearing mode of resistant action, coupling process between bond action and resistant action were analyzed. The next test was to verify the feasibility of a new anchorage method named intersect-type anchorage method of CFRP grid in mortar based on bidirectional pull-out tests. The maximum loads, failure modes and strains of the CFRP grid in the intersecting part were obtained. The tensile strength utilization and failure mechanism were analyzed. Based on the analysis of two stages of pull-out experimental results, the following main innovative results were achieved: (1) The minimum number of nodes for full use of the tensile strength of CFRP grid was attained; (2) The tensile bearing mode of CFRP grid with multiple nodes and the corresponding calculation formula of the maximum tensile load were proposed; (3) The coupling mechanism between bond action and resistant action was revealed; (4) A new anchorage method named bidirectional intersect-type anchorage method of CFRP grid in mortar was proposed. The main procedure of this new method is cutting the middle part of the horizontal bar between two adjacent vertical bars and assembling two parts of CFRP grids by intersecting with a certain   a number of nodes.

The result from investigating the tensile behavior of the crossing point in CFRP grid showed that; (1) Two mechanical models (Elastic Layer Model (ELM) and Spring Model (SM)) of the crossing point in CFRP grid were proposed. Based on the proposed models, the tensile behavior and failure mechanism of the crossing point can be clarified clearly. (2) The influencing mechanism of the mortar on the tensile stress transfer mode of multiple crossing points along the vertical bar in CFRP grid was revealed. (3) The failure mechanisms corresponding to different failure modes of pull-out specimens with multiple crossing points were publicized.

2.6.2. Tran Vu Dung's thesis

The study aims to assess the factors that influence to the strengthening work. The factors, such as: bond behavior between 2 materials, characteristics of CFRP and mortar, etc., will be analyzed, evaluated and compared in each chapter to clarify their roles. The research was conducted under both experimental and FEM analysis approaches. Detail contents in each chapter are shown in the following paragraphs.

In the experimental program, he studies about one of the most important factors for success of the repair, the shear bond strength of the interface between substrate concrete and repair mortar was evaluated through experimental and analytical investigations. There are five types of shear bond test were carried out, namely, Direct shear test, Push-off test, Bi-surfaces shear test, Slant shear test and Punching shear test. The bond interface of each type has 3 kinds of roughness index: High, medium and smooth. The results reflected the difference of shear bond strength between these tests and its correlation with roughness index. Next, the macrotexture of the interface is exemplified by a new model like a saw-tooth shape. This model is evaluated based on the assumption that every saw-tooth always exists two bonding components on the surface to restrain slip between 2 parts that is adhesion and friction. By analyzing and calculating force diagram of each type of test, it can explain why the shear bond strength quite differs in each kind of tests. Simultaneously influence of the interface's roughness or the adhesion is also clarified. This study helps to estimate the bond strength of the interface and suggests measures to make a better bond behavior.

Tran V.D assumed that the shear resistance capacity of a reinforced concrete beam is reduced because of corroded stirrups. This beam should be strengthened by using a CFRP grid and repair mortar. However, in the first stage of the research, only the part potentially appears diagonal crack in this beam would be taken out to analyze. Pullout tests were carried out to evaluate the shear capacity of specimens reinforced by a CFRP grid and sprayed mortar. In the analysis section, to describe the behavior of CFRP grid inside the mortar layer as well as bond behavior between mortar layer and substrate concrete, a new model which includes CFRP frame put on an elastic-brittle spring foundation was proposed. The system is analyzed to investigate the failure process and the impact of CFRP and mortar's characteristic to the load capacity. After that, the corresponding 3D FEM models are also analyzed based on Cohesive Zone Model (CZM) and Crack Data theory. As a result, from both experimental and analytical investigation, it is suggested that the shear resistance area moved stepwise from the bottom to the top of all specimens. As well, it can be concluded the resistance of the structure mainly depends on tensile strength of the mortar, bond strength of the interface and strength of CFRP. The higher tensile strength mortar or the stronger bond method is applied, the better bearing capacity will be accomplished. The larger thickness and smaller grid spacing of CFRP grid can be sustained better. For that reason, to increase the effective resistance, choice of appropriate factors is required. Three large RC

beams were conducted by 4-point bending tests and simulated by FEM computational program to obtain overall assessment about the effectiveness of the repair method. The three beams differ in arrangement of shear reinforcements which is responsible by steel stirrups and CFRP grid. RC1 is a normal reinforced concrete beam; RC2 is a strengthened beam with CFRP grid and Sprayed mortar; the last one has CRRP grid and Sprayed mortar but not use steel stirrups. In FEM analysis approach, outcomes of the study in chapter 3, as CZM, Crack Data for concrete material, are applied. There is a good agreement between simulations and experiments about the load capacity, the failure process and effects of the repair method. The role and effectiveness of CFRP-Sprayed mortar layer in the strengthening work for age reinforced concrete structures are confirmed. It is noted that, in this chapter, bond behavior of the substrate concrete's surface in the model are simulated not only as good condition like in the experiments but also various conditions through adjusting parameters in CZM.

2.6.3. Experimental direction

The Bo Wang's thesis mainly focus on the tensile behavior of the CFRP grid in sprayed mortar, the behavior of cross-point. While Tran VD's thesis mostly studies on shear behavior between 2 materials. In the experimental program, Tran VD conducted the test with the specimens made by concrete and mortar. Various types of shear bond test were carried out. In a certain point of view, they didn't reflect correctly the actual work of concrete and mortar in the composite structures. In the real structure, the force is transferred from the CFRP to the mortar and then through the contact surface between concrete and mortar or in an opposite direction, the principle diagram is shown in Fig. 2-16. For a better adequate understanding of the behavior of CFRP grid and sprayed mortar in strengthening RC beams, additional experiments are necessary. These tests need to be modeled much more closely to the actual work of CFRP and mortar. All of these investigations are described in detail in the following chapters.
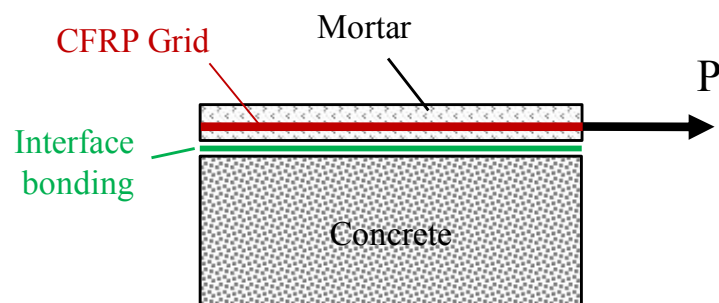
Figure 2-16: Forces transfer mechanism between materials

Chapter 3:

BEHAVIOR OF MATERIALS IN REINFORCED CONCRETE SPECIMENS STRENGTHENED BY CFRP GRID AND MORTAR

This chapter aims to investigate the capability of four materials: concrete, steel, Carbon Fibre Reinforced Polymer (CFRP) grid, and mortar, acting together in composite specimens. In this experimental program, three concrete prisms are reinforced by different schemes of steel bars and/or CFRP grid in the axial direction. Specimen 1, as the control, with a square section of concrete is axially reinforced by steel rebars. Specimen 2 was reinforced by CFRP grid and Specimen 3 was reinforced by both rebars and CFRP grid. CFRP grid and spray mortar were applied on two sides of concrete prisms 2 and 3. The strengthened specimen 2 and 3 have the same dimensions as specimen 1 (100 x 100 x 500 mm), they were applied the axial tensile force until fail. Though specimens 2 and 3 the concrete surface is well-treated for the high adhesive property between concrete and mortar, the failure still occurs at the bonding interface. The result of the test shows the effect of strengthening by CFRP grid, the behavior of reinforcing materials and the capability of CFRP grid influenced by the bonding interface between concrete and mortar.

3.1. INTRODUCTION

Regarding the effect of the strengthening of CFRP grid and sprayed mortar, the capacity of CFRP grid and bonding strength of the interface between materials are influential factors. Many studies on CFRP grid reinforcement (Ding, Wu, and Wu 2010) and bonding of interface between two materials (TRAN Vu Dung 2016), (Austin, Robins, and Pan 1999) have been reported. (Júlio, Branco, and Silva 2004) Concluded that sandblasting is a consistent preparing method to provide the best bond strength between two layers of materials. On the other hand, (Santos, Santos, and Dias-Da-Costa 2012) supposed that the higher surface roughness the greater number of non-adhesive failure was detected (Ding et al. 2010). But there are not many studies focus on the problem of the combination of old and reinforced materials in a real strengthened structure. The purpose of this chapter is to study the behavior of materials such as concrete, steel, mortar and CFRP grid as they act together in a composit specimen. The maximum load, failure modes and the bonding characteristics of the interface of concrete and mortar are also investigated. In this study, sandblasting and primary epoxy resin application methods was chosen to apply to the bonding surface for a high interface strength. Among all considered techniques, sandblasting is such the preparation method of substrate surface that provides the highest values of bonding strength in shear (Júlio et al. 2004).

Prismatic concrete specimens with a cross-section of rectangular or square have been cast to examine the capability of these materials working together. These concrete prisms are reinforced with steel bars and/or CFRP grid in the axial direction then applied the tensile force on the specimens until failure by the hydraulic tensile testing machine. The behavior of materials was analyzed to make clear the effect of the strengthening work. The original goal of the research project was to investigate the maximum stress of CFRP grid in the composite specimen. In reality, the fracture didn't happen as expected. The result showed another important factor influencing strongly the effect of strengthening; the influence of surface preparation on the effect of strengthening.

3.2. EXPERIMENTAL PROGRAM

3.2.1. Experimental design

Three prismatic RC specimens have been fabricated then applied the axial tensile force. The reinforcement scheme of the three specimens is shown in Fig.3-1. Specimen 1 (SP1) is a control one with the length of 500 mm, made of concrete, the square cross-section of 100×100 mm, reinforced with two D6 steel bars along with the length direction of the specimen. Two D6 steel bars are welded to the D16 steel bar.

When the tensile test is carried out, the tensile force is transmitted from the chucks through the D16 rebar to the D6 rebar & concrete to apply the load on the specimen. Strengthening scheme of the three specimens is shown in Fig.3-1. In specimen 1, the weakest cross-section is the middle one with two bars of D6. Specimen number 2 (SP2), has no steel bar at the middle section, but strengthened with CFRP grid and sprayed mortar.

The dimension of substrate concrete prism is 500×100×60 mm. Then, on both sides of this original concrete specimen, two additional 20 mm layers of CFRP grid and mortar, have been installed for strengthening. Like the SP1, the middle center section is also the weakest cross section as applying the axial tensile force. The middle section   consists of 60×100 mm concrete, two layers of 20 mm mortar, and 4 bars of the CFRP grid.

Specimen number 3 (SP3) is reinforced by the same steel bars of D6 as in SP1, but the size of the cross-section after casting concrete is 60×100 mm, the length is 500 mm. This specimen is strengthened with two additional layers of CFRP grid and mortar, like SP2. The dimension of the cross-section after strengthening is square of 100×100 mm. And the middle section of SP3 is the weakest section; it consists of 60×100 mm concrete at the middle, two steel bars of D6, two layers of 20 mm mortar on both sides, and four bars of CFRP grid.
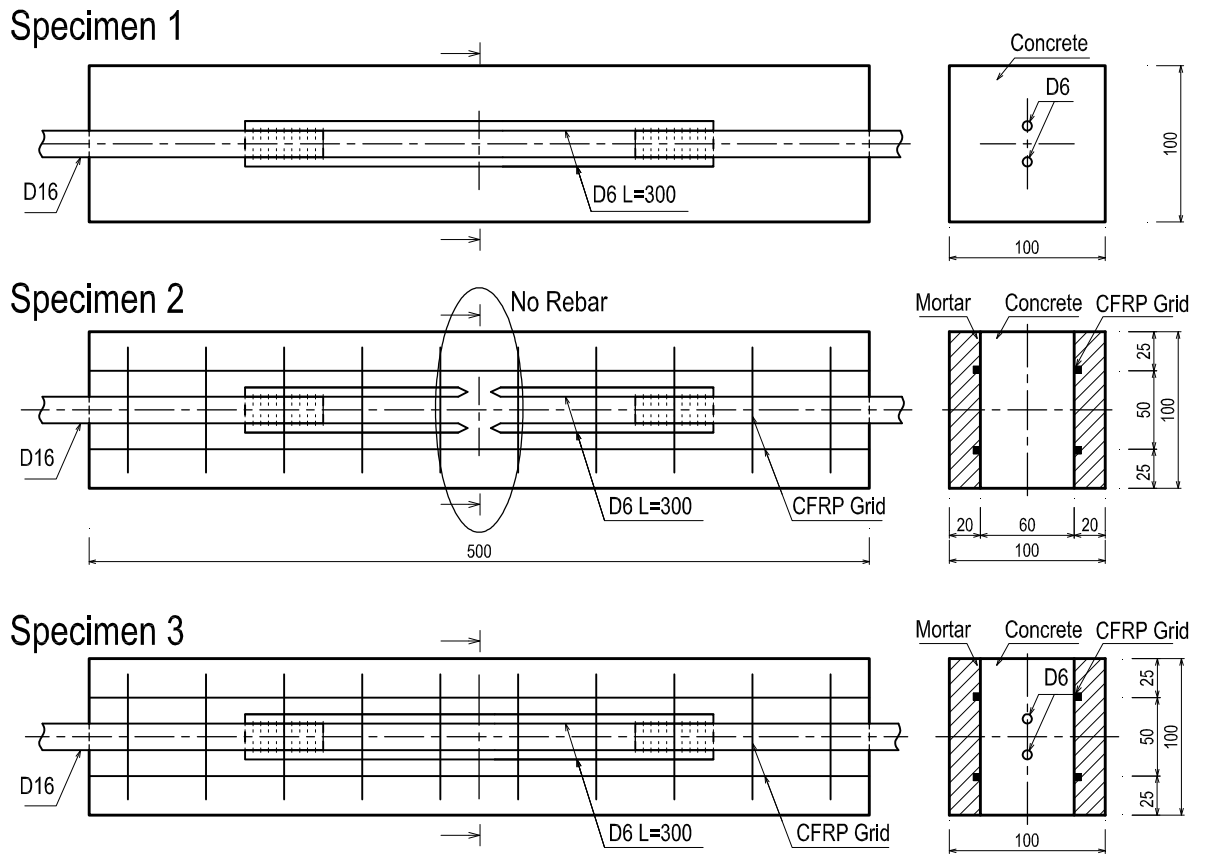
Figure 3-1: Strengthening scheme for the three specimens
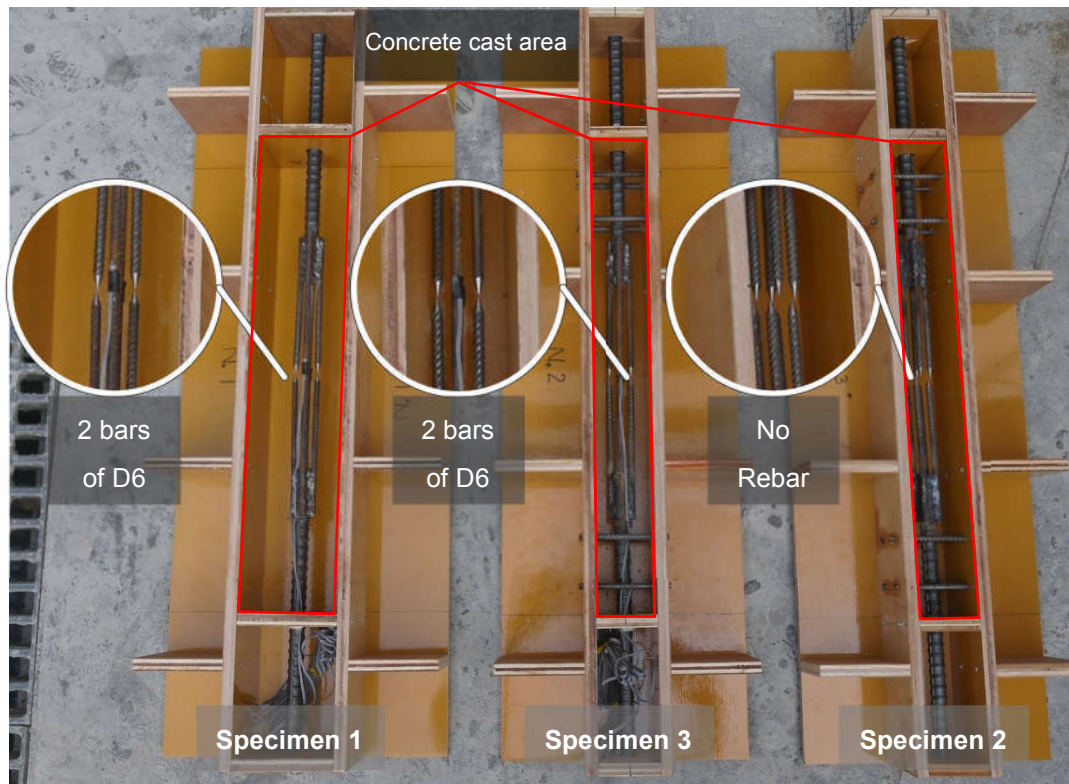
Figure 3-2: Prepared molds and reinforcing bars

3.2.2. Concrete and mortar

The mix proportion of concrete is presented in Table 3-1. The concrete has the aggregate with a maximum size of 20 mm. The water/cement ratio is 50%. Its unit cement content is 319 kg/m^3. The fresh concrete has an air content of 4.5% and a slump of 100 mm. A cubic meter of concrete contains 750 Kg of sand and 5.8 Kg of admixture. Mortar is polyacrylate ester (PAE) powder polymer modified type. It contains Vinylon fiber (PVA fiber) mixed type. The mixing ratio of mortar is 25 kg premixed mortar with 3.4 kg of water, according to Table 3-2. The fresh mortar has slump flow test of 16 cm、 diameter of slump cone downside and upside are 100 mm and 70 mm, respectively, slump cone tube height is 60 mm. The mechanical properties of concrete and mortar are tested on the same day with the tensile test, as shown in Table 3-3.

A layer of epoxy primer is applied before spraying mortar to increase the adhesion between the concrete and the mortar. Parameters of the epoxy primer are listed in Table 3-4.

3.2.3. Reinforcing materials

The steel bars used in the experiment have the mechanical properties listed in Table 3-5. Reinforcing bars with 6 mm of nominal diameter are used in this experiment.

CFRP grid is 50 x 50 mm grid size, other related parameters are indicated in Table 3-6. The name of CFRP grid, FTG-CR5-50P, is specified by the manufacturer.

Table 3-1: Mix proportion of concrete

Gravel (mm)	Slump (mm)	Air (%)	W/C (%)	Unit content (kg/m^3)				
				Water	Cement	Sand	Gravel	Admixture
20	100	4.5%	50%	157	319	750	879	5.8

Table 3-2: Mix proportion of mortar

Primixed Mortar	Water
25 kg	3.4 kg

Table 3-3: Mechanical properties of concrete and mortar

Type	Compressive strength (MPa)	Elastic modulus (GPa)	Tensile strength (MPa)
Concrete	47.4	27.7	3.2
Mortar	21.8	49.0	3.0

Table 3-4: Properties of epoxy primer

Main component	Modified vinyl acetate-ethylene copolymer emulsion
Solid content	45 to 48 (% by weight)
Appearance	Milky white liquid
Viscosity	500-2000 (mPa.s)
pH	4.5-6.5
Density	1.06 (g/ cm^3)
Low-temperature stability	Good

Table 3-5: Mechanical properties of reinforcing bars D6

Section area (mm^2)	Yield strength (MPa)	Tensile strength (MPa)	Elastic modulus (MPa)
31.67	417	570	2×10^5

Table 3-6: Mechanical properties of CFRP grid FTG-CR5-50P

Reinforcement Fiber	Resin ma-trix	Section area (mm^2)	Tensile strength (MPa)	Elastic modulus (MPa)
High-strength carbon	Vinyl ester	13.2	1,400	10^5

Table 3-7: Reinforcement ratio of specimens

Specimen	Reinforcement type	Reinforcement area (mm^2)	Ratio (%)
SP1	2 steel bars of D6	2 x 31.67 = 63.34	6.3
SP2	4 bars of CFRP grid	4 x 13.2 = 52.8	5.3
SP3	2 steel bars of D6 and 4 bars of CFRP grid	2 x 31.67 + 4 x 13.2 = 116.14	11.6

Table 3-7 presents the reinforcement ratio of each specimen. For a simple calculation, the section squares of CFRP grid and steel bar are added together without concerning the difference in the elastic modulus.

3.2.4. Casting and strengthening the specimens

Pictures of demolded concrete specimens are shown in Fig.3-3. After pouring the concrete prisms 1, 2 and 3 were cured seven days in a water tank at 20°C. Then the specimen 2 and 3 are sandblasted to prepare a high adherence of the surface. The arithmetic average roughness of surface after treating is 0.158 mm. The surface of the specimens before and after sandblasting is exhibited in Fig.3-4.

Next, the CFRP grid is embedded on the two sides of the specimen 2 and 3, they are set to the concrete substrate by D6 steel anchors, see Fig.3-4. And the epoxy primer is painted to the concrete surface (shown in Fig.3-5). Finally, spraying mortar to make a layer of 20 mm thickness on both sides of specimens 2 and 3 (see Fig.3-5 and Fig.3-6).

Figure 3-3: Substrate concrete specimen after casting

Figure 3-4: Concrete surface before and after sandblasting

Figure 3-5: Applying epoxy primer

Figure 3-6: Spraying mortar
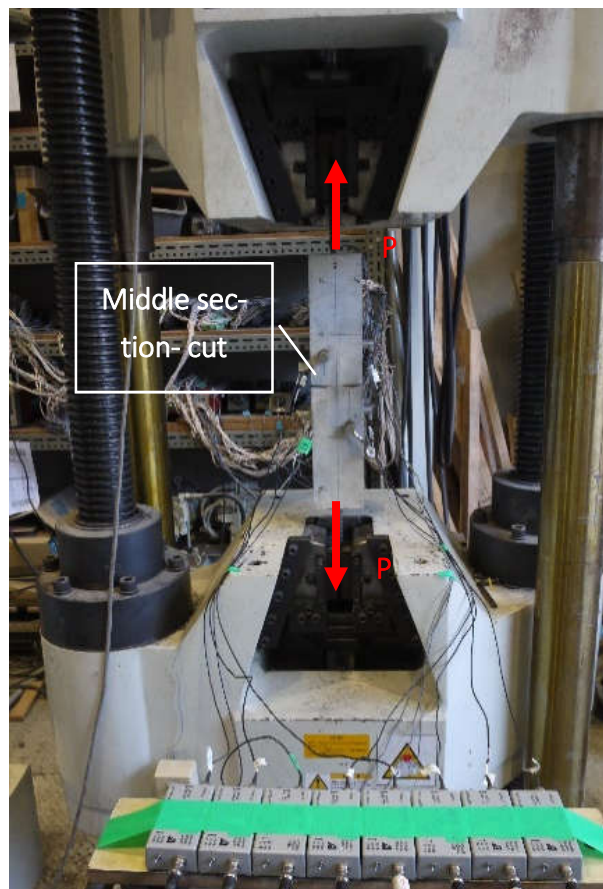
Figure 3-7: Tensile test
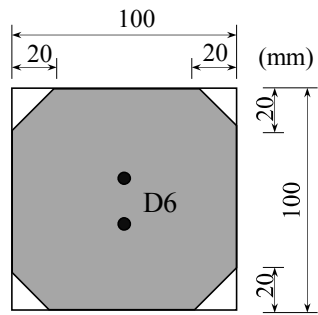
Figure 3-8: Cutting joint at the middle-section of concrete prisms
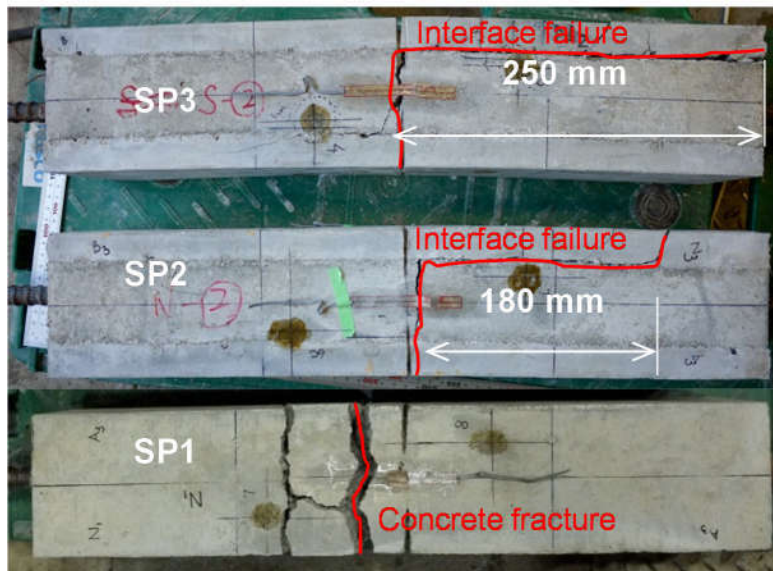
Figure 3-9: Specimens after the tensile test

Then, all the specimens are cured by wet towels until 28 days old of the mortar.

3.2.5. Tensile test

On the testing date, the age of the concrete was 90 days, while the age of the mortar was 39 days. To make sure that the ultimate crack crosses the middle cross-section of prisms the specimens are cut at four corners at the middle section by a cutting machine before testing. Cut edges are 20 mm in length, cut section is exhibited Fig.3-8.

Specimens are kept and applied load by a hydraulic tensile testing machine, and the load increased until the specimen completely failed (Fig.3-7). The incremental load on the testing machine is set to the movement of grips of 1 mm/min.

3.3. RESULTS AND DISCUSSIONS

When applying the load on all three specimens, the first cracks occur on the middle part of the concrete prisums as expected. As the load increases, the cracks progressively propagate, and more cracks appear perpendicular to the axial. The pictures about the cracks of the specimens after the tensile test are displayed in Fig.3-9.

The results obtained from the experiment were collected, processed and graphed correspondingly between load, strain, and displacement. Load-displacement curves of specimen 1, 2 and 3 are shown in the Fig.3-10, 3-12, and 3-14, respectively. Load-strain curves of specimen 1, 2 and 3 are drawn in Fig.3-11, 3-13, and 3-15, respectively.

3.3.1. Result of specimen 1

As the applying tensile force rises, the normal stress in the concrete increases. When it reaches the tensile strength of concrete, the first crack occurs at the middle section. The first crack becomes the critical crack at the ultimate stage. In this section, the crack is perpendicular to the centroid axis, as shown in Fig.3-9. The crack propagates, the bearing capacity of the cracked cross-section reduces, in order to maintain the established increasing load speed (displacement speed is 1 mm/min), the load decreases simultaneously with the increase of the tensile stress in reinforcing bars.
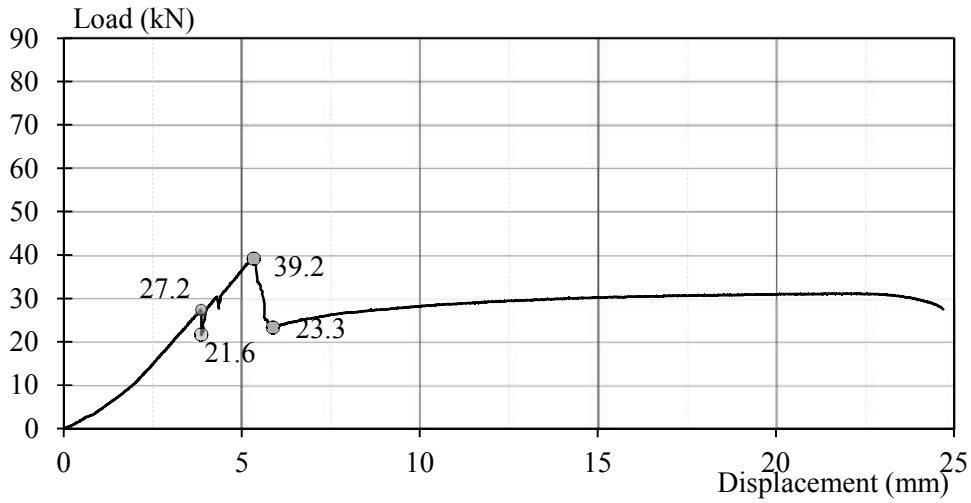
Figure 3-10: Load-displacement curve of specimen 1
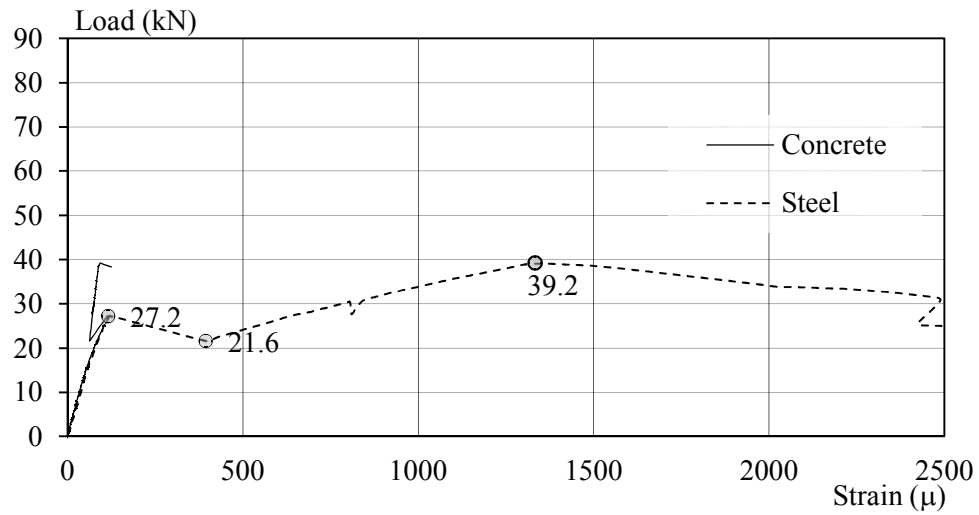
Figure 3-11: Load–strain curves of concrete and steel of specimen 1
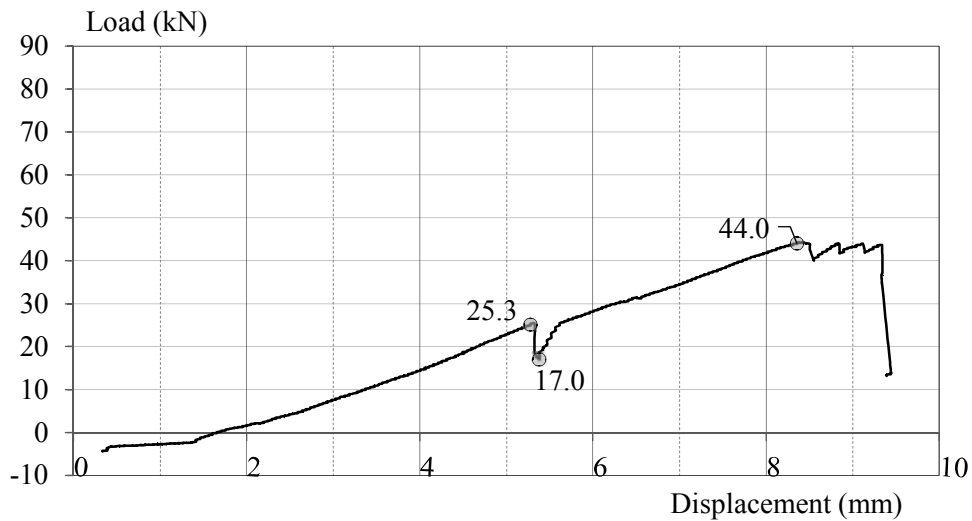
Figure 3-12: Load-Displacement curve specimen 2

42
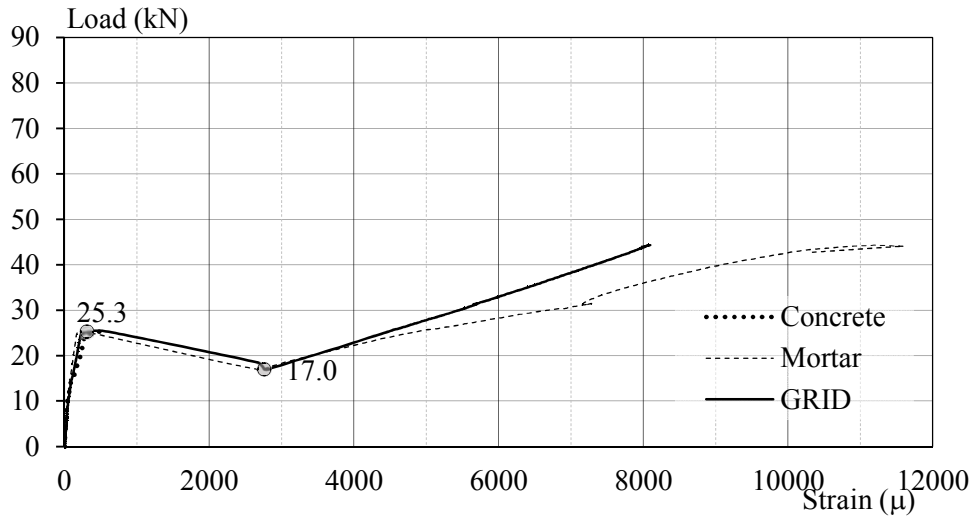
Figure 3-13: Load – strain curves of concrete, mortar and CFRP grid of specimen 2
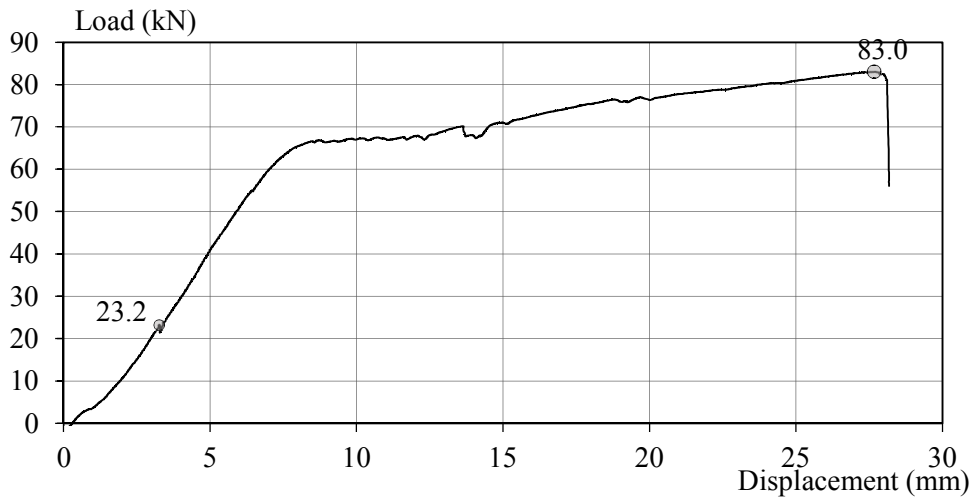
Figure 3-14: Load-Displacement curve of specimen 3
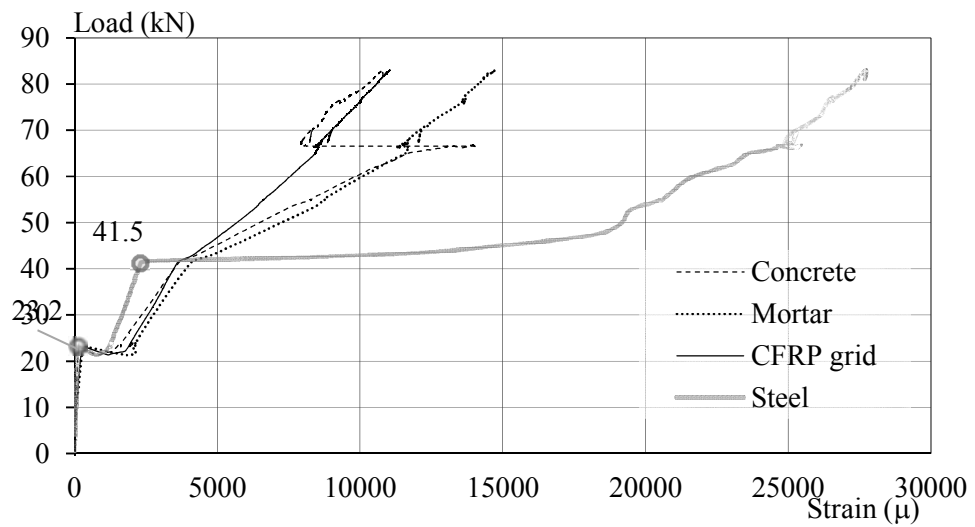
Figure 3-15: Load – strain curves of concrete, mortar, CFRP grid and steel - specimen 3

43
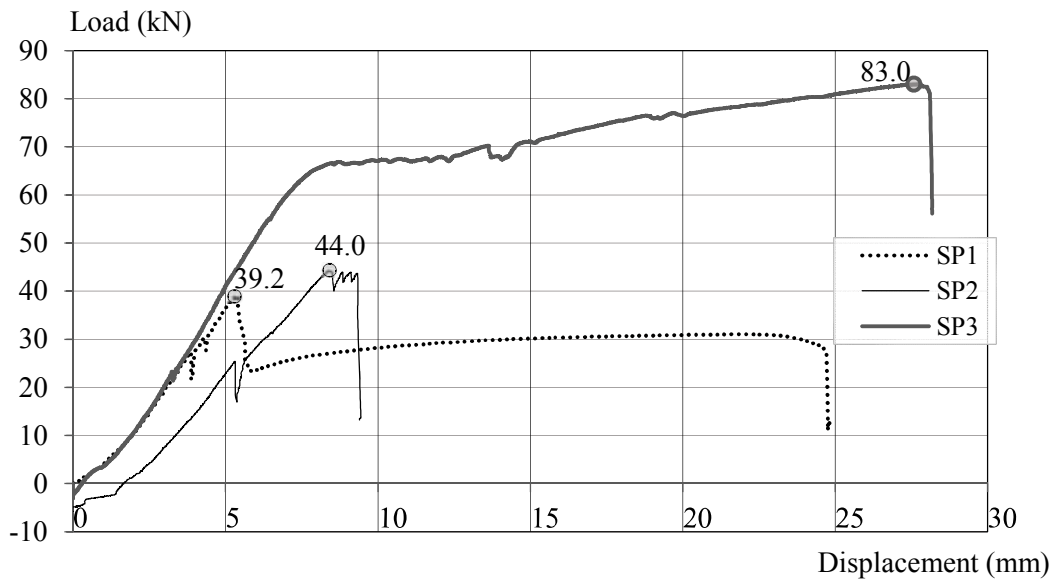
Figure 3-16: Load-displacement curves the three specimens

According to the Fig.3-10, the first crack occurred corresponding to the load level of 27.2 kN. The tensile stress of concrete is given as follow:

$$\sigma_c = \frac{P}{A} = \frac{27.2 \times 10^3}{100^2 - 20^2 \times \frac{1}{2} \times 4 + \left(\frac{2 \times 10^5}{27.7 \times 10^3} - 1\right) \times 31.67 \times 2} = 2.97 \text{ MPa}$$

where;

σ_c: stress in concrete (MPa),

P: load value (N),

A: transformed section (mm²), section area of 2 bars of D6 is transformed into concrete area. The transformed section is considered the cut edge by cutting machine; the cut corner is a triangle with two edges of 20 mm (Fig.3-8).

The stresses in the steel bars also increase rapidly to compensate for the loss of concrete strength. This tendency of the variability of the stress is exhibited in Fig.3-11.

In the process of increasing the load from 27.2 kN to 39.2 kN, the cracks continue forming and developing.

The maximum load of SP1 is 39.2 kN. At the maximum load, both concrete and steel are subjected to this maximum tensile force, based on data recorded by the strain gauges, normal stresses in concrete and reinforcing bars at this load level is given as:

$$\sigma_s = \varepsilon_s \times E_s = 1333 \times 10^{-6} \times 2 \times 10^5 = 266.6 \text{ MPa}$$

$$\sigma_c = \varepsilon_c \times E_c = 93 \times 10^{-6} \times 27700 = 2.58 \text{ MPa}$$

44

σ_c, σ_s: Stress of concrete and steel bars, respectively;

ε_c, ε_s: Strain of concrete and steel bars (99×10^{-6}, 1333×10^{-6}), respectively, taken from experiment data correspond to the load of 39.2 kN;

E_c, E_s: Elastic modulus of concrete and steel bars, respectively; taken from Table 3-3 and Table 3-5.

After reaching the peak of 39.2 kN, the load dropping rapidly by 23.3 kN, the concrete cracked and the whole tensile capacity of the section is provided by the steel bar. The strain of reinforcing bars was recorded by 2445 x 10^{-6}. The stress of steel bar is calculated as:

$$\sigma_s = \varepsilon_s \times E_s = 2445 \times 10^{-6} \times 2 \times 10^5 = 489 \text{ MPa}$$

Comparing to the mechanical properties in Table 3-5, and regarding the load value of 23.3 kN, it is supposed that the reinforcing bars yielded already and the whole concrete part of the section has been cracked. Then, the load continues increasing, the steel becomes hardening, reaches ultimate strength and fracture.

3.3.2. Result of specimen 2

As the applying load on specimen 2 increase, the crack occurs and propagates at the middle section as on specimen 1. The initial crack is perpendicular to the centroid axis of the prism. At the end of loading process, the crack propagates along bonding surface between concrete and mortar. Finally, the fracture of CFRP grid does not occur as expected. The observed damage happens at the interface between two materials: concrete and mortar. The critical crack on specimen 2 is presented in Fig.3-9.

According to the Fig.3-12, the first crack is observed at the load level of 25.3 kN. The tensile stress of the concrete is calculated as follow:

$$\sigma_c = \frac{P}{A} = \frac{25.3 \times 10^3}{100^2 - 20^2 \times \frac{1}{2} \times 4 + \left(\frac{10^5}{27.7 \times 10^3} - 1\right) \times 13.2 \times 4} = 2.71 \text{ MPa}$$

where;

σ_c: stress in concrete (MPa),

P: load value (N);

A: transformed section (like specimen 1).

The stresses in the CFRP grid also increases to balance for cracks of concrete and mortar. The increase of the stress is exhibited in Fig.3-13. The maximum tensile load acting on specimen 2 is 44 kN. Corresponding strain recorded by strain gauge on CFRP grid is 8040×10^{-6}. The stress in CFRP grid is given as follow:

$$\sigma_G = \varepsilon_G \times E_G = 8040 \times 10^{-6} \times 10^5 = 804 \text{ } MPa$$

The maximum stress of CFRP grid (804 MPa) in specimen 2 equals to 57.4% of the nominal tensile strength (1400 MPa, shown Table 3-6).

3.3.3. Result of specimen 3

When the load increases, the normal stress in concrete prism hit the tensile strength, cracks initially occur at the middle cross-section of the prism and are perpendicular to the longitudinal axis of the specimen. Then the crack propagates on the bonding surface between concrete and mortar till the tip of the prism. At the ultimate stage, similar to the specimen 2, the failure occurs at the interface between concrete and mortar. The ultimate cracks are illustrated in Fig.3-9.

Based on Fig.3-14, it is supposed that the load-displacement is more smoothly, with no sudden change of phase. Comparing to SP1, there is no phase where the load significantly drops and as suddenly as in SP1. The first major cracks were recorded when the load was 23.2 kN. The tensile stress of concrete is calculated as follow:

$$\sigma_c = \frac{P}{A}$$

$$= \frac{23.2 \times 10^3}{100^2 - 20^2 \times \frac{1}{2} \times 4 + \left(\frac{2 \times 10^5}{27.7 \times 10^3} - 1\right) \times 31.67 \times 2 + \left(\frac{10^5}{27.7 \times 10^3} - 1\right) \times 13.2 \times 4}$$

$$= 2.38 \text{ MPa}$$

where;

σ_c: stress in concrete (MPa),

P: load value (N);

A: transformed section (mm^2), similar to SP1.

According to Fig.3-14, as the load increase from 0 to 65 kN the load-displacement curve is nearly a straight line. The stiffness of the general structure has almost no change. But, from the Fig.3-15, it is found that at the values of the load 23.2 kN and 41.5 kN, deformations of the materials: concrete, mortar, steel, and CFRP grid have a significant jump.

At a load of 41.5 kN, the steel bars yield, shown in Fig.3-14. Stress in rebars and CFRP grid is given by following:

$$\sigma_s = \varepsilon_s \times E_s = 2407 \times 10^{-6} \times 2 \times 10^5 = 481.4 \text{ MPa}$$

$$\sigma_G = \varepsilon_G \times E_G = 3623 \times 10^{-6} \times 10^5 = 362.3 \text{ MPa}$$

σ_s, σ_G: Stress of steel bars and CFRP, respectively;

ε_s, ε_G: Strain of steel bars and CFRP, respectively; taken from experiment data at the load of 41.5 kN;

E_s, E_G: Elastic modulus of steel bars and CFRP grid, respectively; taken from Table 3-3 and Table 3-6.

After rebars yielded at the loading stage of 41.5 kN (concrete and mortar cracked), CFRP grid carries all the later incremental load. When load hits the value of 83 kN, SP3 completely

fails. The maximum stress in the CFRP grid is determined as:

$$\sigma_G^{max} = \varepsilon_G \times E_G = 12008 \times 10^{-6} \times 10^5 = 1200.8 \, MPa$$

12008×10^{-6} is strain value recorded by gauges attached to CFRP grid at the load level of 83 kN.

The maximum stress of CFRP grid (1200.8 MPa) in specimen 3 equals to 85.8% of the nominal tensile strength (1400 MPa, shown Table 3-6).

3.3.4. Comparison and discussion

Fig.3-16 shows the comparative chart of the load - displacement of all three specimens. Table 3-8 presents the compared results between three specimens.

Table 3-8: Compare results with SP1

	Reinforcement area		Designed load (kN)	Maximum load (kN)			Failure mode
	Rebar and CFRP (mm^2)	%		P$_{max}$	Compare to SP1 %	Compare to design %	
SP1	63.34	100	36.1	39.2	100	108.6	Concrete fracture
SP2	52.8	83	73.9	44	112	59.5	Interface failure
SP3	116.14	184	110.0	83	212	75.5	Interface failure

According to Table 3-8, by comparing the maximum load of the three specimens, among themselves, the SP3 shows the highest (83 kN), followed by the SP 2 (44 kN) then SP1 (39.2 kN). The maximum load of SP3 is 212% higher than that of SP1 when the cross-sectional area of reinforcement is only 184% higher.

At the ultimate stage, the failure mode of specimen 2 and 3 is interface-failure, fracture does not occur in CFRP grid as expected. In this experimental program, through the concrete surface have been treated quite well, the failure still occurred at the interface between two materials; concrete and mortar.

The maximum stress recorded in SP2 and SP3 reaches a high level when compared with a designed value (59.5% in SP2 and 75.5% in SP3). The maximum stress in the CFRP grid in SP3 is (1200.8MPa) is lower than the nominal tensile strength of CFRP (see Table 3-6). The failure of specimen 2 happens at a low stress of CFRP due to reasons; first, the concrete surface even is well-prepared but not enough for a high shear stress at interface, second, when the critical crack propagates along the bonding surface, the cross-section is no longer symmetry and the axial tensile force causes a bending moment on the specimen 2. This phenomenon is restrained in specimen 3 due to a more stability by the appearance of two bars of D6.

In SP3, despite significant changes in the deformation of reinforcing bars, the overall stiffness of the entire specimen does not change abruptly. Thanks to the support and good combination of materials with each other, SP3 shows a valuable effect of reinforcement by using CFRP grid and sprayed mortar.

3.3.5. Shear stress in the bonding interface

In two cases of strengthening, the failure occurs at the interface between two materials: concrete and morta, see Fig. 3.9.

To investigate the cause of the failure, internal forces applying on half parts of SP2 and SP3 are depicted on Fig.3-17. In SP2, after the middle cross section was totally cracked, there are four bars of CFRP grid carry the axial force. While, in SP3, there are four bars of CFRP grid and two yielded rebars. The anchor bars, shown in Fig. 3-4, is just for setting the CFRP grid. Without concerning the effect of these anchor bars, the shear stress at the interface between concrete and mortar at the ultimate stage can be determined as follow:

$$\tau = \frac{P_i}{A_i}$$

where:

τ: shear stress on the bonding interface

P_i: shear force applies to the interface

A_i: failed bonding area by the shear force

In specimen 2, the shear stress on bonding interface τ_2 is calculated as below:

$$\tau_2 = \frac{2 \times P_2}{A_i} = \frac{11 \times 10^3}{180 \times 100} = 1.22 \, MPa$$

Specimen 2
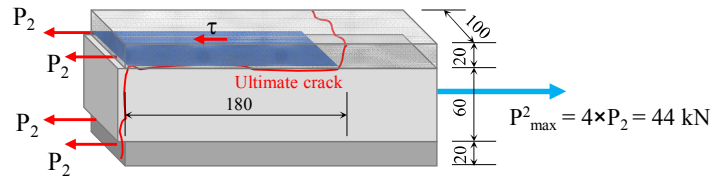
Specimen 3
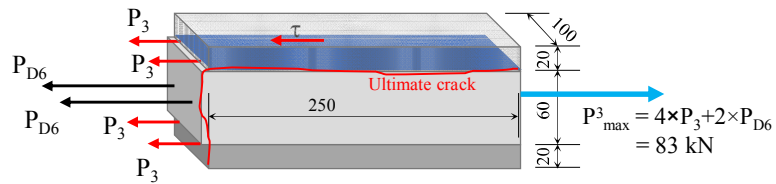
P_2 , P_3 : maximum force applying on CFRP bar in SP2 and SP3

P^2_{max} , P^3_{max}: maximum load of specimen 2, specimen 3

Figure 3-17: Shear force applied to the interface of specimens

where;

P_2: tensile force in a CFRP bar in specimen 2

$P_2 = P_{max}/4 = 44 \times 10^3/4 = 11 \times 10^3$ N (Fig.3-17)

In specimen 3, the shear stress on bonding interface τ_3 is calculated as below:

$$\tau_3 = \frac{2 \times P_3}{A_i} = \frac{2 \times 14146}{250 \times 100} = 1.13 \, MPa$$

Where:

$P_{D6} = A_{D6} \times \sigma_{yield} = 31.67 \times 417 = 13206$ N

$P_3 = (P^3_{max} - 2 \times P_{D6})/4 = 14146$ N (Fig.3-17)

The fracture area at the ultimate stage in bongding surface of specimen 3 is larger than it of specimen 2. Specimen 3 is more stable under the tensile force comparing to specimen 2 due to the apperance of two steel bars. In this experimental program, both specimens 2 and 3 are well-surfaced treated to obtain good adhesion. The concrete surface is sandblasted to get the roughness of 0.158 mm. Authors expected that the failure at the ultimate stage of specimen 2 and specimen 3 is the fracture of the CFRP grid. Actually, the fracture occurs on the interface between two materials. The average shear stress on the surface of the contact between the two layers of concrete and mortar is about 1.18 MPa (average of 1.13 MPa and 1.22 MPa). Regarding the previous studies, about shear strength, V.D Tran reported in (TRAN Vu Dung 2016) that, in the direct shear test, with the average roughness from 0.05 to 0.85 mm, the shear strength is from 0.51 – 2.77 MPa, and the result is significantly changed depending on the type of the test method. Austin S stated that, in the twist-off shear

test, shear strength ranges from 1.9 – 4.2 MPa, depends on surface condition and repair material (Austin et al. 1999). If the concrete surface is better prepared, the maximum tensile stress in the CFRP grid is even higher than the present result. It would make use the capacity of the CFRP grid. This research, calculated shear stress is in the real composite structure. The average shear stress of 1.18 Mpa, this result is consistent with it's of the earlier investigates (TRAN Vu Dung 2016),(Austin et al. 1999). The above assumes that the shear stress is uniformly distributed on the interface. In fact, the shear stress at the location near the cracks is much higher and mainly causes the failure.

3.4.   CONCLUSIONS

From these above comments about the behavior of materials in the composite specimens, following conclusions are drawn;

-   The reinforcing effect of CFRP grid material is demonstrated in a simple experiment. Specimen 2 and specimen 3 strengthened by CFRP grid exhibited a effective combination of 4 materials: concrete, steel, mortar and CFRP grid. Both strengthened specimens perform the very high bearing capacity comparing to the control one – specimen 1. Comparing between specimen 3 and specimen 1, the maximum load of SP3 is 212% higher than that of SP1 when the cross-sectional area of reinforcement is only 184% higher.

-   As reinforced with CFRP grid material, the strengthened specimens perform the high stiffness and less brittle. The deformation occurs smoothly due to the high adhesion between materials; concrete and mortar.

-   The interface bonding plays an important role in the reinforcing effect. In this study, although the bonding surfaces are repaired by an appropriate method such as sandblasting, epoxy primer applying, both specimens the fracture still occurs at the bonding surface, CFRP –CR5 did not show the full capacity. To take advantage of CFRP grid and to enhance the effect of strengthening work, a better condition of surface roughness and an adequate length of bonding interface is necessary.

Chapter 4:

EXPERIMENTAL INVESTIGATION OF THE USE OF CFRP GRID FOR SHEAR STRENGTHENING OF RC BEAMS

This section examined the effectiveness of CFRP grid and sprayed mortar in enhancing the shear capacity of RC beams. Three RC beams were fabricated and two of them were strengthened by CFRP grid and sprayed mortar. Then the four-points bending test was carried out to collect the data on the behavior of CFRP grid and stirrups. The results are presented and discussed in this paper. This chapter evaluated the strengthening effectiveness of CFRP grid and sprayed mortar and the behavior of stirrups and CFRP grid. The difference in behaviors between stirrups and CFRP grid was analyzed.

4.1.   INTRODUCTION

CFRP currently plays a key role in strengthening and retrofitting concrete structures in Japan. The area of CFRP sheet used was 980,000 m^2 in 2006 and 1,310,000 m^2 in 2013 (Anon n.d.). CFRP is usually used in the form of a sheet. The consumption of CFRP in the form of a grid was only about 5% of that of CFRP sheets in 2006. CFRP grid and sprayed mortar have advantages in dealing with the damaged concrete surface. Scheme of CFRP grid application is shown in Figure 4-1:
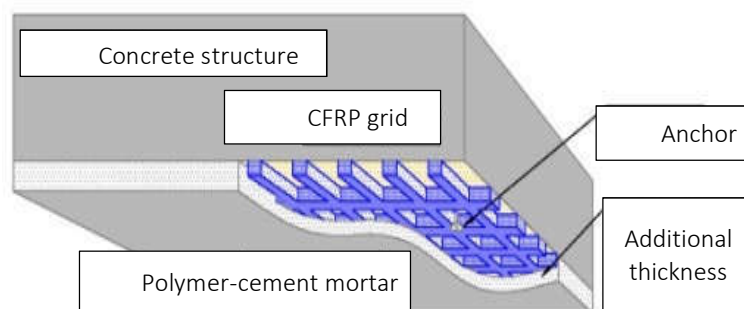
Figure 4-1: Schematics of CFRP grid reinforcement application

Many experimental studies have been conducted over the past decade to study the performance of concrete beams strengthened in shear with externally bonded FRP composites. Bukhari (Bukhari et al. 2010) reviewed the existing design guidelines for strengthening continuous beams in shear with CFRP sheets and proposed modification to Concrete Society Technical Report. Chen (Yi, Xiaobing, and Wenyong 2011) studied the shear behaviour of RC beams with FRP grid and concluded that RC beams strengthened with CFRP grid perform the effect in terms of both increasing the shear capacity and controlling of the crack width. (Guo et al. 2014) examined the effect of shear capacity of RC beams reinforced with a haunch using the PCM shotcrete method with CFRP grid and investigated the adhesive properties of the reinforced interface between PCM and the existing concrete. CFRP grid reinforcement represents a suitable replacement for steel rebars in some concrete structural members subjected to aggressive environmental conditions that accelerate corrosion of the steel reinforcement and cause deterioration of the structures (Zhang, Masmoudi, and Benmokrane 2004). These studies have not focused on the difference in behaviours between stirrups and CFRP grid. Besides, the result from chapter 3 shows the effect of CFRP grid when applied for the composite specimens. The further experiment need to be implemented to access the capability of CFRP grid when applying for large beams. The main purpose of this chapter is to study the capacity of CFRP grid and the behavior of stirrups and CFRP grid in shear strengthening. This session illustrates the use of CFRP grid combined with sprayed mortar to improve the shear strength of RC beams. The existing guidelines are related to the application of CFRP sheet, and there are no specific

guidelines for the application of CFRP grid. The material factor in calculating the effectiveness of CFRP grid in providing shear resistance capacity was evaluated. Based on the experimental result, the effectiveness of CFRP grid and sprayed mortar in enhancing the shear strength of RC beams were also evaluated. The difference in behavior between stirrups and CFRP grid was analyzed in detail. CFRP grid consists of vertical and horizontal components but this study only focused on researching the vertical component of the CFRP grid, the effect of horizontal part will be ignored.

4.2. EXPERIMENTAL PROGRAM

Three RC beams were fabricated and tested. The control RC beam was not strengthened while the two other beams were shear strengthened by CFRP grid and sprayed mortar. The three RC beams were designed such that their flexural strength was much higher than their shear strength to ensure that failure was controlled by the shear force.

4.2.1. Materials

The three RC beams were fabricated using ready-mixed concrete with a compressive strength of 34.1 N/mm^2 and maximum aggregate size of 20 mm. In the concrete mix, high-early-strength Portland cement was used and the water-cement ratio was 0.556 with the addition of water-reducing and air-entraining agents. The other parameters of the concrete mix are shown in Table 4-1. The mortar to be sprayed was made by mixing 25 kg of premixed mortar, 1.21 kg polymer, and 4.1 kg water. In order to increase interface adhesion, the epoxy primer was applied to the surface of concrete before spraying mortar. The properties of the polymer and epoxy primer are shown in Tabel 4-2: D32 was used as the main reinforcing bar in the tension zone. D6 and D10 were used as the stirrup and reinforcing bar, respectively. The CFRP grid used in this test was CFRP-CR8 (The CR8 label is given by the manufacturer) with a grid spacing of 100 mm × 100 mm. Fig. 4-2 shows the strain gauges are attached on the bars of CFRP grid. The mechanical properties of concrete and mortar are given in Table 4-3. Mechanical properties of the reinforcing bars and the CFRP grid are listed in Table 4-4.

Table 4-1: Mix proportion of concrete

Gravel (mm)	Slump (mm)	W/C (%)	Air (%)	Unit content (kg/m^3)				
				Water	Cement	Fine Aggregate	Coarse Aggregate	Admixture
20	120	55.6	4.5	158	284	792	1126	1.3

Table 4-2: Properties of polymer and epoxy primer

Properties	Polymer	Epoxy primer
Main component	SBR synthetic rubber	vinyl acetate-ethylene copolymer
Solid content	45-46 (% by weight)	45-48 (% by weight)
Appearance	white milky liquid	white milky liquid
Viscosity	below 50 (mPa.s)	500-2000 (mPa.s)
pH	8.0-9.0	4.5-6.5
Density	1.0 (g/cm^3)	1.06 (g/cm^3)

Table 4-3: Mechanical properties of concrete and mortar

Type	Compressive strength (N/mm^2)	Elastic modulus (kN/mm^2)	Tensile strength (N/mm^2)
Concrete	34.1	31.9	2.92
Mortar	36.7	31.0	2.87

Table 4-4: Mechanical properties of reinforcing bars and CFRP

Type	Type	Cross sectional Area (mm^2)	Yield strength (N/mm^2)	Tensile strength (N/mm^2)	Elastic modulus (N/mm^2)
Rebar	D32	794.2	389	587	2×10^5
	D10	71.33	413	561	2×10^5
	D6	31.67	417	570	2×10^5
CFRP grid	CR8	26.5	*	1400**	1×10^5*

Note:

* CFRP grid has no yield strength;

** manufacturer's data.
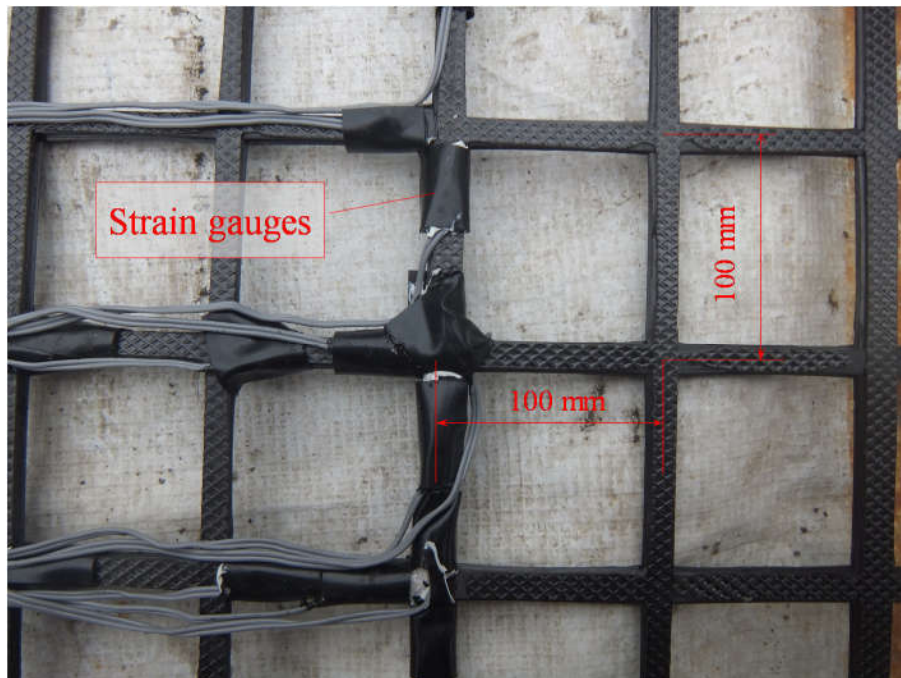
Figure 4-2: CFRP CR8 100 x 100 mm

4.2.2.   Reinforcement scheme

The RC beams had the dimensions 200 mm × 500 mm × 2,750 mm. They were labelled RC beam 1 (control beam), RC beam 2, and RC beam 3. RC beam 1 and RC beam 2 were reinforced with 6D32 longitudinal rebars at the bottom and 2D10 longitudinal rebars on the top. The stirrup spacing was 200 mm (see Fig. 4-4). In RC beam 1, D10 bar was used for stirrups while, in RC beam 2, D6 bar was used as stirrups, which is smaller than the type used in the RC beam 1. With the assumption that the shear strength in this beam was lost due to corrosion, the cross-sectional area of the stirrups was reduced. RC beam 3 was reinforced with 6D32 longitudinal rebars at the bottom. RC beam 3 had no stirrups in order to evaluate the capacity of CFRP grid for enhancing shear resistance without stirrups. RC beam 2 and RC beam 3 were strengthened by CFRP grid and sprayed mortar. The CFRP grid was placed along the beam web and mortar was sprayed to create an additional 20 mm layer on both sides of the two beams.

Table 4-5 shows the total shear reinforcement area of each beam. Reinforcement area in RC beam 1 is the total of cross sections of D10, while, in RC beam 3, it is the total cross sections of CFRP grid (vertical grid only) and, in RC beam 2, it is the total of cross sections of D6 and CFRP grid in 200 mm beam length of each beam. Fig. 4-3 presents the reinforcing bars before being put in the formwork. Fig 4-4 shows the longitudinal and transverse cross-sections of three RC beams and strengthening scheme using CFRP grid and sprayed mortar.

Figure 4-3: Reinforcing bars and stirrups

Table 4-5: Total cross-sectional area of shear reinforcement: CFRP grid and stirrups

No.	Shear reinforcement	Total reinforcement area $(mm^2/200\ mm$ length)	Total reinforcement area $(mm^2/mm$ length)	Ratio of shear reinforcement $p = \frac{A_s}{b \times s}$ (%)
RC beam 1	D10 @200 mm	142.66	0.7133	0.37%
RC beam 2	D6 @200 mm and CFRP grid CR8 @100 mm	169.34	0.8467	0.35%
RC beam 3	CFRP grid CR8 @100 mm	105.60	0.528	0.22%

NOTE:

A_s - area of shear reinforcement (mm^2);

b - beam width (b_{RC1} = 200 mm; b_{RC2} = b_{RC3} = 240 mm);

s - shear reinforcement spacing (mm).
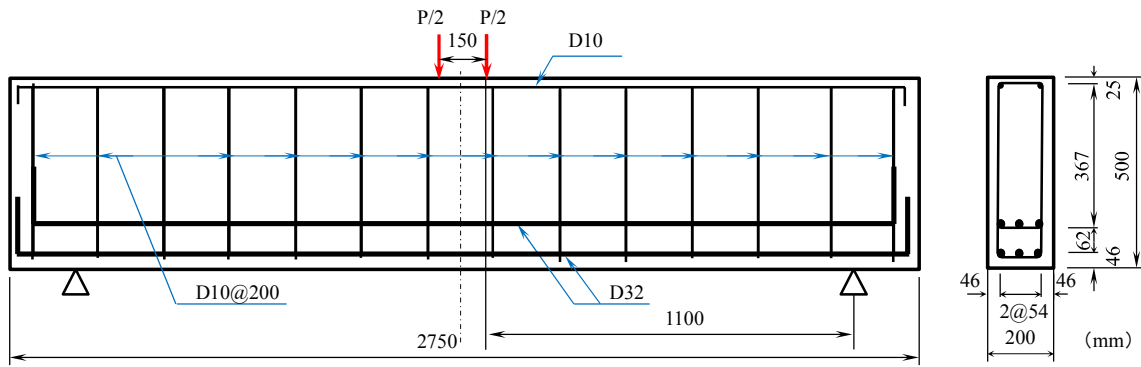
a) RC beam 1
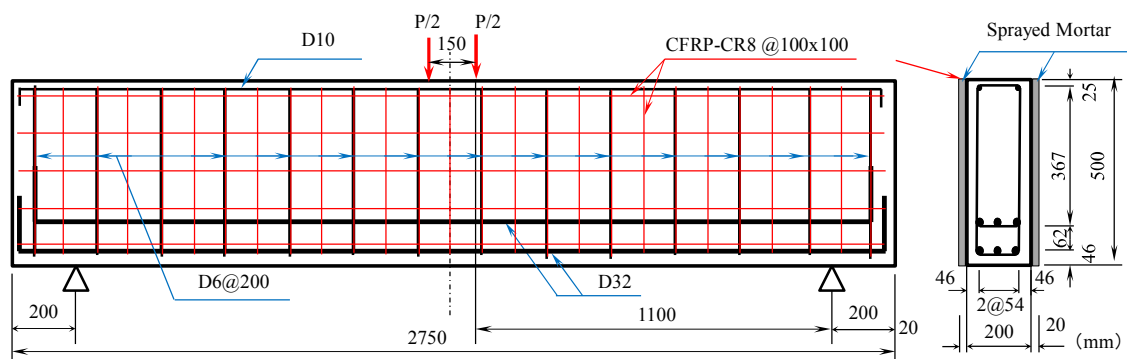
b) RC beam 2
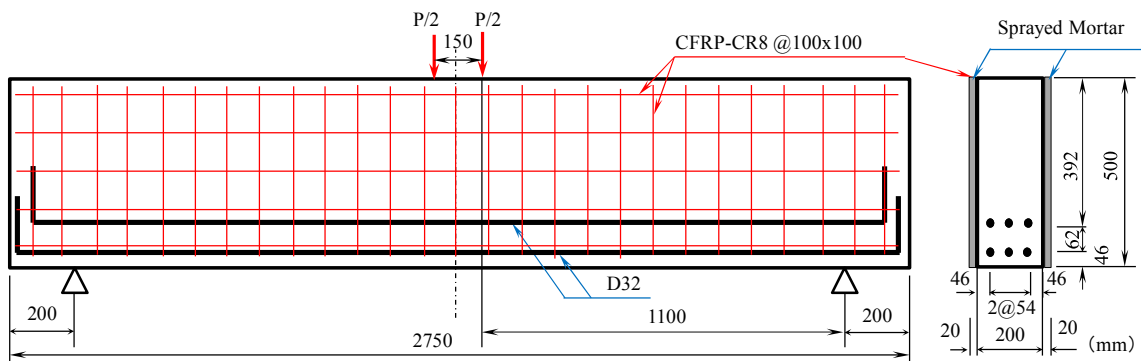
c) RC beam 3

Figure 4-4: Longitudinal and transverse cross-sections of three RC beams and strengthening scheme using CFRP grid and sprayed mortar

4.2.3. Casting RC Beams

First, concrete for the RC beams was cast in wooden formwork and cured by the moisture-retaining cover (see Fig. 4-5 and 4-6). Eight days after casting the web's surfaces of RC beam 2 and RC beam 3 were sandblasted. The average roughness of the beam surface after sand blasting was 0.15 mm. Four days later, CFRP grid was fixed on both sides of the beam by steel bolt anchors (Fig. 4-7). On the next day, the epoxy primer was applied. The roughness of the beam surface after applying epoxy was 0.13 mm. After the epoxy layer had hardened, the repair mortar was sprayed (see Fig. 4-8). Finally, a curing compound was sprayed on the mortar surface. Tests of the RC beams were carried out at the age of 27th, 28th, and 29th day.

4.2.4. Instrumentation and Test method

Four-point-bending test was performed (see Fig. 4-9) on the three beams, with a span length (L) of 2,350 mm and a shear span (a) of 1,100 mm. The effective depth (d) was 423 mm. The shear span to effective depth (a/d) ratio was 2.6. During the test, when the first flexural crack and the first diagonal crack appeared, the specimens were unloaded to trase the cracks and take photographs. After that the load was continually increased until the beams failed. The failure processes were monitored by strain gauges installed on concrete, reinforcing bars and the CFRP grid, and by displacement transducers placed at mid-span and two end supports of each beam.

Figure 4-5: Reinforcing bars placed in wooden formwork before casting concrete

Figure 4-6: Concrete beam after demolding

Figure 4-7: CFRP Grid is fixed to two sides of RC beam 2 and 3

Figure 4-8: Spraying the mortar to RC beam 2 and 3
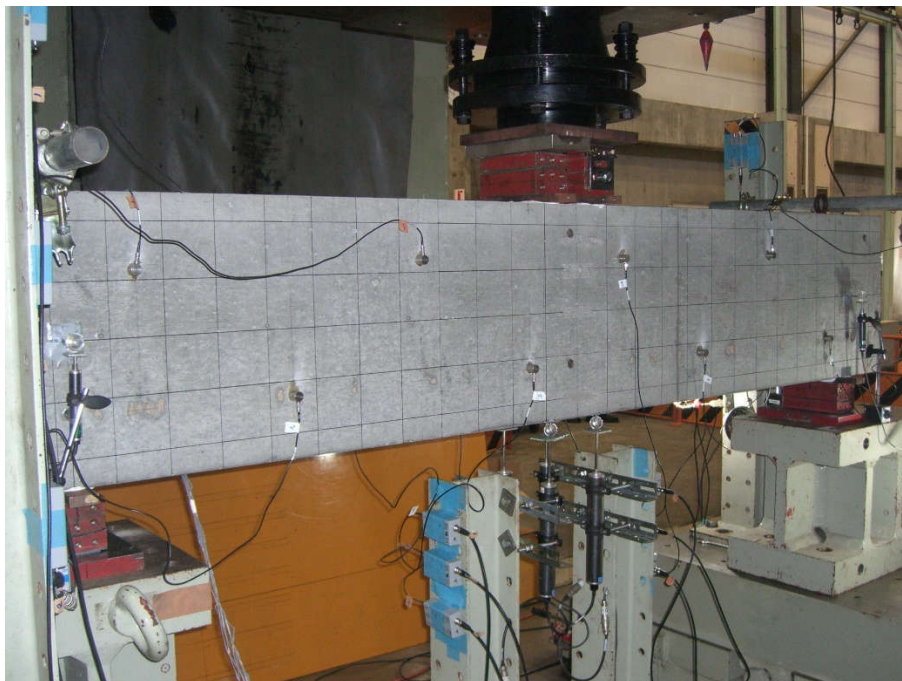
Figure 4-9. Apply four-point bending test on beams

4.3. RESULTS AND DISCUSSIONS

4.3.1. Load – displacement behavior, crack development and failure mode

Based on the observation of cracks for the three beams, it is supposed that all beam failures were due to diagonal tension. The test results of all beams are summarized in Table 4-6. RC beam 2 exhibited the highest maximum load (757 kN) while RC beam 3 exhibited the lowest (617 kN) and RC beam 1 showed a value between the two extremes (690 kN). Compared to the control beam (RC beam 1), the maximum test load of RC beam 2 was higher by 10% while that of RC beam 3 was lower by 10%.

Table 4-6: Summary of test results

Beam index	Cracking load (kN)	Maximum load (kN)		Max. mid-span displacement. (mm)
		Design	Test	
RC beam 1	225	354	690	8.4
RC beam 2	300	697	757	7.4
RC beam 3	300	656	617	7.1

The total cross-sectional area of shear reinforcement placed in 200 mm beam length was 142.6 mm^2 (two bars of D10) in RC beam 1, while, in RC beam 2 and RC beam 3, it was 169.3 mm^2 (two rebars of D6 and four bars of CFRP CR8) and 105.6 mm^2 (four bars of CFRP CR8), equivalent to 118.7% and 74.3% of that of RC beam 1, respectively. The ratio of shear reinforcement of RC beam 1 was 0.37%, while, in RC beam 2 and RC beam 3, it was 0.35% and 0.22%, comparing to RC beam 1, they are equivalent to 94.6% and 59.5%, respectively. The total cross-sectional areas of reinforcing bars and CFRP grid and the ratios of shear reinforcement are shown in Table 4-5. From test results, in two cases of strengthening, CFRP grid and sprayed mortar perform the high effect for enhancing the shear capacity of RC beams

Fig. 4-10 through Fig. 4-12 describe cracks generated during the test. The cracks shown in bold lines were the largest cracks at the ultimate state of each beam. Fig. 4-10 through Fig. 4-12 also show locations of the displacement transducers and strain gauges installed on rebar, concrete, and CFRP grid in the three RC beams.

RC BEAM 1
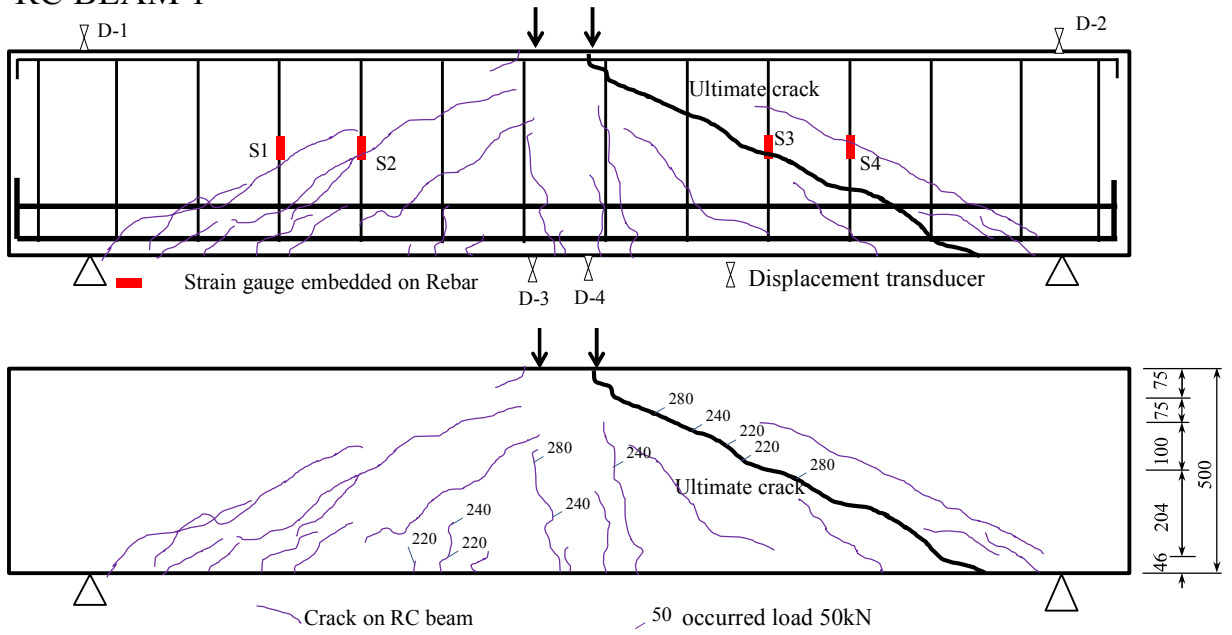
Figure 4-10: Locations of strain gauges on stirrups and experimental cracks in RC beam 1

RC BEAM 2
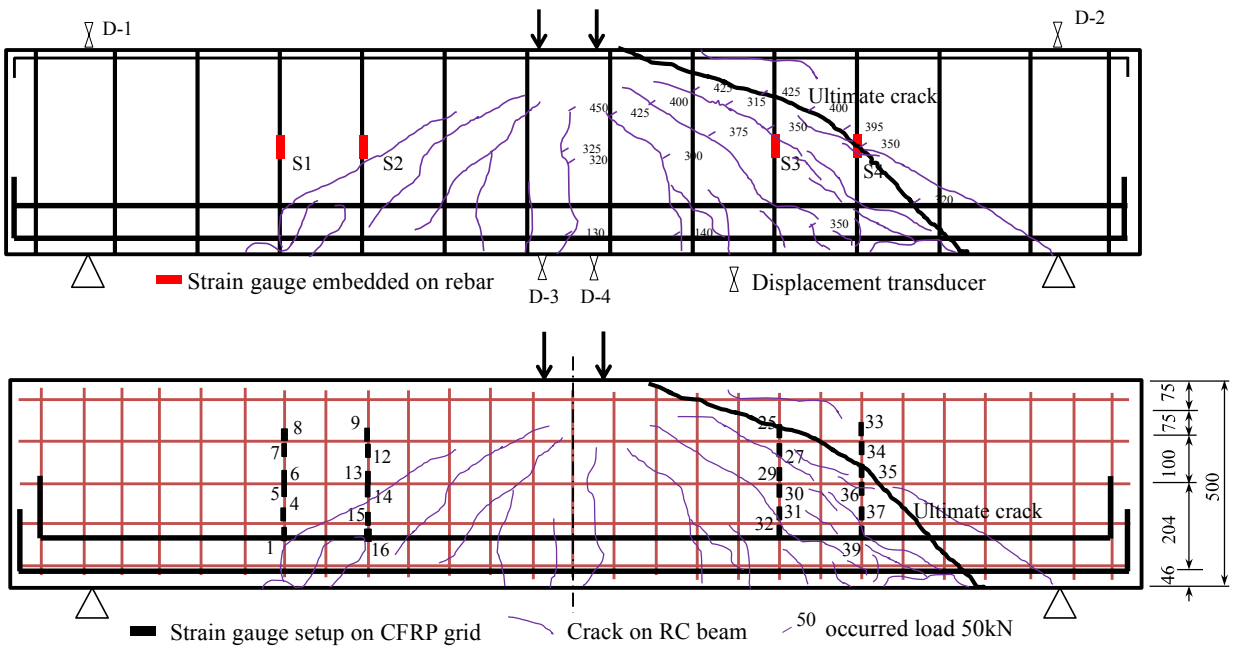
Figure 4-11: Locations of strain gauges on stirrups and experimental cracks in RC beam 2
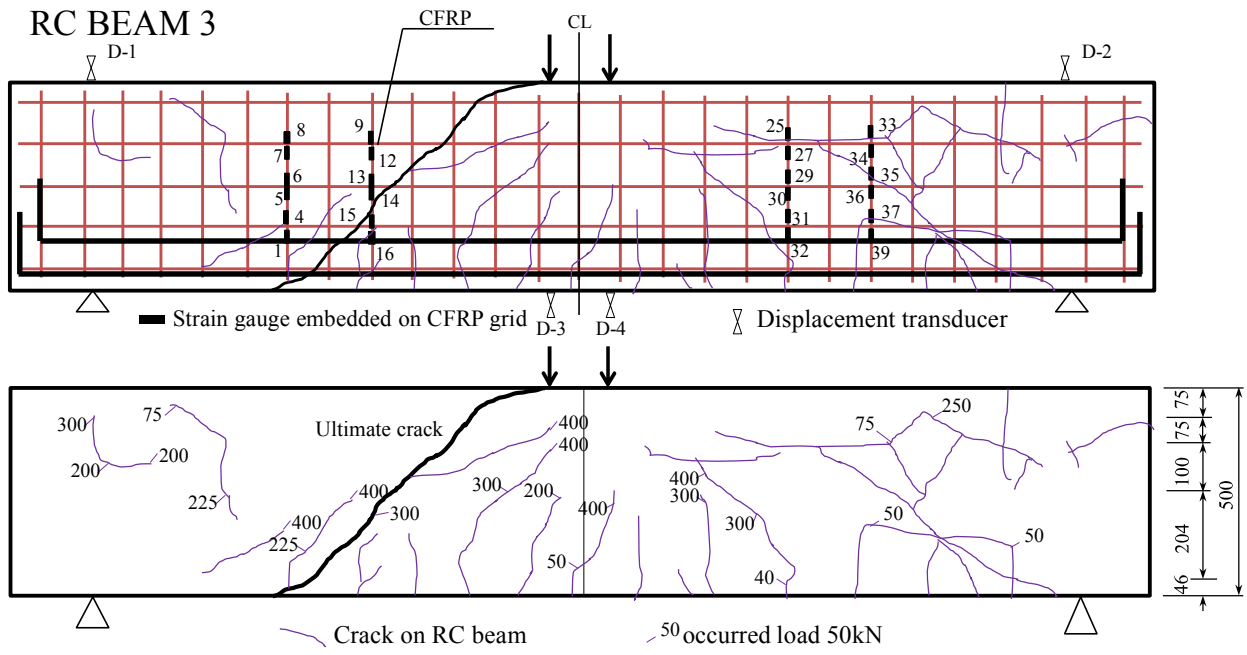
Figure 4-12: Locations of strain gauges on CFRP grid and experimental cracks in RC beam 3
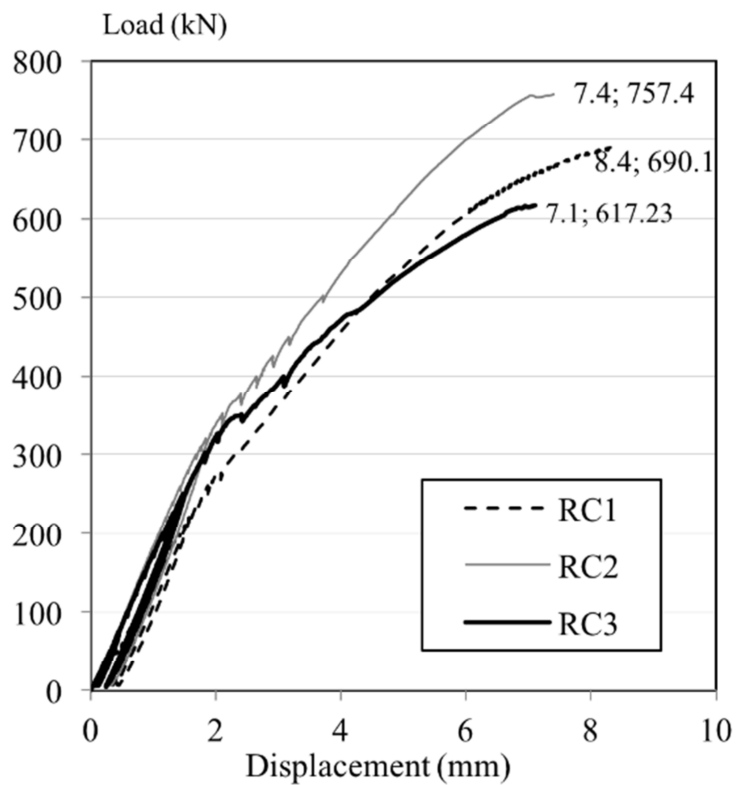
Figure 4-13: Load vs. mid-span displacement curves

Fig. 4-13 shows the load versus mid-span displacement curves for the three beams. The maximum mid-span displacements of the three beams are listed in Table 4-6. RC beam 1 had the highest mid-span displacement of 8.4 mm while RC beam 2 and RC beam 3 had lower values of 7.4 mm and 7.1 mm (lower than 11.9% and 15.5% compared to RC beam 1), respectively. Each load versus mid-span displacement curve (see Fig. 4-13) could be divided into two stages. The first stage is before the cracking (225 kN for RC beam 1, 300 kN for RC beam 2 and RC beam 3). In this stage, RC beam 2 and RC beam 3 showed higher stiffness than RC beam 1 because their width was larger (240 mm) compared to that of RC beam 1 (200 mm). In the second stage after the cracking, there is a distinct difference between RC beam 1 and RC beam 3. The stiffness of RC beam 3 became lower than that of RC beam 1 due to cracks developed and the cross-section reduced. The Young's modulus of the stirrups is higher than that of CFRP grid (200,000 N/mm^2 versus 100,000 N/mm^2, respectively, in Table 4-4. RC beam 3 had CFRP grid but no stirrups. Therefore, stirrups provide higher stiffness to the beam and result in smaller displacement value compared with the CFRP grid. In general, after strengthened by CFRP grid and sprayed mortar, both RC beam 2 and RC beam 3 had higher stiffness, ductility characteristic, and the cracking loads were also improved (except in the final period for RC beam 3, when the load was over 500 kN).

4.3.2. Behavior of stirrups in RC beam 1 and CFRP grid in RC beam 3

As the load increased, the RC beams deformed, cracks appeared and developed, and the beams failed. The behavior of the stirrups in RC beam 1 and that of the CFRP grid in RC beam 3 were different. Figure 4-14 illustrates the load versus strain curves of stirrups in RC beam 1 and CFRP grid in RC beam 3. Strain gauges S3 and S4 with locations shown in Fig. 4-10 were installed on the stirrups in RC beam 1. Strain gauges G13 and G35 with locations shown in Fig. 4-12 were installed on the CFRP grid in RC beam 3. These strain gauges were near the cracks in each beam.

From Figure 4-14, in general, strain values on CFRP grid in RC beam 3 are lower than those on stirrups in RC beam 1. The strain recorded by G13 was the highest in RC beam 3 and the strain recorded by S3 was the highest in RC beam 1. These gauges were close to the ultimate cracks in each beam (see Fig. 4-10 and Fig. 4-12). The load versus strain curves consist of 3 stages: In the first stage, there are no cracks in each beam. Cracking load of RC beam 3 was around 300 kN while, for RC beam 1, it was around 225 kN (see Fig. 4-15). In this stage, at the same load levels, the strain of G35 was lower than that of S4 and the slope of the experimental load-strain curves of RC beam 3 was higher than that of RC beam 1. The reason was the beam width of RC beam 3 was 240 mm (two layers of 20 mm including CFRP grid and sprayed mortar were applied on two sides of the RC beam) compared to the

200 mm width of RC beam 1. Thus, the bending stiffness of RC beam 3 increased by about 10%.

In the second stage, when the diagonal cracks appeared and developed, the length and the width of the cracks increased, the cross-sectional area reduced gradually, and the shear capacity of both beams provided by concrete and mortar reduced.

The shear strength of RC beam 1 was mainly provided by stirrups whereas that of RC beam 3 was mainly provided by CFRP grid. Moreover, the Young's modulus of CFRP grid (1×10^5 N/mm^2) is a half of that of the stirrup (2×10^5 N/mm^2) as shown in Table 4-4. Therefore, strains in RC beam 3 are higher than those in RC beam 1 as shown in Fig. 4-15 and Fig 4-16.
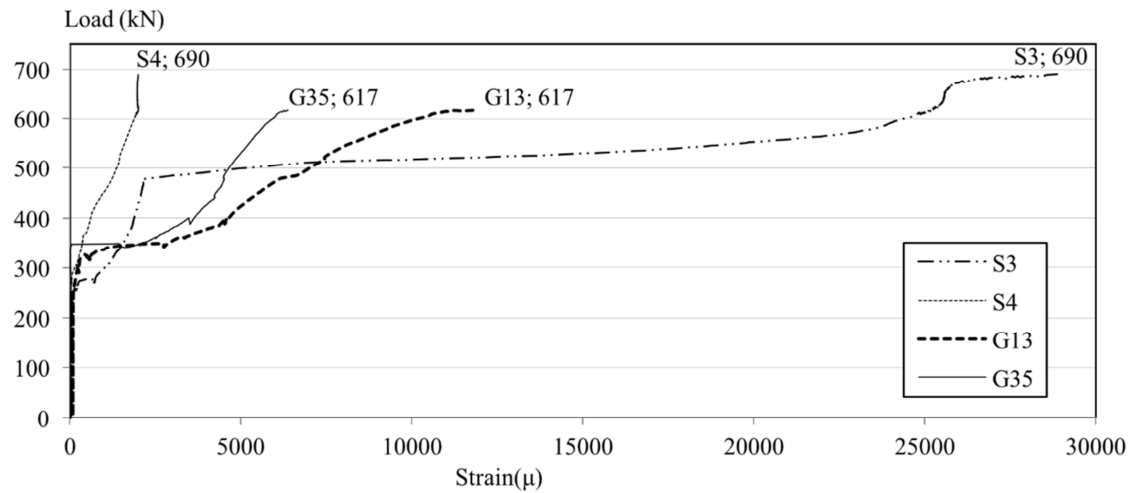
Figure 4-14: Load vs. strain curves of stirrups in RC beam 1 and CFRP grid in RC beam 3
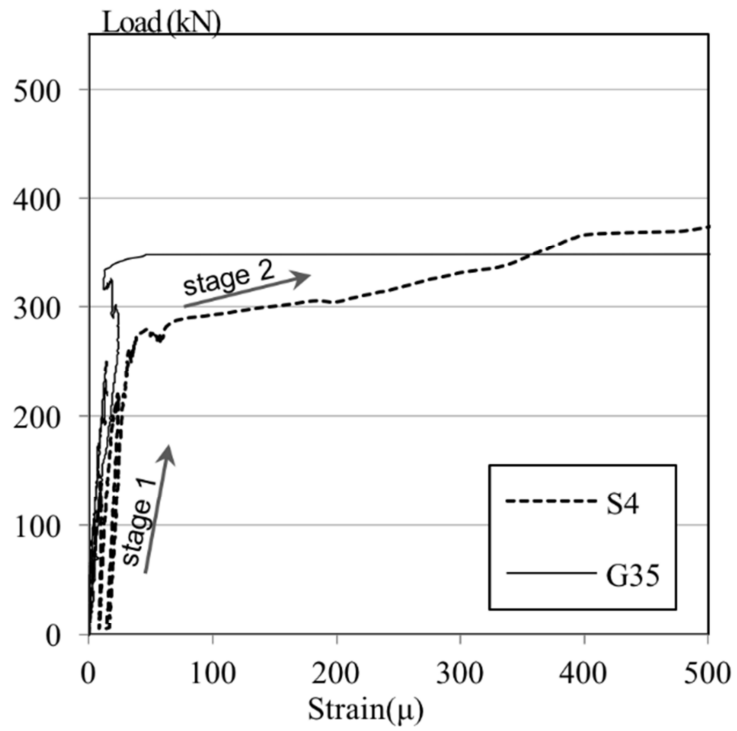
Figure 4-15: Load vs. strain curves of S4 (RC beam 1) and G35 (RC beam 3)
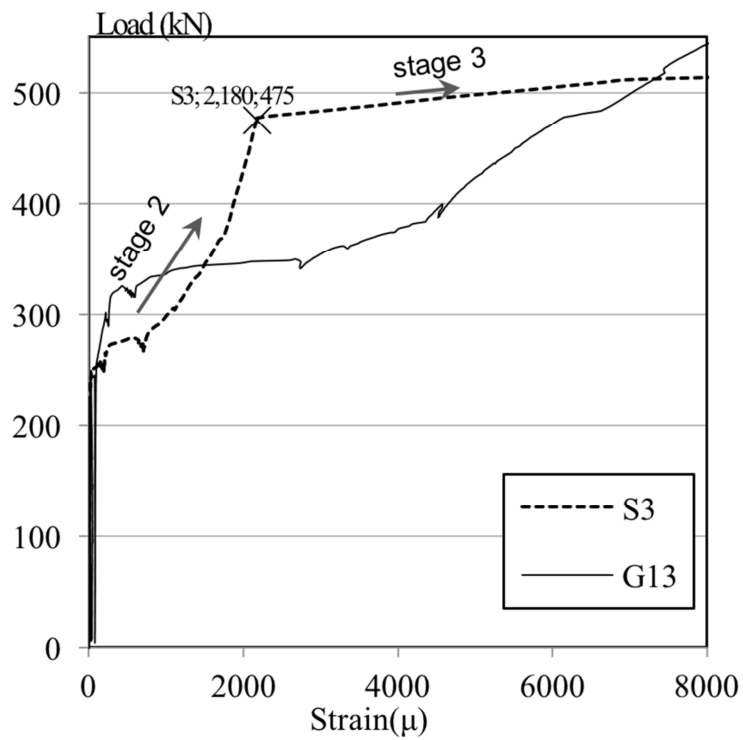
Figure 4-16: Load vs. strain curves of S3 (RC beam 1) and G13 (RC beam 3)

In the third stage, when the load continued increasing, the stress on the stirrup reached the yield strength. From the values given in Table 4-4, the stirrup is expected to yield at a strain of

$$\varepsilon_{yield} = \frac{\sigma_{yield}}{E_s} = \frac{417}{2\times10^5} = 2{,}085 \times 10^{-6}.$$

In the test, stirrup S3 yielded at a strain of $2{,}180 \times 10^{-6}$ equivalent to a load of 475 kN as shown in Fig. 4-16. When the stirrup yielded, the elastic modulus of shear reinforcing bars reduced rapidly, whereas CFRP grid was elastic until fracture. This is the reason why strains in RC beam 3 were lower than those in RC beam 1.

4.3.3. Difference in behavior between CFRP grid and stirrups in RC beam 2

Bonding between concrete and sprayed mortar is one of the most important factors that influence the effectiveness of reinforcement. The difference in behaviors between the stirrups and CFRP grid at the same positions in RC beam 2 may provide the information on the bonding between concrete and sprayed mortar. The strain gauges on CFRP grid G4, G14, G30, and G35 and those on the stirrups S1, S2, S3, and S4 were respectively at the same positions in RC beam 2. Locations of these strain gauges are shown in Fig 4-11 and 4-12. The data of the bending test are listed in Table 4-7. Fig. 4-17 illustrates the load versus strain curves of the stirrups and CFRP grid in RC beam 2.

The strain curves for the load between 300 kN and 550 kN (see Table 4-7 and Fig. 4-17 show the following behavior: When the load is greater than 350 kN, the strain values on the stirrup are higher than that on the CFRP grid (except stirrup S1), S3/G30 and S4/G35 are higher than S2/G14. At a load greater than 700 kN, the difference in strains between stirrup S4 and CFRP grid G35 becomes larger. At the ultimate stage, the strain recorded by S4 is about 5 times higher than that by G35 (4.9 times higher at a load of 750 kN). Thus, strain gauge readings at the same position differed significantly. This observation proved that, these materials (the CFRP grid and the stirrup) no longer worked together and the bonding between concrete and mortar was damaged. The possible reasons are as follows: First, when the strain on stirrups S2, S3, and S4 was greater than $2{,}085 \times 10^{-6}$ (as calculated in section 3.2), the stirrups yielded and deformed rapidly after this point. Second, when the load was increased from 320 to 425 kN, cracks appeared and propagated towards the loading point, the compression area of the cross-section reduced. Most of these cracks were located in the same positions as S2, S3, and S4 (see Fig. 4-11). Once a crack crossed the locations of stirrups and CFRP grid, the adhesion of mortar to concrete surface was also damaged.
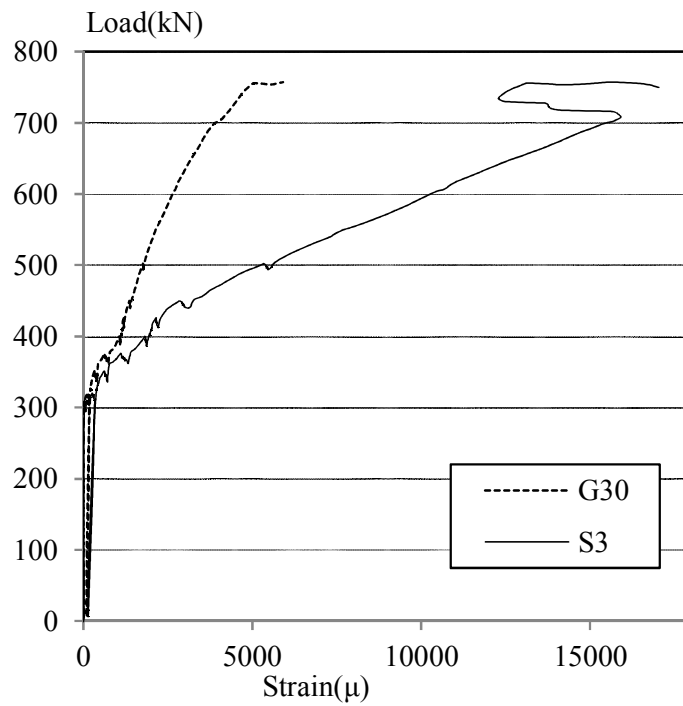
a) Stirrup S4 and CFRP grid G35
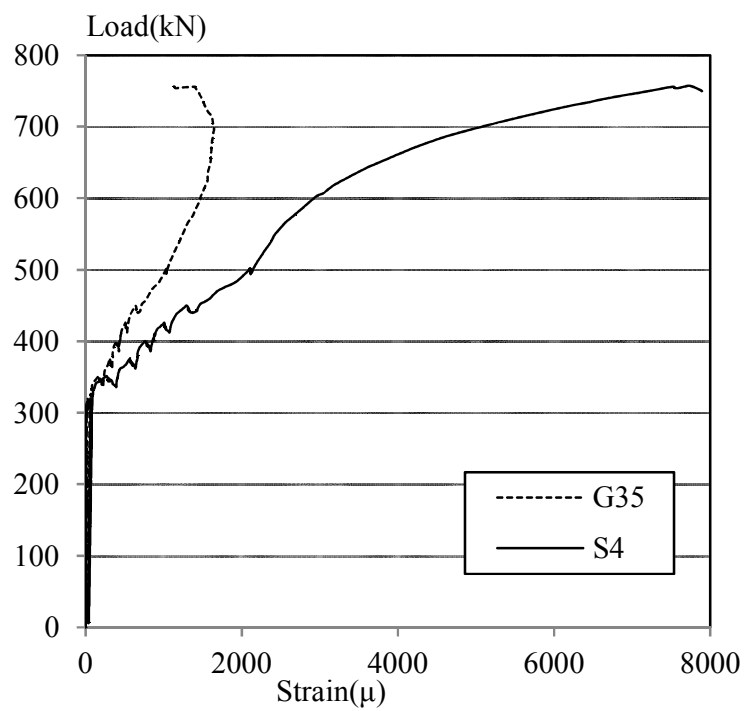
b) Stirrup S3 and CFRP grid G30

Figure 4-17: Load vs. strain curves of stirrup and CFRP grid in RC beam 2

4.3.4. Contribution of CFRP grid in shear strengthening of RC beams

This section is to determine the suitability of using shear design methods given by the (Japan Society of Civil Engineers 2007) to estimate the shear strength of a beam reinforced with a CFRP grid. Design shear capacity values were calculated for different values of shear strength as shown in Table 4-6. Flexural cracks appeared when the flexural cracking strength of concrete was exceeded by the applied stress. After that, if the stress reached the shear strength of concrete, diagonal cracks would occur. The design shear capacity of RC beam 1 is the sum of shear resistances contributed by concrete and reinforcement while those of RC beam 2 and RC beam 3 are the sums of shear resistances contributed by concrete, reinforcement, and CFRP grid. According to Equation (9.2.3) in (Japan Society of Civil Engineers 2007), the design shear capacity was calculated using following equations:

$$V_{yd} = V_{cd} + V_{sd} \qquad (1)$$

V_{cd}: design shear capacity of linear members without shear reinforcing steel.

V_{sd}: design shear capacity of reinforcement,

Table 4-7: Comparison of strains on stirrups and CFRP grid in RC beam 2

Load (kN)	CFRP (μ)				Stirrup – RC beam 2 (μ)				Comparison			
	G6	G14	G30	G35	S1	S2	S3	S4	S1/G6	S2/G14	S3/G30	S4/G35
50	1.0	1.0	–2.0	3.0	2.0	2.0	1.5	1.5	2.0	2.0	–0.8	0.5
100	8.0	8.0	0.1	9.0	8.0	7.0	5.5	6.0	1.0	0.9	55.0	0.7
150	12.0	11.0	1.0	14.0	15.0	8.5	7.5	7.5	1.3	0.8	7.5	0.5
200	13.0	13.0	–3.0	15.0	17.0	8.5	6.0	7.0	1.3	0.7	–2.0	0.5
250	14.0	16.0	2.0	15.0	21.5	9.0	7.0	6.5	1.5	0.6	3.5	0.4
300	18.0	13.0	20.0	12.0	29.0	6.0	45.5	4.5	1.6	0.5	2.3	0.4
350	4.0	–14.0	418.0	154.0	32.5	5.0	592.0	247.5	8.1	–0.4	1.4	1.6
400	126.0	1111.0	1064.0	392.0	57.0	1248.0	1822.0	854.0	0.5	1.1	1.7	2.2
450	338.0	1785.0	1358.0	640.0	158.5	2264.0	3246.0	1443.5	0.5	1.3	2.4	2.3
500	636.0	2305.0	1789.0	1027.0	438.0	4046.5	5592.0	2091.0	0.7	1.8	3.1	2.0
550	864.0	2748.0	2126.0	1232.0	632.0	6475.0	7606.0	2417.5	0.7	2.4	3.6	2.0
600	1234.0	3273.0	2622.0	1467.0	782.0	9382.0	10198.5	2905.5	0.6	2.9	3.9	2.0
650	1451.0	3759.0	3168.0	1596.0	826.5	11489.5	12621.0	3714.0	0.6	3.1	4.0	2.3
700	1573.0	4243.0	3882.0	1645.0	864.5	13727.5	15415.5	5050.0	0.5	3.2	4.0	3.1

Design shear capacity in RC beam 1:

$$V_{yd1} = V_{cd1} + V_{sd1} \qquad (2)$$

Design shear capacity in RC beam 2:

$$V_{yd2} = V_{cd2} + V_{sd2} + V_{CFRP} \qquad (3)$$

V_{cd}: design shear capacity without shear reinforcement

$$V_{cd} = \beta_d \times \beta_p \times \beta_n \times f_{vcd} \times b_w \times d / \gamma_b \qquad (5)$$

$$f_{vcd} = 0.20 \sqrt[3]{f'_{cd}} \ (N/mm^2) \text{ where } f_{vcd} \le 0.72 \ (N/mm^2)$$
$$\beta_d = \sqrt[3]{1000/d} \ (d \text{ in mm}) \text{ when } \beta_d > 1.5, \ \beta_d \text{ is taken as } 1.5$$
$$\beta_p = \sqrt[4]{100 \times p_v} \text{ when } \beta_p > 1.5, \ \beta_p \text{ is taken as } 1.5$$

$\beta_n = 1$

b_w: web width (*mm*)

d: effective depth (*mm*)

$p_v = A_s/(b_w \times d)$

where,

A_s - area of tension reinforcement (mm²);

f'_{cd} - design compressive strength of concrete (N/mm²);

f'_{cd} is taken as 34.1 N/mm² with concrete and 36.7 N/mm² with mortar (see Table 4-3:);

γ_b - member factor, may generally be taken as 1.3;

V_{cd1} - shear resistance contributed by concrete;

V_{cd2} - shear resistance contributed by concrete and sprayed mortar;

V_{cd3} - shear resistance contributed by concrete and sprayed mortar.

-        V_{sd}: design shear capacity of shear reinforcement, taken from Eq.(9.2.6) of Ref (Japan Society of Civil Engineers 2007)

$$V_{sd} = A_w \times f_{wyd} \times z/S_s/\gamma_b \qquad (6)$$

where,

A_w - total area of shear reinforcement placed in S_s;

f_{wvd} - design yield strength of shear reinforcement (yield strength of stirrup, D10 for RC beam 1 and D6 for RC beam 2, was taken, f_{wvd} of RC beam 1 is as 413 N/mm² and f_{wvd} of RC beam 2 is 417 N/mm² in Table 4-4);

z - distance from location of compressive resultant to centroid of tension steel, which may be taken as $d/1.15$;

S_s - spacing of shear reinforcement;

γ_b - member factor, may generally be taken as 1.1.

- V_{CFRP}: design shear capacity of CFRP grid. In Japan, there is no standard specification for shear strengthening concrete structure using CFRP grid. In this case, the CFRP grid was taken as shear reinforcement.

According to Eq.(9.2.6) of (Japan Society of Civil Engineers 2007), the following equation was suggested for calculating V_{CFRP}.

$$V_{CFRP} = A_{CFRP} \times f_{CFRP} \times z/S_s/\gamma_b \qquad (7)$$

where,

A_w - total area of shear reinforcement placed in S_s (mm^2);

f_{CFRP} - design yield strength of shear reinforcement (In this experiment, there is no yield strength of CFRP and CFRP can be considered as a linear-elastic material. f_{CFRP} was taken as tensile strength, equal to 1,400 N/mm^2);

γ_b - member factor of CFRP material (as there is no standard specification for CFRP grid, the safety ratio of 1.3 for CFRP sheet taken from "Guideline for repair and strengthening using CFRP sheet for concrete structure" (JSCE et al. 1996) was used.

According to test results in Table 4-6, RC beam 1 and RC beam 2 showed the maximum test loads of 690 kN and 757 kN, respectively, much higher than design loads of 354 kN and 697 kN, respectively, due to the following reasons. First, the value of the design load is calculated for linear-elastic material, while at the load of 690 kN, the stirrup in RC beam 1 already yielded; second, there is safety ratio included in the formula in standard specifications. For RC beam 3, the design loads are higher than the maximum experimental load, due to the following reasons. First, applying the formula for stirrups to calculate shear strength of CFRP grid was not appropriate as some coefficients in the formula were not reasonable for CFRP grid, the stirrup has yield strength but CFRP grid does not. Second, when computing the design shear strength, it was assumed that the CFRP grid would work at full capacity. Actually, the maximum stress in the CFRP grid was less than 1,400 N/mm^2 as shown in Table 4-4. At the ultimate state of strengthened beams, the maximum load of RC beam 3 was 617 kN and the maximum strain values of CFRP grid in RC beam 3 were recorded by strain gauges G13 and G35 (location of strain gauges are shown in Fig. 4-12). The maximum strains were $11,943 \times 10^{-6}$ and $6,377 \times 10^{-6}$ as shown in Fig. 16, respectively. The stress on the CFRP grid was calculated as follows.

$$\sigma_{CFRP}^{G13} = E_{CFRP}\varepsilon_{max}^{G13} = 1 \times 10^5 \times 11,943 \times 10^{-6} = 1194.3 \, N/mm^2$$

$$\sigma_{CFRP}^{G35} = E_{CFRP}.\varepsilon_{max}^{G35} \quad = 1 \times 10^5 \times 6,377 \times 10^{-6} = 637.7 \, N/mm^2$$

The maximum stress values on the CFRP grid recorded by G13 and G35 were 85.3% and 45.5% of the tensile strength of CFRP grid (1,400 N/mm^2) as shown in Table 4-4.

Guideline for repair and strengthening using CFRP sheet for concrete structure (JSCE et al. 1996) suggests that the material factor for calculating CFRP sheet capacity is 1.3. There is no mention of the corresponding value for CFRP grid. Here, using material factor of 1.3, the shear design load of RC beam 3 would be 656 kN, which is not appropriate. In the present research work, a coefficient of 1.5 is proposed, indicating that the CFRP grid works at 66.7% of its tensile strength. Using the coefficient of 1.5, the design load will be 637 kN for RC beam 2 and 600 kN for RC beam 3.

4.4.   CONCLUSIONS

Experiments were conducted to study the performance of CFRP grid and sprayed mortar for shear strengthening of RC beams. Based on the collected data, the following conclusions are drawn:

(1)   CFRP grid and sprayed mortar could be significantly effective in shear strengthening. In this experiment, RC beams strengthened with CFRP CR8 and sprayed mortar (RC beam 2 and RC beam 3) attained 110% and 90% of shear capacity compared with the ultimate load of the control beam (RC beam 1). The cross-sectional area of reinforcing materials in RC beam 2 and RC beam 3 were equivalent to 119% and 74%, respectively, of the cross-sectional area of stirrups in RC beam 1. In general, the stiffness, ductility characteristic, and the cracking load of the strengthened RC beams (RC beam 2 and RC beam 3) using CFRP grid and spayed mortar were improved.

(2)   The behavior between the CFRP grid and the stirrups reflects the bonding between concrete and sprayed mortar. It is one of the most important factors that influence the reinforcement effectiveness. According to experimental results, as the load increased, variations of the stirrup strains and the CFRP grid strains at the same position in a strengthened RC beam had similar tendencies. After the stirrups yielded and the cracks developed in a strengthened RC beam, the bonding between concrete and sprayed mortar was considerably affected.

(3)   In an application of CFRP grid and sprayed mortar, CFRP grid could not work at 100% of the tensile strength. Ref (JSCE et al. 1996) reports the material factor of 1.3 for calculating CFRP sheet capacity, but the maximum stress of CFRP grid was 85.3% of the tensile strength in our experiments. Therefore, a material factor of 1.5 is proposed for the CFRP grid when applying the formula in Ref (Japan Society of Civil Engineers 2007) to calculate the shear strength of a RC beam strengthened with CFRP grid and sprayed mortar. Using a coefficient of 1.5 means the CFRP grid works at 66.7% of its capacity.

It is concluded that the shear-strengthening of RC beams by CFRP grid and sprayed mortar is effective. CFRP grid and sprayed mortar are useful in strengthening and retrofitting

of concrete structures. CFRP grid can support or replace stirrups in RC beams in providing shear strength.

Chapter 5:

CRACK PROPAGATION AND THE ROLE OF HORIZONTAL AND VERTICAL COMPONENTS OF CFRP GRID IN SHEAR STRENGTHENING FOR RC BEAM

This chapter takes the data from the previous experiment in chapter 4. Acoustic emission (AE) sensors were attached on the two beams to monitor the crack development from the starting point to the ultimate state. The actual observed fact of the crack propagation is combined with AE technique result to conclude the better understanding of the formation and propagation of diagonal cracks.   As a result of the experiments, micro-cracks in concrete beams occur and develop very early, even when the load is very low and in the compressed area of the beam. In this research work, based on the result from AE sensor and observation, the comparison between the crack propagation of control beam and the shear strengthened beam is also presented. The test result also reveals that CFRP grid provides the significant part for the shear strength of RC beam. From the analysis, it illustrates that the roles of horizontal and vertical components of CFRP grid are different and depend on the strengthening locations, the properties of materials.

5.1. CRACK PROPAGATION OF RC BEAM STRENGTHENED IN SHEAR BY CFRP GRID

5.1.1. Introduction

Many researchers have studied on diagonal crack propagation, and diagonal failure mechanism also. Shear failure is devided into two types; diagonal tensile failure and shear compression failure. According to previous studies, shear compression failure can be simulated by Finite Element (FE) analysis. It is not an easy task to simulated diagonal tensile failure, which is a brittle failure, by FE analysis (Sato et al. 2004). But not many researches have been published on the development of cracks in the interior of RC beams, and especially for RC beams shear-strengthened with CFRP grid. To investigate the damage occurring inside the concrete structure, the method uses a system of sensitive sensors combining with converter equipment and computer systems to capture and process the wave sounds emitted by fractures of elements inside the concrete structures. AE technology was first investigated in the middle of the 20th Century. It is one of the non-destructive evaluation techniques, a useful method for the investigation of local damage in concrete. Thus, AE techniques have been applied to crack detection in concrete structures (Ohtsu et al. 1996). The damage degree in concrete structures can be easily estimated, taking account of the number of AE hits and the maximum amplitude of AE signal (Ohtsu et al 2006). Also, AE source localization due to micro-cracks can be performed by taking into account the arrival time differences of AE waveforms at each AE sensor (Mclaskey et al. 2007). Taking advantage of the AE technique, it is possible to determine precisely the location of the fracture cracks that occur and develop in concrete beams, thereby more clear understanding and analyzing of the performance of the concrete beam strengthened with CFRP grid have been found out. A better understanding of the formation and development of cracks can help us find effective reinforcement methods when applying CFRP grids to concrete structures.

The objective of this part is to investigate the crack propagation in shear-strengthened RC beams and compare with its formation in the control beam. The diagonal crack of RC beams shear-strengthened by CFRP grid and sprayed mortar was studied in detail. The propagating process of crack was analyzed base on the actual facts observed in the experiments and the Acoustic Emission (AE) result. The difference between the crack propagation of the control beam and the shear strengthened beam using AE result combining with the observed result is also presented. Some of the differences in results obtained from direct observations on the beams and the results obtained from the AE sensor are also stated and clarified. The experimental data is taken from the four-point bending test applying on RC beam 1 and RC beam 2 in chapter 4.

5.1.2. AE system

In this test, used PA sensors are F15a - 100-450 kHz High-Sensitivity Flat Frequency Response AE Sensor, the preamplifiers are 2/4/6 - switch selectable gain single ended and differential preamplifier. Fig. 5-1 shows the application of AE system to the concrete test, the image of Sensor F15a and Preamplifier 2/4/6. These are the product of Physical Acoustic Company (homepage: *http://www.physicalacoustics.com/*).

a) Application of AE to concrete specimens　　b）Sensor F15a　　c) Preamplifier 2/4/6
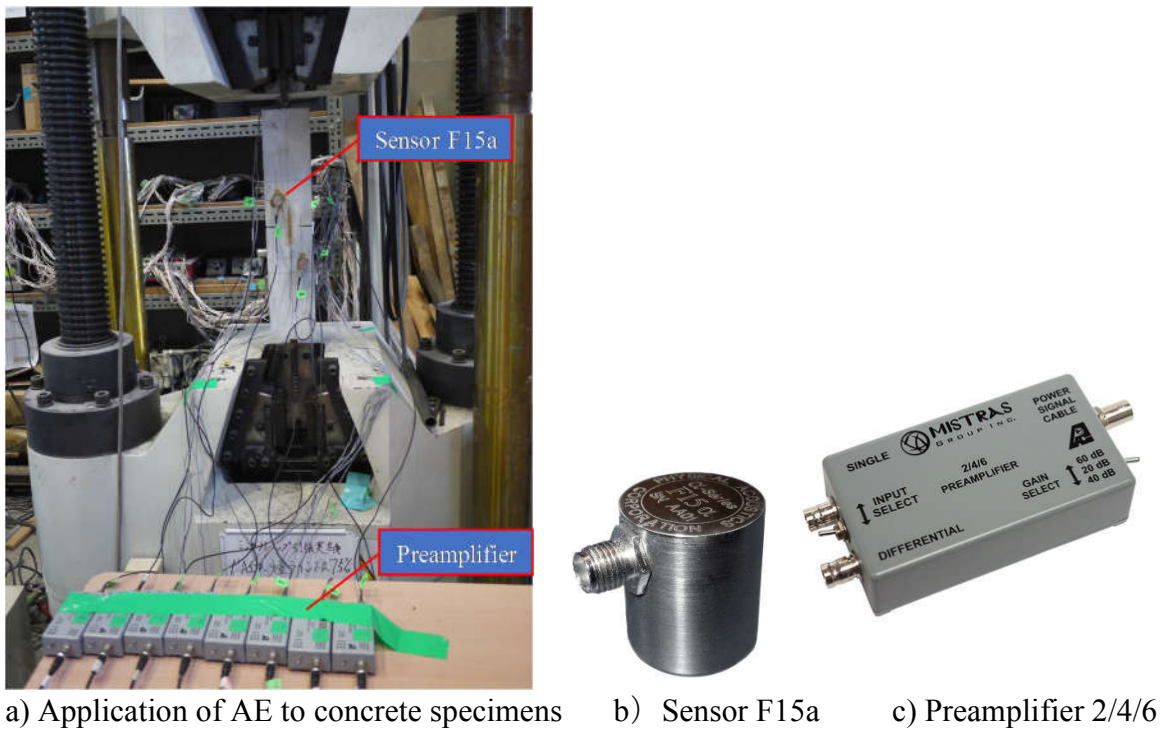
Figure 5-1: AE system and its application

5.1.3. Results and discussions

5.1.3.1. Results

The detail of the experimental program is presented in chapter 4. Strengthening scheme of two beams is shown in Fig. 4-4.

AE sensors were set on two beams to capture the wave sound emitting from the crack occurring inside the beams. 16 AE sensors were attached to both sides of each beam to get the signal of the failure process. Eight channels of AE sensor were used on each side of the beam; the locations of the AE sensor are displayed in Fig. 5-2.
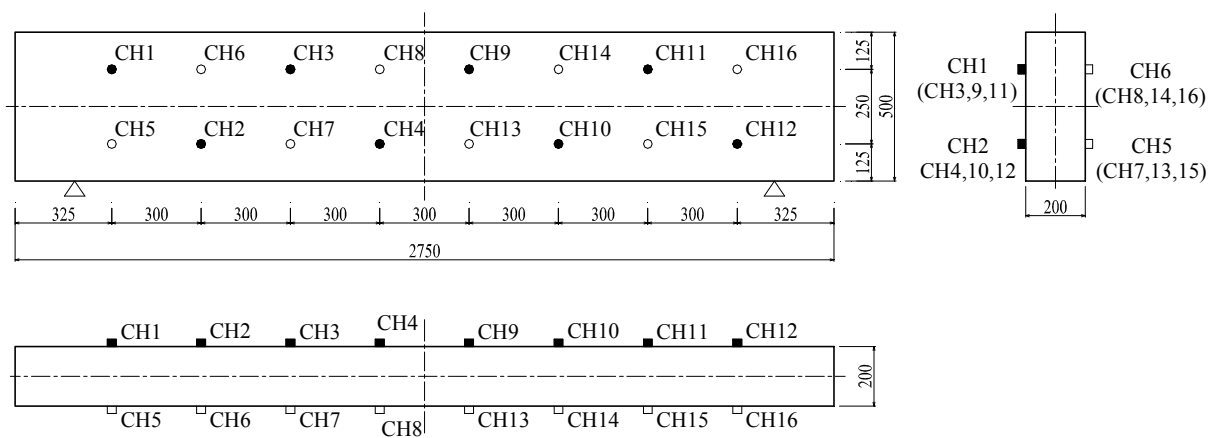
Figure 5-2: Location of AE sensors set on beams

The test results of two beams are summarized in Table 5-1.

Table 5-1: Summary of test results (from Chapter 4)

Beam index	Calculating crack load	Cracking load (kN)	Maximum load (kN)
RC beam 1	88	225	690
RC beam 2	97	300	757

Fig. 5-3 shows the crack pattern of RC beam 1 and RC beam 2. The above image is the real one taken after the loading test, and the below one is redrawn by the software of the computer. The ultimate cracks are the cracks cause the collapse of beams. The bold continuous lines are the ultimate cracks.
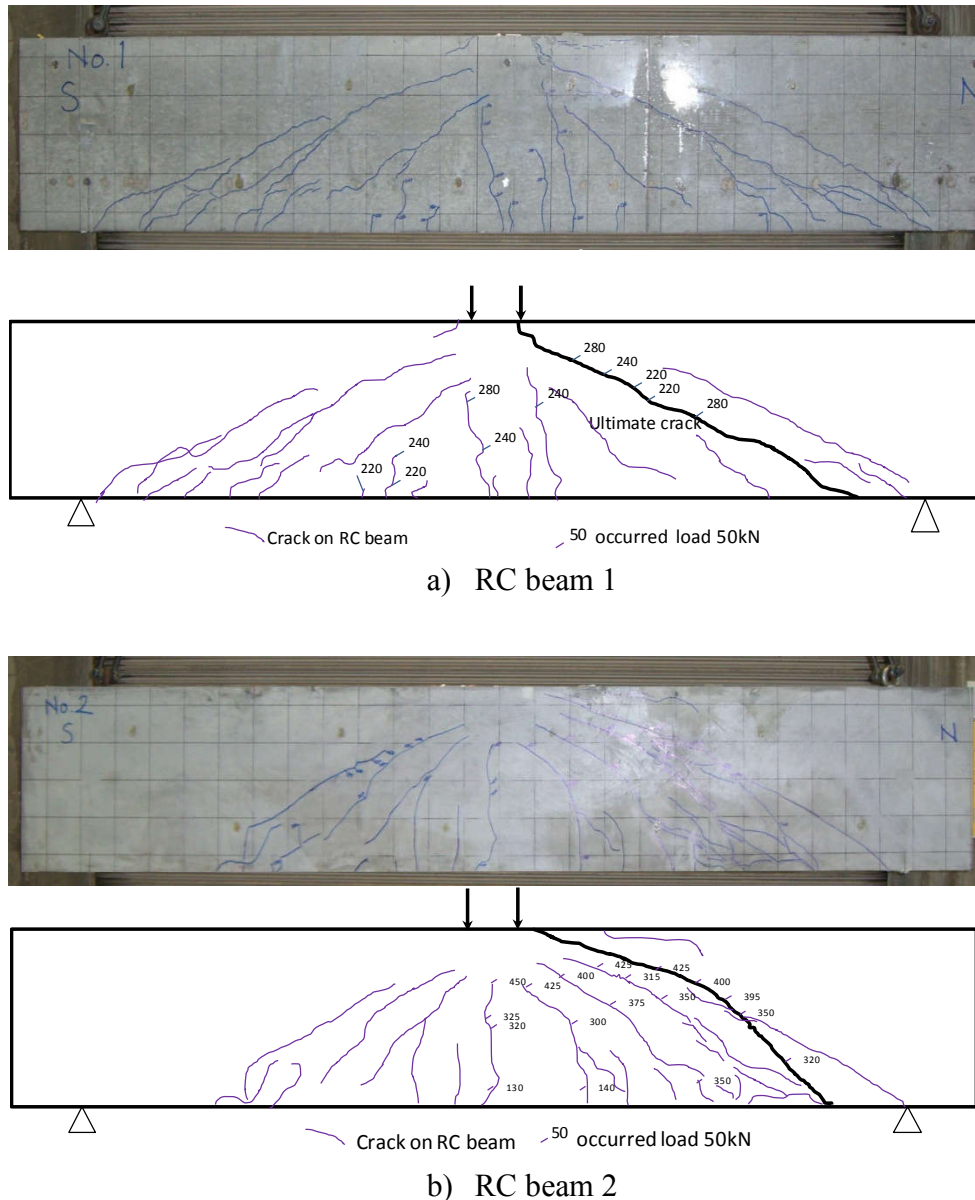
a) RC beam 1

b) RC beam 2

Figure 5-3: Crack pattern of two beams: RC beam 1 and RC beam 2

As increasing the load on the beams, firstly, the micro-crack is formed inside the concrete chords. The wave sound emitted from the appearance of micro-cracks are detected and recorded by AE sensors. The received signal is automatically processed by the computer to give the exact position of cracks corresponding to each level of the load. Fig 5-4 shows the distribution of the fracture points identified by the AE sensor. Each point in the graph in Fig. 5-4 represents for a signal absorbed. From the start time to the failure stage of load increment, there are so many signals that have been treated. To analyze clearly the formation and development of diagonal cracks, each beam, the distribution of cracks was divided into four stages corresponding to the load increment: 0-100 kN, 100-200 kN, 200-300 kN, 300-

400 kN. Fig. 5-4.1a, 5-4.1b, 5-4.1c, 5-4.1d shows the location of the crack in RC beam 1; Fig. 5-4.2a, 5-4.2b, 5-4.2c, 5-4.2d) performs the location of the crack in RC beam 2. The red dots present for the crack occurring at present load stage. The blue dots present for the crack formed from the all previous stages.
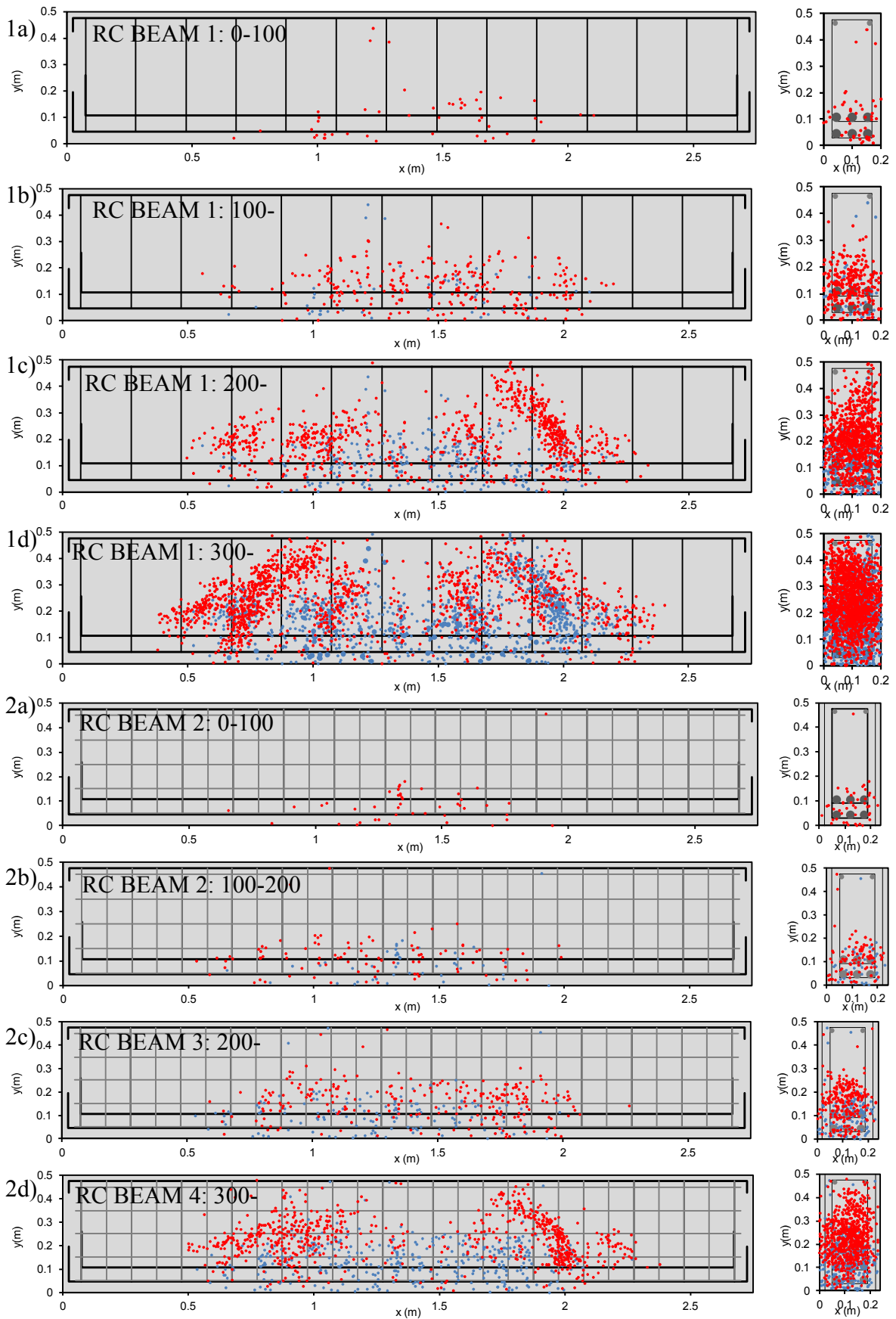
Figure 5-4: Distribution of the crack sound detected in two beams: RC beam 1 and 2

Red dots: Location of the cracks occurs corresponding to each stage of load increase;

Blue dots: Location of the cracks occurs corresponding to all the previous stages of load increase.

5.1.3.2.   Discussions

5.1.3.2.1.   Crack propagation in the RC beam 1 and RC beam 2, combine two results

According to the Table 5-1, RC beam 2 exhibited the higher maximum load (757 kN) while RC beam 1 showed the lower (690 kN). Compared to the control beam (RC beam 1), the maximum test load of RC beam 2 was higher by 9.7% (Vu et al 2016). RC beams 2 is able to withstand a higher bending load than RC beam 1 because it has been strengthened in shear by two layers CFRP grid and mortar with a thickness of 20 mm on two sides of the beam.

Base on the observation of the cracks on two beams, see Fig. 5-3, in both cases the failure mode is diagonal tension failure as expected. With a span length (L) of 2.35 m and a shear span (a) of 1.1 m, the effective depth (d) was 0.423 m, the shear span to effective depth (a/d) ratio was 2.6. These two beams are the slender beam.

As the load increases, cracks occur and develop on the beam. Based on the observed results, on both beams, the crack was initially formed at the mid-span of the beam (RC beam 1 - the first observed cracks were discovered at the value 225 kN of load, with RC beam 2 this value is 300 kN, Table 5-2), near the mid-span section, as the load increases, the cracks also grow upwards (flexural crack). Next, more cracks occur on support sides, which are also perpendicular to the member axis. The cracks continue to incline towards the bearing points (diagonal crack), the width of the crack also increases. When the load is high enough close to the maximum value, a crack opens wilder and becomes the critical crack. According to Fig. 5-3, the crack pattern displays the mostly the symmetry propagation. This is in line with the scheme for the beam load as symmetric. At the force stage of more than 400kN, the cracks have propagated much more in the tension area of cross-section, concrete has cracked, the tensile strength of the section is totally provided by reinforcing bar with RC beam 1 and reinforcing bars and CFRP grid with RC beam 2. After this period, new main cracks do not occur, but the formed cracks continue growing toward the loading point and open its width.

As shown in Fig. 5-4, the distribution of cracks is classified correspondently to each stage of load increase. The first cracks sound occurred when the load is still very low, less than 100 kN (Fig. 5-4.1a with RC beam 1 and Fig. 5-4.2a, with RC beam 2.

In the first stage of load increase, Fig. 5-4 (1a, 2a) Micro-cracks occur scattered on the tension area of RC beams 1 and 2. Even, in the compression area micro-cracks also arise. As the load increases, the cracks occur much more and faster. From Table 5-2, it is found

that the number of cracks in both beams increased rapidly until the load was equal to 400 kN. In particular, the crack sound appears denser in some specific locations. This is consistent with the results of the cracks seen above the beam surface (Fig. 5-4.1c, 5.1d, and 5.2d). It is also assumed from the Fig. 5-4 that (vertical cross-section), the crack mainly locates in the middle area of the section. There are fewer cracks that found at the boundary of the section. This also is the reason for the difficulty to observe the crack from outside of the beams.

The stage of the load from 200-400 kN (Fig. 5-4:1c, 1d) with RC beam 1 and 300-400 kN (Fig. 5-4:2d) with RC beam 2, the number of cracks increases rapidly, and mostly the crack sound occurred in this stage. This matches with the crack pattern in Fig. 5-3.

After the above-listed stages, the crack occurs continuously but with a slower speed. The main crack doesn't occur more. They develop toward the compression zone and open widely. That the reason why in this paper, the author doesn't enclose the distribution of the crack the period of load after 400 kN (400-690 kN with RC beam 1, and 400-757 kN with RC beam 2). Besides, when the crack opens widely, it splits the RC beams into many separate parts and influences the signal transmission of AE sensor system (AE system can detect a crack sound only if at least 4 AE sensors receive the signal).

5.1.3.2.2.   Compare the result of two RC beam

From these above result, it is possible to come to the comment that the cracks resulting from the AE sensor are, of course, more reliable, since they exhibit cracks development from the micro-cracks stage and can determine the exact location of the crack. Table 5-2 and Fig 5-5 shows the number of crack signals in the two beams classified corresponding to the incremental stages of the load. AE result shows that the number of the crack sounds received from two beams is extremely different. Base on the observed result, initial cracks on RC beam 2 occurred later (after the load of 300kN) than RC beam 1 (after the load of 225). According to the AE result, most of the crack of RC beam 1 occurs in the load period of 200-400kN. Table 5-2 and Fig. 5-5. show this obviously. In the period of load 200-400 kN, in RC beam 1, there are 2315 cracks have been detected, while that number of RC beam 2 is 983. The crack sound of RC beam 2 also much more scattered than that of RC beam 1.

Table 5-2: Number of cracks detected in two beams by AE sensor

	0-100 kN	100-200 kN	200-300 kN	300-400 kN	400-500 kN	500-600 kN	600-700 kN	700-757 kN
RC beam 1	49	67	865	1450	540	467	337	-
RC beam 2	45	94	242	741	521	367	275	250
% (RC2/RC1)	91.8	140.3	28.0	51.1	96.5	78.6	81.6	

Number of crack signals
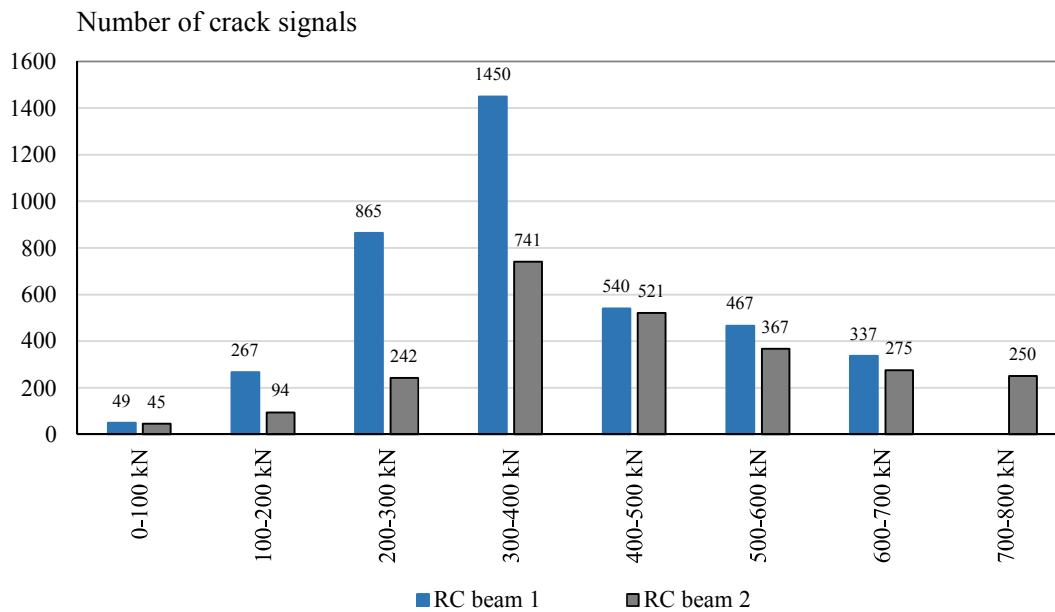
Figure 5-5: Number of cracks recorded by AE sensor in two beams

5.1.4. Conclusions

In order to study the crack propagation, the combination of results from the two methods; actual observed fact and AE technique, the more distinct and detail understanding about the formation and development of the crack has been found. Especially, the micro-crack cannot be identified from outside of the beam, but the location and magnitude can be detected accurately by the AE sensor method. In this experimental program, with two beams, the micro-crack appears in beams since the load still low (0-100 kN) in both the tension zone and the compression zone also.

Comparing the number of cracks in RC beam 1 and RC beam 2, it is supposed that the number of cracks in the shear-strengthened beam (RC beam 2) is significantly smaller than the control beams (RC beam 1). It also shows the effect of reinforcing concrete beams with CFRP grid not only increases the strength of the structure but also contributes to the

reduction of cracks and the brittleness of the structure. The reduction of the number of crack sounds is recorded by 51% at the level of load that most cracks occur (load of 300-400kN in this test).

5.2. ANALYSIS OF THE ROLE OF HORIZONTAL AND VERTICAL COMPONENTS OF CFRP GRID IN SHEAR STRENGTHENING FOR RC BEAM

5.2.1. INTRODUCTION

Recently, numerous researchers have studied the CFRP grid applications for flexural strengthening, for example, two-way slabs, bridge decks and arch-slabs in tunnels. Further, there are also a few papers interested in applying CFRP grid for reinforced concrete (RC) beams to increase shear strength. Numbers of studies (Bukhai et al 2010, Chen et all 2010, Guo et al 2014 and VD Tran et al 2014) have been done by other researchers to investigate the behavior of CFRP grid. However, there is no work mentions the difference between the CFRP component bars. However, there is almost no study mentions about the behavior between components of CFRP grid. This present session is concerned with the role of horizontal and vertical components of CFRP grid in shear strengthening for RC beams. It aims to clarify the character of both components of the CFRP grid in shear strengthening for RC beams. The data from the test in Chapter 4 was collected and analyzed to draw the relevant comment about the behavior of CFRP grid.

The behavior of two components of the CFRP grid is analyzed basing on the data from strain gauges embedded in CFRP of the beams in Chapter 4. The location of strain gauges is shown on the Fig5-6.
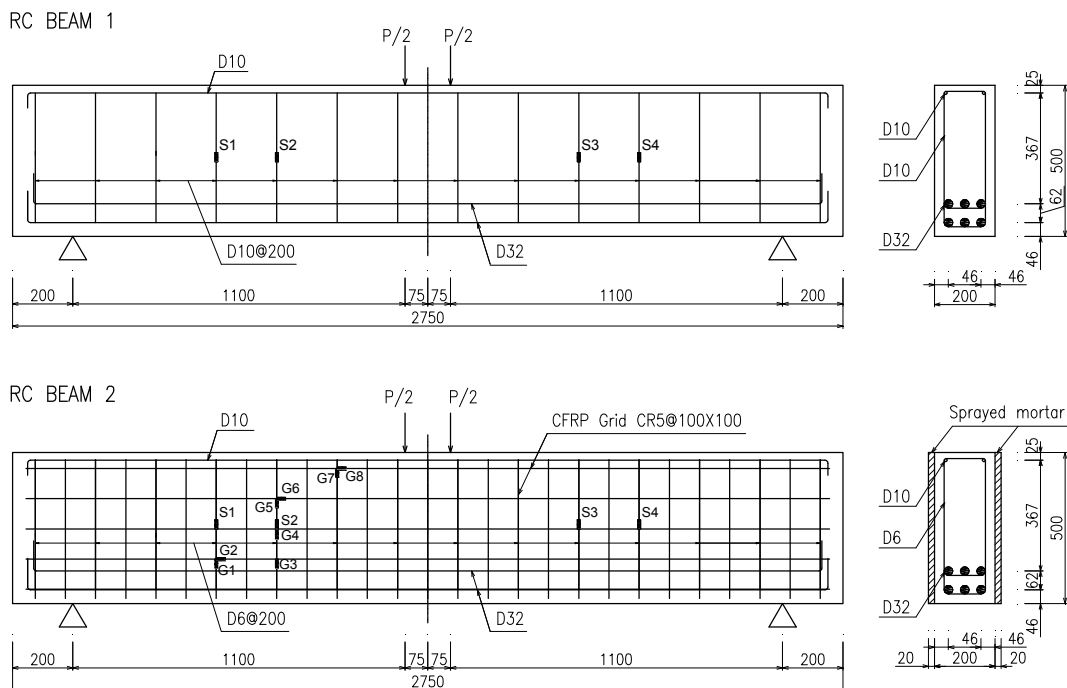
S1, S2, S3, S4: strain gauges installed on stirrups in RC 1 and RC 2

G1, G2, G3, G4, G5, G6, G7, G8: strain gauges installed on CFRP grid in RC 2

Figure 5-6: Location of strain gauges set on horizontal and vertical bars of CFRP grid

5.2.2. RESULTS AND DISCUSSIONS

5.2.2.1. *CFRP grid plays critical roles in providing the shear strength of RC beam 2*

The failure modes of the two beams are shear failure. The summary of shear reinforcement and the test results of two beams was listed in Table 5-3. Fig. 4-10 and Fig. 4-11 in Chapter 4 show crack patterns of two beams after the test, small numbers beside the crack curves are the loading point occurred those cracks; the bold green lines are the ultimate cracks. Fig. 5-7 displays strain-load curves of the stirrups in RC beam 1 and RC beam 2 at the same position of stirrup recorded by strain gauges S2.
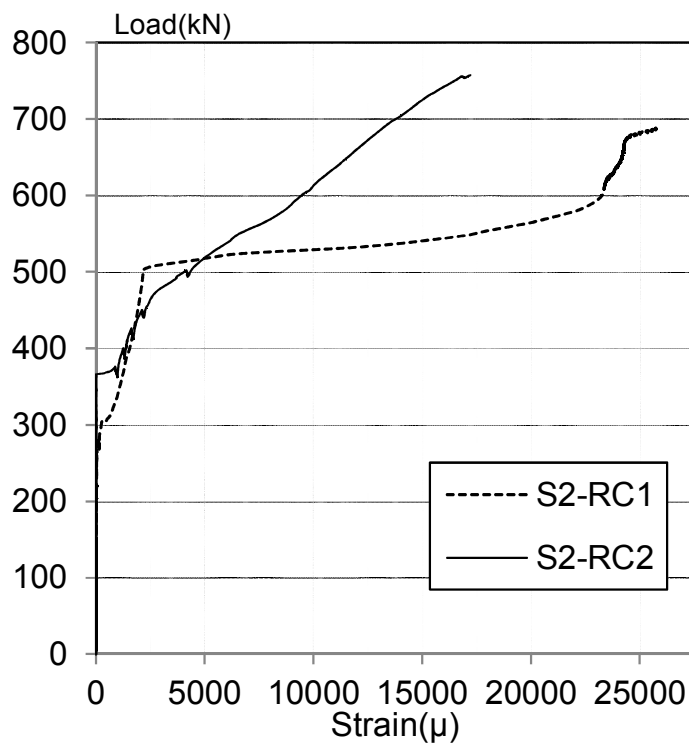
Fig. 5-7: Load-strain curves of stirrup S2 on RC beam 1 and RC beam 2
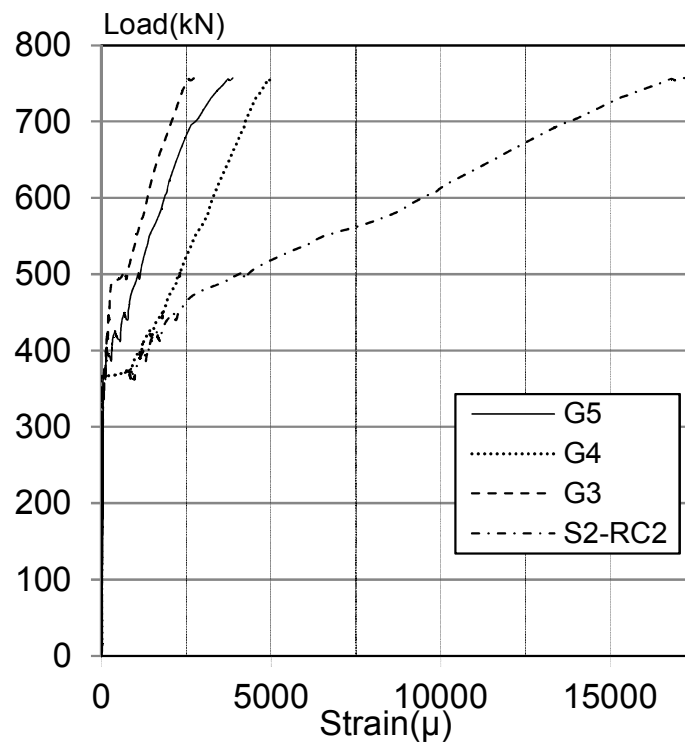
Fig. 5-8: Load-strain curves of stirrups S2 and CFRP grid of RC beam 2

Table 5-3: Summary of shear reinforcement and test results

Beam	Shear reinforcement of 200 mm beam length		Cracking load test (kN)	Maximum load test (kN)
	Stirrup and CFRP grid	Total area		
RC beam 1	2 bars of D10	142.66 mm^2	225	690
RC beam 2	2 bars of D6 and 4 bars of CFRP grid	169.34 mm^2	300	757

Fig. 5-8 illustrates the load-strain curves of the stirrup (recorded by strain gauge S2) and the vertical bars (recorded by strain gauges G3, G4, G5) of CFRP grid in RC beam 2 at the same cross section. The locations of strain gauges were indicated in Fig. 5-7. Strain recorded by gauges G3 and G5 smaller than that of gauge G4. The reason is the location of vertical CFRP bar G4 is near the neutral axis (location of neutral axis is shown in Fig. 5-10). In RC beam 2, gauge G4 and gauge S2 are at the same place, gauge G4 attached on CFRP grid, while gauge S3 attached on the stirrup. By the Fig. 5-8, when the load is under 375 kN, they recorded the same values of strain. However, when the load increased over 375 kN, the strain of stirrup is more than $2,000 \times 10^{-6}$, the stirrup yielded, and the cracks also occurred, the strain recorded by gauges G4 and S2 no longer have the same tendency. The diameter of the stirrup is 6 mm and is the deformed bar, so it had good adhesion with nearby concrete, the strain of yielded stirrup equal to the closed materials. In case of a small crack cross the location of stirrups and strain gauges (the length of gauge is 3 mm), the value of strain gauge increase rapidly because of the open of this crack. While CFRP grid is a plain bar, bonding with mortar is not as good as it of the deformed bar, the strain value recorded by gauge is the average strain value between a grid node and the next one. In this test, the gap between 2 nodes of CFRP grid is 100 mm. From the above analysis, it is seen that shear strength of RC beam 2 has been considerably contributed by CFRP grid and sprayed mortar.

5.2.2.2.   The contribution for shear strength of vertical and horizontal CFRP bars.
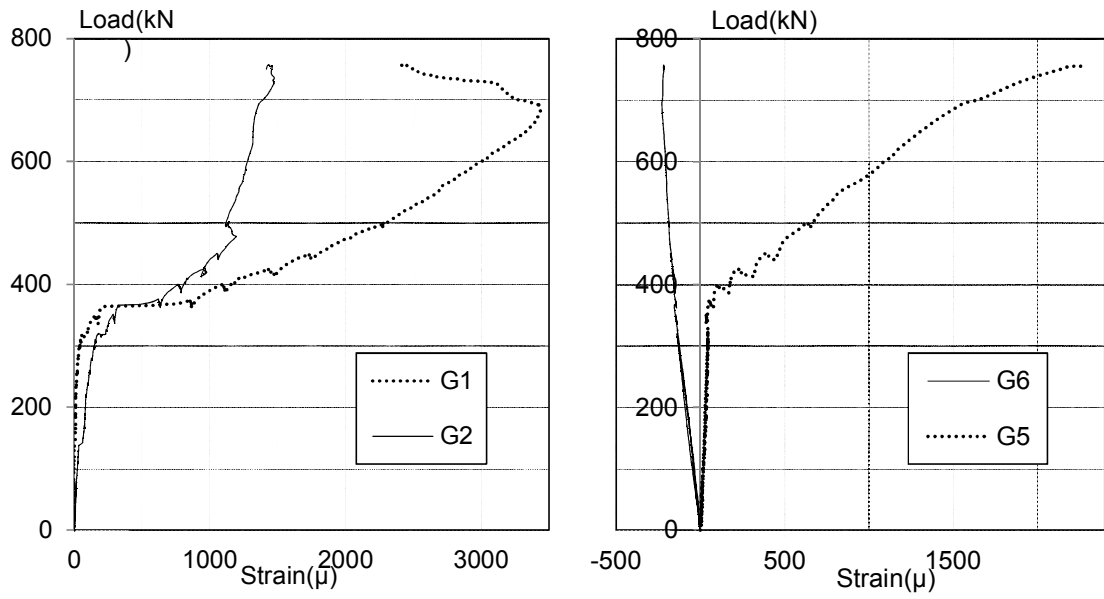
a)

b)
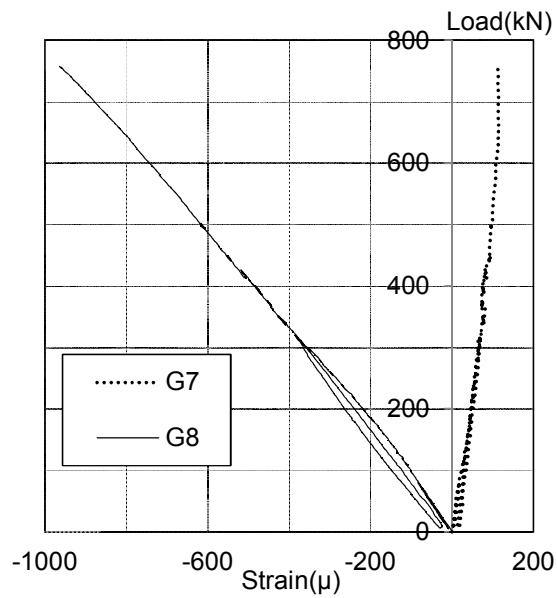
c)

Figure 5-9: Load-strain curves of horizontal and vertical CFRP bars at the same location on RC beam 2
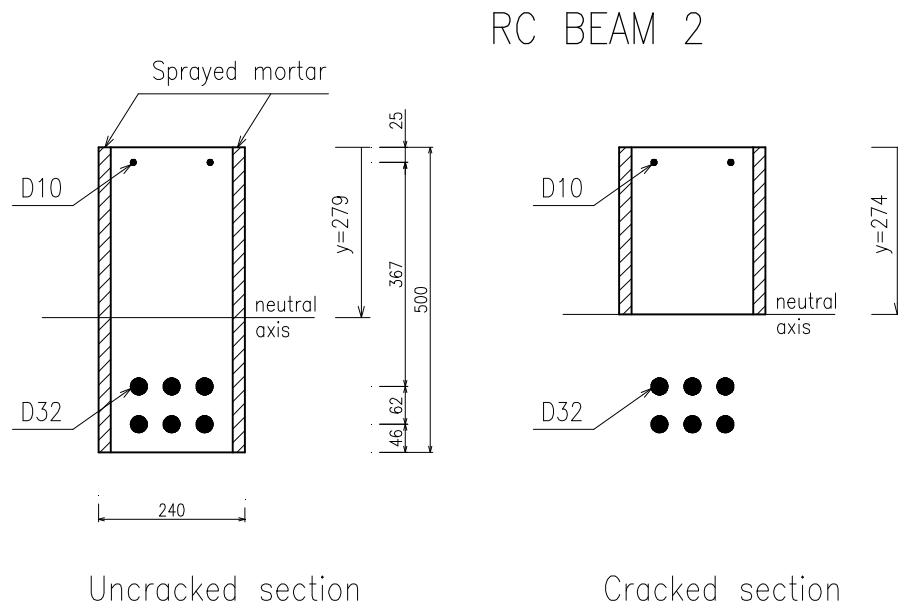
RC BEAM 2

Figure 5-10:   Location of neutral axis in the crack section and un-crack section

To clarify the role of horizontal and vertical components of the CFRP grid, the comparison of those strains was investigated at the same position on RC beam 2. The pairs of compared strain gauges are G1 and G2, G5 and G6, G7 and G8. The locations of these strain gauges were shown in Fig. 5.6. These comparisons are illustrated in Fig. 5-9. When the load increased, the cracks occurred and developed; the loss of concrete and mortar material in the section made the neutral axis move up. Fig. 5-10 shows the displacement of the neutral axis of RC beam 2 before and after cracking.

According to the Fig. 5-9a, the location of strain gauge G1 (vertical component) and gauge G2 (horizontal component) is near neutral axis. In general, the shapes of load-strain curves are the same. However, in particular, the curves could be divided into 2 stages for the detailed comparison. Firstly, when the load under 375 kN, with the same value of the load, the value of strain gauge G1 is smaller than it of gauge G2. When the crack had not occurred and developed, the RC beam 2 can be considered as a homogeneous beam, and all materials: concrete, steel bars, mortar, CFRP grid work together. Secondly, when the load varies from 375kN to 757kN, the crack occurred and developed from the bottom of the beam till the location near neutral axis. Under the neutral axis, concrete and mortar have been cracked; Vertical CFRP bar mainly supports for the shear strength, Horizontal CFRP bar support for the bending strength. The position of horizontal CFRP bar is near the position of the longitudinal reinforcing bar (three bars of D32), while vertical CFRP bar is closed to the location of stirrups (two yielded steel bars of D6). That is the reason for the higher value of gauge G1 when comparing with G2 value.

The position of gauges G5 and G6 (shown in Fig. 5-6) is higher than neutral axis, so it is in the compression zone. Crack pattern (in Fig. 4-11) shows that there is no crack crossing this area. From the Fig. 5-9b, G5 load-strain curve has the breaking point at the load

of around 350 kN, stirrups at this area have the strain about 100×10^{-6}, stirrups has not yielded yet, but it was affected by the under neutral axis cracked area. Fig. 5-9C reveals that horizontal components (recorded by strain gauges G8) were compressed, this position is in the compression zone. Moreover, they are not affected by cracks and yielded reinforcing bars also.

So, the role of each single CFRP bar depends on the location of the CFRP grid node. At the neutral axis, the state of stress is pure shear, and principal direction is 45°, so the vertical and the horizontal components have the same roles in contributing to the shear strength of RC beam 2. Out of the neutral axis area, vertical CFRP bars contribute the key role for the shear strength. Besides, the horizontal component works like anchors for enhancing the bonding between the vertical CFRP bars and the mortar.

5.2.3. Conclusions

According to the above analysis, two following findings about the effect of CFRP grid in shear-strengthening and behavior between horizontal and vertical components have been drawn. The contribution for shear strength of both components depends on the location of the CFRP grid in RC beam. With the CFRP node at the neutral axis, the roles of them are equal while at the remain positions, the vertical component is the important part for the shear strength. In general, vertical bar play a much more important role compared with the horizontal component. It provides more efficiency for control the shear failure. Furthermore, the horizontal component is also an anchor for the excellent adhesion between the vertical component and the mortar. The attitude of applying load, the appearance and the development of cracks also affect the contribution of vertical and horizontal CFRP bar.

Chapter 6:

ANALYSIS ON SHEAR STRENGTH OF RC BEAMS STRENGTHENED BY CFRP GRID BASE ON MECHANICAL MODEL

This section presents the generated theoretical equations to estimate the shear strength of strengthened RC beams base on the mechanical model. The problems are solved in two cases, RC beam shear-strengthened by CFRP grid and/without stirrups. The contribution to the shear strength is assumed to be the sum of the shear transferred by un-crack concrete compression zone, by stirrups, by CFRP grid, by residual tensile and frictional stresses of the critical crack. These equations have been checked with the cases of beams in chapter 4. In both cases of applying the CFRP grid, the un-crack concrete chord plays a vital role in the shear strength contribution (nearly 50%). And the estimated value of shear strength fits the experiment results very well.

Notations

a	shear span
b	width of concrete section
d	effective depth to main tension reinforcement
d_{max}	maximum aggregate size
f_{cc}	uniaxial concrete compressive strength
f_{cm}	mean value of the cylinder concrete compressive strength
f_{ct}	uniaxial concrete tensile strength
f_{yw}	yield strength of the transverse reinforcement
h	overall depth of concrete section
l_{sw}	crack length
l_w	length along the crack where the tensile stresses are extended
n_b	number of longitudinal bars
s	longitudinal coordinate from the support
s_{cr}	location of the section where the critical shear crack starts
s_t	stirrups spacing
s_u	location of the shear critical section
v_c	dimensionless contribution to the shear strength of the un-cracked concrete chord
v_l	dimensionless contribution to the shear strength of the longitudinal reinforcement
v_s	dimensionless contribution to the shear strength of the transverse reinforcement
v_w	dimensionless contribution to the shear strength of the critical crack
v_G	dimensionless contribution to the shear strength of the CFRP grid
v_u	dimensionless ultimate shear force
x	neutral axis depth
x_w	vertical projection of lw
y	vertical coordinate from the top fibre of the concrete element
A_s	longitudinal reinforcement area
A_{sw}	area per unit length of the transverse reinforcement
C	compression force in the un-cracked concrete chord
E_c	modulus of elasticity of concrete
E_s	modulus of elasticity of steel
G_c	modulus of shear deformation for the un-cracked concrete chord
G_f	concrete fracture energy
I_s	modulus of inertia of the longitudinal reinforcement
M	bending moment

M_{cr}	cracking moment
T	tensile force in the longitudinal reinforcement
V	shear force
V_c	contribution to the shear strength of the un-cracked concrete force
V_l	contribution to the shear strength of the longitudinal reinforcement
V_{pred}	predicted value of the ultimate shear force
V_s	contribution to the shear strength of the transverse reinforcement
V_{test}	experimental value of the ultimate shear force
V_u	ultimate shear force
V_w	shear force resisted along the crack
α_e	modular ratio ($E_s \backslash E_c$)
δ_w	crack opening in the vertical direction
δ_v	crack sliding in the vertical direction
ϕ	diameter of reinforcement bar
$\varepsilon_{ct,cr}$	concrete strain at the beginning of micro-cracking
$\varepsilon_{ct,u}$	ultimate tensile strain
ζ	size effect factor
γ	distortion
θ	inclination angle of the strut
λ	distance from the neutral axis
ρ	longitudinal tension reinforcement ratio
ρ_w	transverse reinforcement ratio
σ_1, σ_2	principal stresses
σ_{st}	stress in the transversal reinforcement
σ_x	normal stress in the longitudinal direction
$\sigma_{x,max}$	maximum normal stress in the longitudinal direction
σ_y	normal stress in the transverse direction
σ_w	normal stress in a horizontal fibre in the cracked web
τ	shear stress
τ_{max}	maximum shear stress
τ_{max}	maximum shear stress
τ_λ	shear stress at y= λ.x
H_G	horizontal force by CFRP grid at the critical section
V_G	vertical force by CFRP grid at the critical section

6.1. INTRODUCTION

From the result of chapter 4, there is a clear difference of maximum load between the estimated value and the experiment value when applying the equation of (JSCE et al. 1996) to calculate the shear strength. This difference is shown in Table 4-6. The application of shear strength estimating formula for stirrups to CFRP grid and the safety ratio of CFRP sheet for CFRP grid is not reasonable. There is a requirement for a formula to predict much more accurately the shear strength of the RC beam strengthened with CFRP grid.

Shear failure of a beam is a dangerous phenomenon of RC beams. Many previous studies have researched shear mechanism contribution. To assess the shear transfer mechanism, a large number of experiments have been conducted. To model such a complicated behavior, analytical and numerical models have been developed (Bairan Garcia and Mari 2006), Ferreira, Bairán, and Marí 2013; Mohr, Bairán, and Marí 2010; Vecchio and Collins 1986). Above models have contributed to the more adequate awareness of the evolution of the resisting mechanisms according to the experimentally observed behavior.

The applying these models in practical work, however, still includes a lot of difficulties, time consumption, and dependency on the numerous input parameters required. On the other hand, most simple equations recommended by the Code (ACI 2015; Can/Csa 2012; Canadian Standards Association 2014; JSCE et al. 1996). Fig. 6-1 shows the diagonal crack of RC beam failed due to the shear stress.
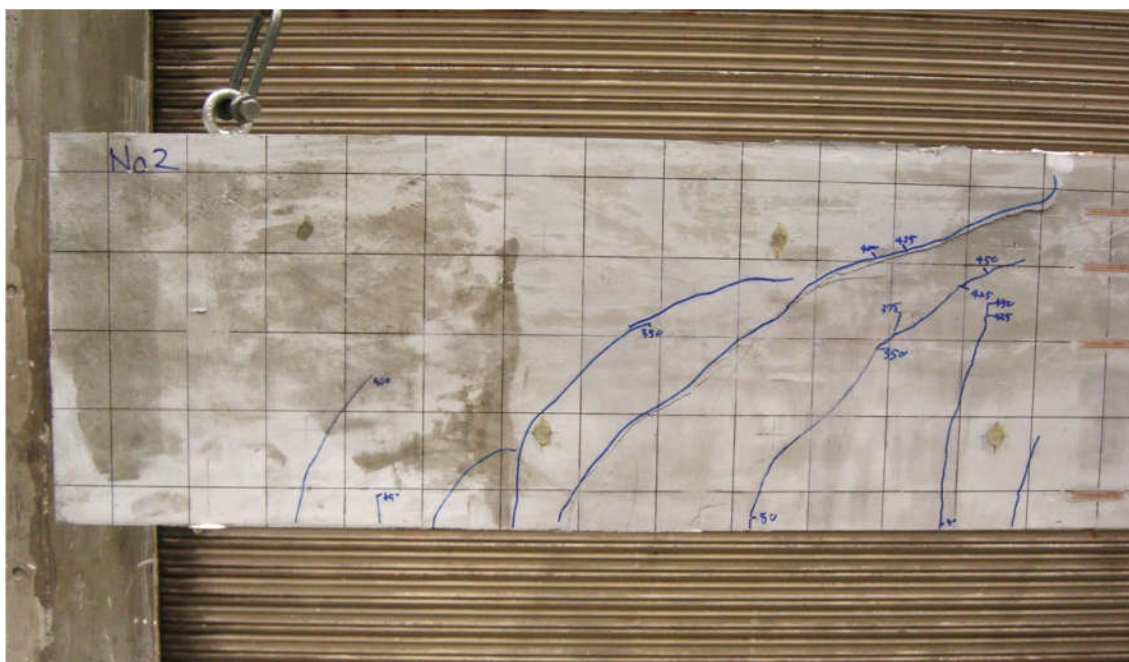
Figure 6-1: Failure crack pattern of shear-strengthened beam

6.2. PRINCIPLE OF PROPOSED METHOD

6.2.1. Shear transfer mechanism

When applying a load to a RC beam, it can be considered as an elastic body. Hence, the maximum principal tensile stress occurs at the extreme tension fiber within the mid span, and its direction is parallel to the member axis. As this principal tensile stress increases and exceeds the tensile strength of concrete, crack occurs in the direction perpendicular to the direction of principal tensile stress. This crack is called "flexural crack". After the flexural crack is formed, a RC beam is no longer considered to be an elastic body. However, since the tensile force is carried by longitudinal reinforcement, the state of stress even after flexural cracking is still similar to that of the principal stress of an elastic beam. When applied load is increased, the flexural crack propagates to the compression zone of the cross section. Also in both of side spans, the formulation of cracks occurs with an inclination with respect to the member axis. This crack is called "diagonal crack". The most rapidly propagating crack will be com the crictical crack. The critical crack is the one that leads to the collapse of the beams. with the slender beams with transverse reinforcement under 4 point-bending test, the damaged cracks normally consist of two branches.
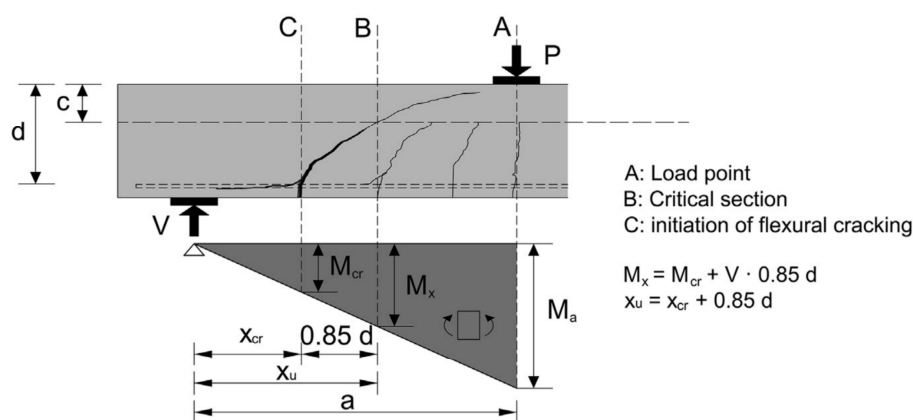
Fig. 5. Position of the critical section in the beam.

Figure 6-2: Position of the shear critical section in the beam.
Adapted from (Marí et al. 2015)

Generally, these two branches are formed at the different stage of load and are due to various other reasons. The first branch is an inclined shear crack, which develops from the starting of nearby flexural cracks till the intersection point with the neutral axis. It often occurs in the middle of flexural cracks and is formed at the end of bending cracks. Flexural cracks and inclined cracks have the same height as Fig. 6-2. As the load increases, the second branch of the crack occurs inside the compression concrete zone. The formation of the second branch of the critical crack causes the damage of beam. From the end of the first

branch, the second part of critical crack propagates, abruptly or gradually, toward the loading point crossing the compression zone. This failure mode is conventionally called diagonal tension failure, and it occurs only in slender beams (which have the shear span to depth ratio (a/d) greater than 2.5). In this section, analytical expressions are derived describing the characteristics of these two branches, as well as the mechanism of shear failure based on the following considerations. (Zararis and Papadakis 2001).

It is commonly admitted that the shear in RC beams is transferred in cracked concrete members by various action such as aggregate interlock, dowelling action, inclining compressive concrete zone, the transverse reinforcement and the residual tensile stresses along the crack. The attitude of shear transmitted by each action is considerably changed by the shape of the crack and by the kinematics at failure (Campana et al. 2013).

When applying the CFRP grid to increase the shear strength of concrete beams, CFRP grid has the same contribution as stirrups. They provide the following favorable effects:

- constraint to the diagonal crack opening, increasing the friction and the residual stresses;
- vertical confinement stresses on the compressed concrete chord, increasing its strength;
- support to the longitudinal bars, constraining their vertical displacement and enhancing their capacity;
- prevent brittle shear failure.

6.2.2. Assumption of the method

a) As widely adopted by many authors (Cladera et al. 2015, 2016; Marí et al. 2015; Oller et al. 2015), it is considered that the shear strength, V, in Eq. (1) is the sum of the shear resisted by the un-cracked concrete zone (V_c), the tensile stresses transferred along the crack, (V_w), the shear transferred by the longitudinal reinforcement in the presence of stirrups, (V_l), and the transverse reinforcement crossing the diagonal critical shear crack, (V_s). Fig. 6-3 presents the qualitative distribution of the shear stresses at the imminent shear failure section. The shear strength of sections can be calculated as below:

$$V = V_c + V_w + V_l + V_s = f_{ct}.b.d.(v_c + v_l + v_w + v_s) \tag{1}$$

The shear strength of strengthened beams, V_{st}, in Eq. 2, CFRP grid also contributes to the shear strength. The joint contribution of CFRP grid, V_G, shown in Fig. 6-4.

$$V_{st} = V_c + V_w + V_l + V_s + V_G = f_{ct}.b.d.(v_c + v_l + v_w + v_s + v_G) \tag{2}$$
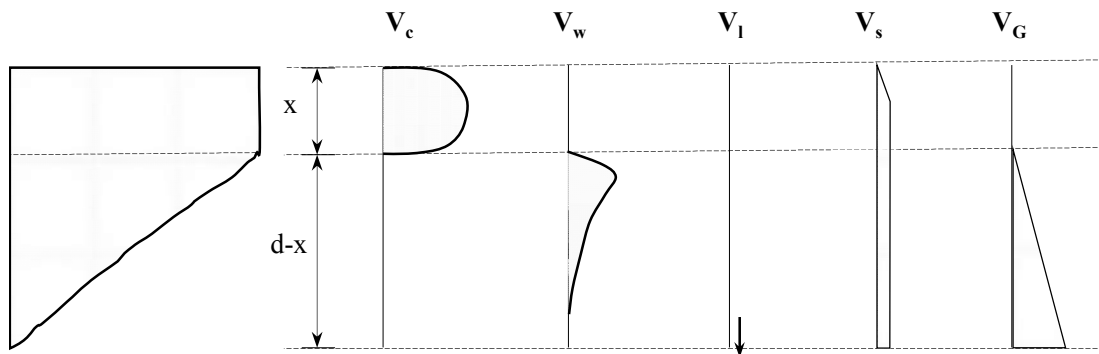
Figure 6-3: Qualitative distribution of shear stresses at imminent shear failure and distribution

Un-cracked concrete chord

Inclined crack

Longitudinal reinforcement (dowel action)

Transverse reinforcement

CFRP grid
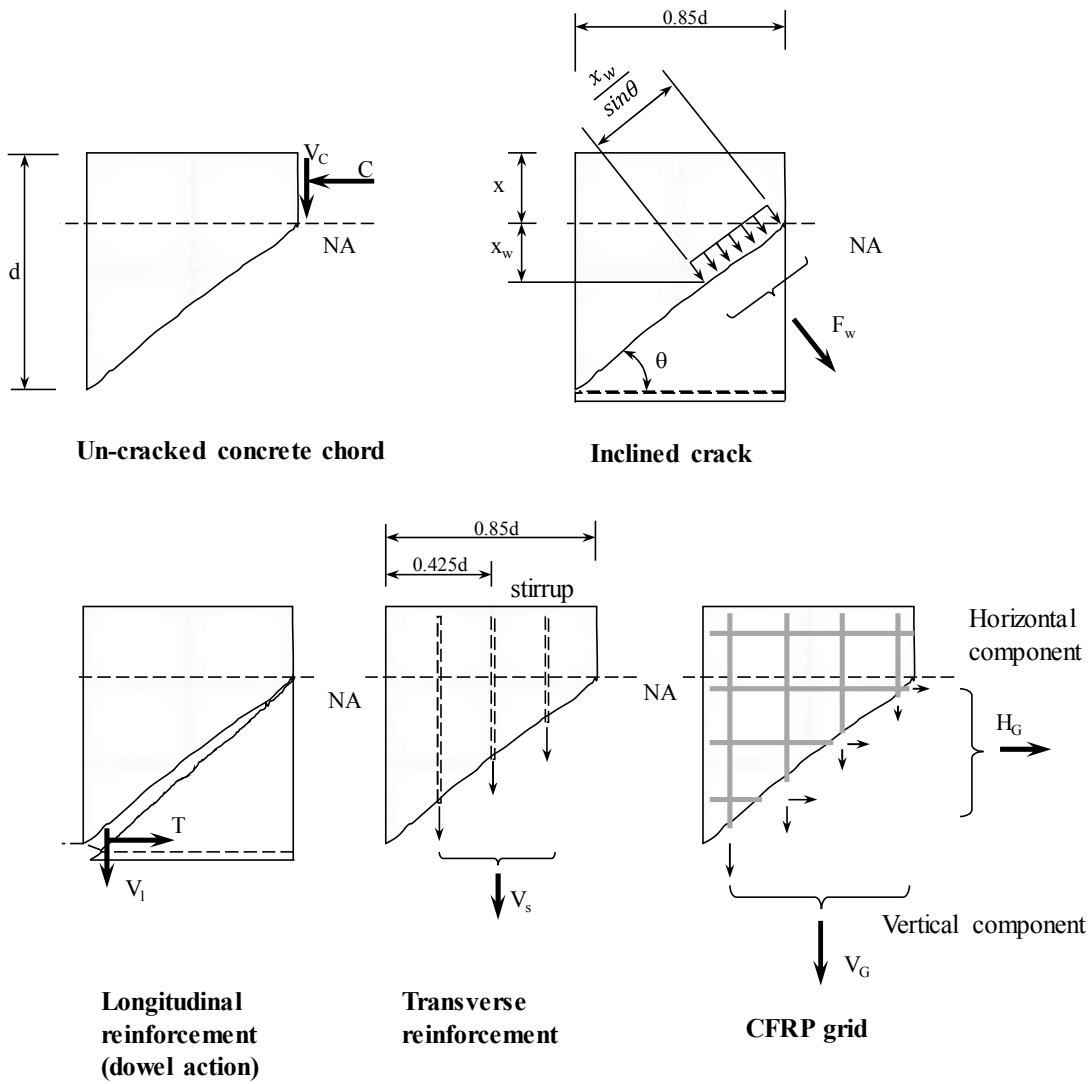
Figure 6-4: All joint contributions for the shear strength
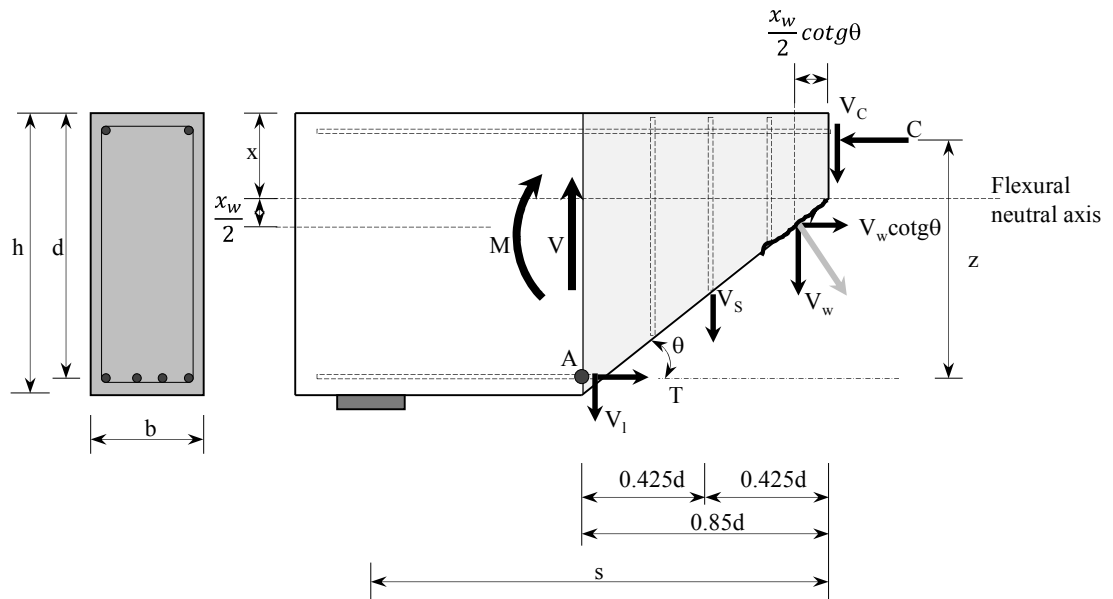
Figure 6-5: Shear transfer mechanism of RC beam with transverse reinforcement
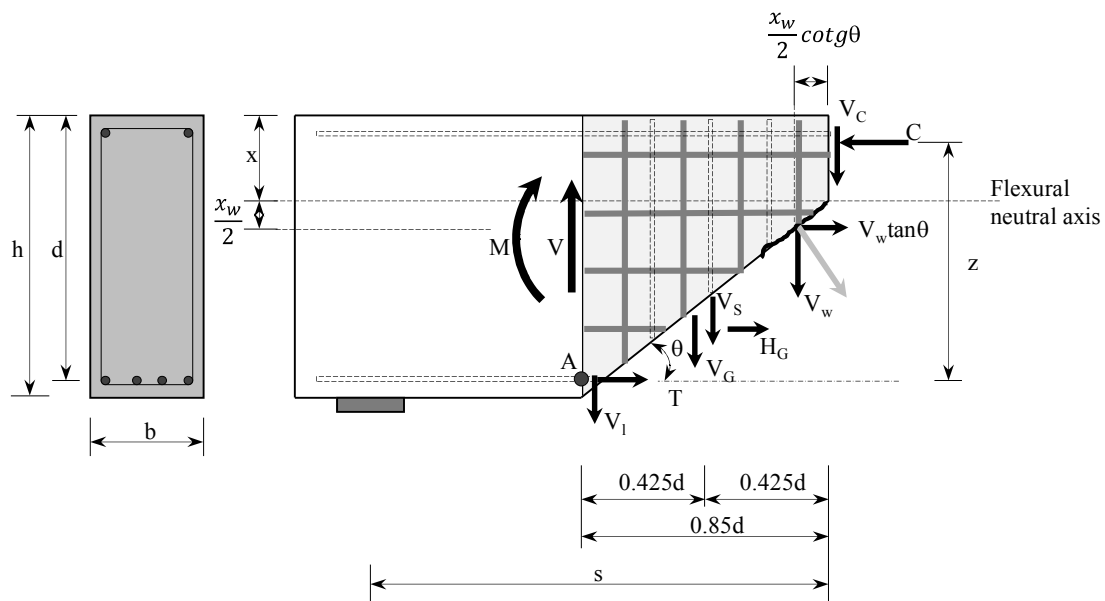
Figure 6-6: Shear transfer mechanism of RC beam

b) Neutral axis depth and the height of the un-crack concrete chord are the same. It can be determined by traditional analysis of cracked reinforced concrete section under pure flexure (Cladera et al. 2015);

c) According to many previous experimental studies, the horizontal projection of the critical crack that equals to *0.85d*, as shown in Fig. 6-2, has been widely adopted by the authors (Cladera and Marí 2005) (Marí et al. 2015). And θ is the inclined angle of the first branch with the central axis of beams. θ can be calculated by the Eq. (3) as follow:

$$cotg\theta = \frac{0.85}{1-\frac{x}{d}} \tag{3}$$

Actually, the inclination of the cracks depends on the longitudinal and transverse reinforcement ratios ρ and ρ_w, respectively. This value is in agreement with experimental observations from other researchers (Karayannis and Chalioris 2013). In general, the influence of longitudinal reinforcement ratio is more important. That influence is expressed through the neutral axis depth. As a result of this statement, the inclining angle is of critical crack decreases as the longitudinal reinforcement ratio increases, it means for the same strain, γ, the longitudinal tensile strain, ε_x, is lower.

d) Assumptions about the distribution of stresses along the un-cracked concrete chord. Fig. 6-8 describes the considered distributions of the normal stress and the shear stress on the failure section.

- σ_x distributes linearly; is consistent with the moderate level of normal stresses that exist in the critical section

- τ, shear stress distributes parabolically, is equal to 0 at the top fiber and the neutral axis, is maximum at $y = x/2$.
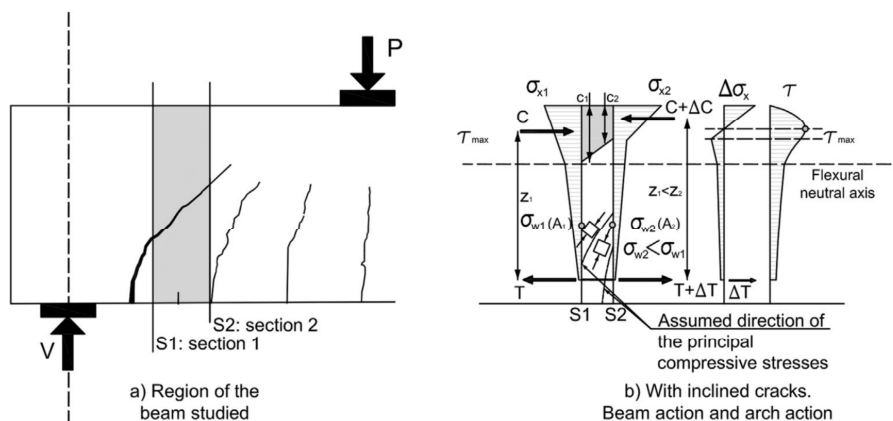
Figure 6-7: Stresses distribution in diagonally cracked reinforced concrete members
Adapted from (Marí et al. 2015)
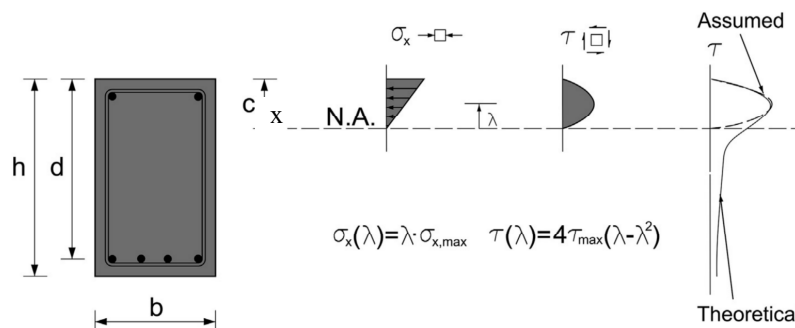
Figure 6-8: Considered distributions of stressed at the un-cracked concrete zone
Adapted from (Marí et al. 2015)

e) The compression concrete zone is subjected to a biaxial state of stresses. Failure is assumed to happen when the principal stresses (σ_1, σ_2) reaches the Kupfer's biaxial

failure envelope (Kupfer and Gerstle 1973). Fig 6-9 shows the Kupfer's biaxial failure envelope.
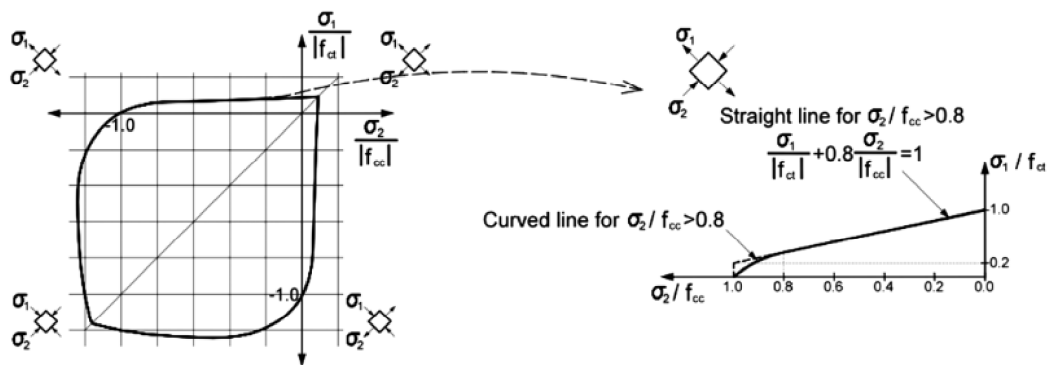
Figure 6-9: Adopted failure envelop for concrete under a biaxial stress state.
Adapted from (Kupfer and Gerstle 1973)

f)   At the ultimate state, all the present stirrups crossed by the critical cracks yielded.

g)   Generally, the longitudinal reinforcing bars are made from the deformed bars, excellently bonded with concrete, so that all reinforcement is effective at the critical section.

h)   At ultimate state, the CFRP bar that gets the maximum stress reaches the tensile strength of CFRP grid. The horizontal component of CFRP grid works as effective anchors. Internal horizontal forces of horizontal bars of CFRP grid is small when compared to the internal forces of longitudinal reinforcing bars. So, the vertical effect to shear contribution of the horizontal bars of CFRP grid is neglected.

i)   Ignore the compression capability of CFRP grid in the compression concrete chord. CFRP grid is supposed that the compressive strength is considerably smaller than the tensile strength (Ueda, Hiraga, and Nishimura 2011).

j)   Ignore the direct contribution of CFRP horizontal component to the shear strength, even the longitudinal reinforcement is much higher contribution when compared with a horizontal bar of CFRP grid but, contribute less than 5% of the total shear strength of RC beams (Oller et al. 2015).

Contributing part of longitudinal bars, in general, depend on the relative neutral axis depth and neutral axis depth is also influenced by reinforcement ratio of CFRP grid.

k)   In the compression zone, the mortar works as well as the concrete.

6.3. FORMULATION OF THE METHOD

6.3.1. Contribution of cracked concrete web

The shear transferred along the critical crack is considered due to the residual tensile stresses and the frictional forces. All of these factors relate to the roughness of the crack surface. The residual stressed are the tensile stresses that concrete can resist in tension, up to a maximum crack width. Frictional forces are those, which oppose the slip between both surfaces of the crack and decrease as the crack width increases. Both types or stresses are interrelated as crack opening and crack slip are too, but it is difficult to obtain them separately. For this reason, in this work, only the residual stresses are considered and it will be assumed that the resulting principal stresses are normal to the averages crack surface. The residual stress is considered distributed as a uniform load along the critical crack on the length of $x_w/\sin\theta$.

In order to evaluate the residual tensile stresses, a tensile stress-strain curve with a post-peak linear softening branch will be considered, in which the ultimate tensile strain $\varepsilon_{ct,u}$ depends on the fracture energy. See Fig 6-10.
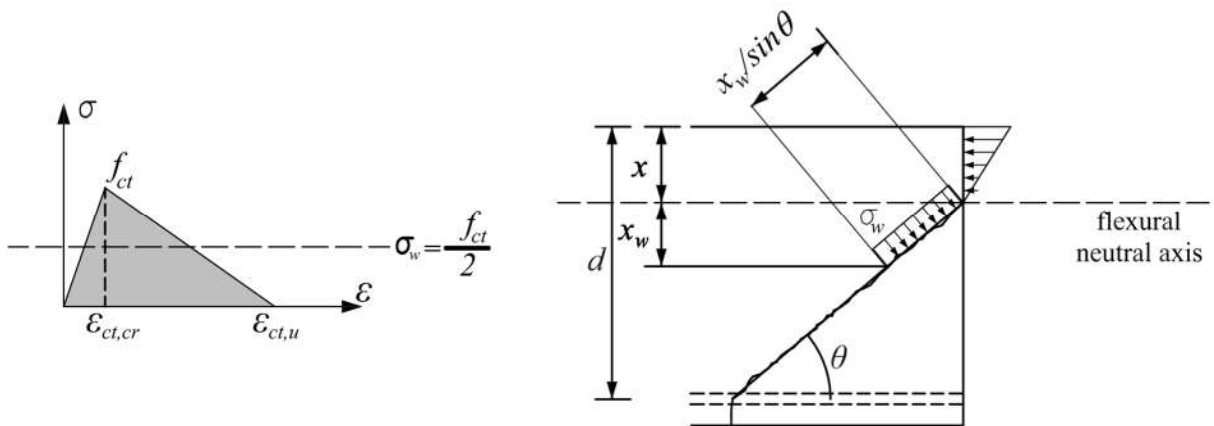
Figure 6-10: contribution of cracked concrete to shear resistance

The expression of the shear force resisted along the crack, V_w, is:

$$V_w = \int_0^{l_w} \sigma_w \cdot b \cdot \cos\theta \cdot dl \approx \frac{x_w}{\sin\theta} \cdot \sigma_w \cdot b \cdot \cos\theta$$

$$= x_w \cdot \sigma_w \cdot b \cdot \cot\theta \tag{4}$$

where

$\sigma_w = f_{cr}/2$ is the adopted constant concrete tensile stress, extended to a length l_w of the crack, which is energetically equivalent to the actual triangular distribution.

x_w the length of the tensile zone, is obtained by setting the compatibility of deformations in the direction normal to the crack, and with the regards to the geometrical relationships indicated in Fig. 4-8.

$$x_w = (d - x) \cdot \frac{\varepsilon_{ct,u}}{\varepsilon_s} \cdot \sin^2 \theta \qquad (5)$$

where

ε_s is the strain in the longitudinal reinforcement.

The ultimate tensile strain of Concrete: The state of stress affects the failure characteristics of concrete. Concrete is most brittle under tension. The tensile strain capacity, which is used to assess cracking in concrete structures, should be chosen judiciously differing on the state of stress. The limiting tensile strain in the uniaxial compressive test lies between 300 μ and 500 μ. The tensile strain capacity of concrete lies between 150 μ and 210 μ in the flexural-strength test and between 100 μ and 140 μ in the direct tension test. (Wee, Swaddiwudhipong, and Lu 2000).

By imposing the compliance between the crack opening at the level of the longitudinal reinforcement and at the point of the crack where the residual tensile stress is zero, and relating the crack opening to the reinforcement longitudinal strain ε_s and the crack spacing. The shear transferred along the closet part of the crack can be expressed as a function of ε_s. At ultimate a strain in the reinforcing bar close to 0.0009 has been assumed. The complete derivation of this equation can be found in (Marí et al. 2015).

$$v_w = \frac{V_w}{f_{ct}.b.d} = 167.\frac{f_{ct}}{E_c}.\left(1 + \frac{2.E_c.G_f}{f_{ct}^2.d}\right) \qquad (6)$$

where

G_f is the fracture energy of concrete, which depends on the concrete strength and the aggregate size. According to (FIB- Bulletin 42 2013) G_f can be computed as Eq. 7;

$$G_f = G_{Fo} \cdot \left(\frac{f_{cm}}{f_{cmo}}\right)^{0.18} \qquad (7)$$

where

f_{cm} is mean concrete compressive strength (MPa);

f_{cmo} = 10 MPa is mean concrete compressive strength (MPa);

$G_{Fo} = 0.11 \ N/mm$ base value of fracture energy which depends on maximum aggregate size.

6.3.2. Contribution of the longitudinal reinforcement

The contribution of the longitudinal reinforcement is strongly influenced by the presence of transverse reinforcing bars. Stirrups constraint the vertical movement of longitudinal reinforcing bars, enable them to carry a certain shear strength. In order to

evaluate such contribution, it is considered that the longitudinal bars are doubly fixed at the two stirrups adjacent to the crack, and subjected to bending due to a relative imposed displacement between the two extremities. This relative vertical displacement is caused by the opening of the critical crack and by the shear deformation of the compression chord. This contribution obviously depends on the tensile steel ratio, which is implicitly represented by means of *c/d*. The contribution of the longitudinal reinforcement is less than 5% of the shear strength. Therefore, a simplified expression is presented in Eq. 8. A more detailed derivation of the equation is carried out in (Marí et al. 2015).

$$v_l = \frac{V_1}{f_{ct}.b.d} \approx 0.23.\frac{\alpha_e \cdot \rho}{1-\xi} \approx 0.25.\xi - 0.05 \qquad (8)$$

where

α_e: modular ratio (E_s/E_c)

ρ: the longitudinal reinforcement ratio

$\xi = \xi/d$: the relative neutral axis depth

6.3.3. Contribution of the transverse reinforcement to the shear strength

The contribution of the transverse reinforcement to shear strength is taken as the sum of the forces in the stirrups that intersect the inclined crack from the bottom of the beam to a height of (d_s-*c*), as shown in Fig. 4-2. In this model, it is supposed that failure, all transverse reinforcement yielded along the ultimate crack height. Then the contribution of stirrups to the shear strength can be calculated as Eq. 9, in non-dimensional terms.

$$v_s = \frac{V_s}{f_{ct}.b.d} = \frac{0.85.d.A_{sw}\cdot f_{yw}}{f_{ct}.b.d} = 0.85.\rho_w.\frac{f_{yw}}{f_{ct}} \qquad (9)$$

where

A_{sw}: is the area per unit length of transverse reinforcement;

ρ_w: is the transverse reinforcement ratio;

f_{yw}: is the yield strength.

6.3.4. Contribution of the CFRP grid

CFRP grid consists of two components: vertical bars and horizontal bars. Fig. 6-11 shows the internal force of each CFRP component; vertical bars and horizontal bars. In this proposed model, the contribution of horizontal bars for the shear strength is small, like the longitudinal reinforcing bars. The CFRP vertical bar acts as anchors to enhance the bonding between the vertical bars and the concrete chord. The role of vertical bars is only concerned with this model.

The contribution of the CFRP vertical bars to shear strength is taken as the sum of tensile stresses at the vertical bars crossing the critical shear crack from the bottom of the beam to a height of (d_s-*c*), whose the horizontal projection is equal to $0.85 \times$ d, as shown in Fig 6-11.

Internal force in vertical CFRP bars   Internal force in horizontal CFRP bars   Internal force in both CFRP components
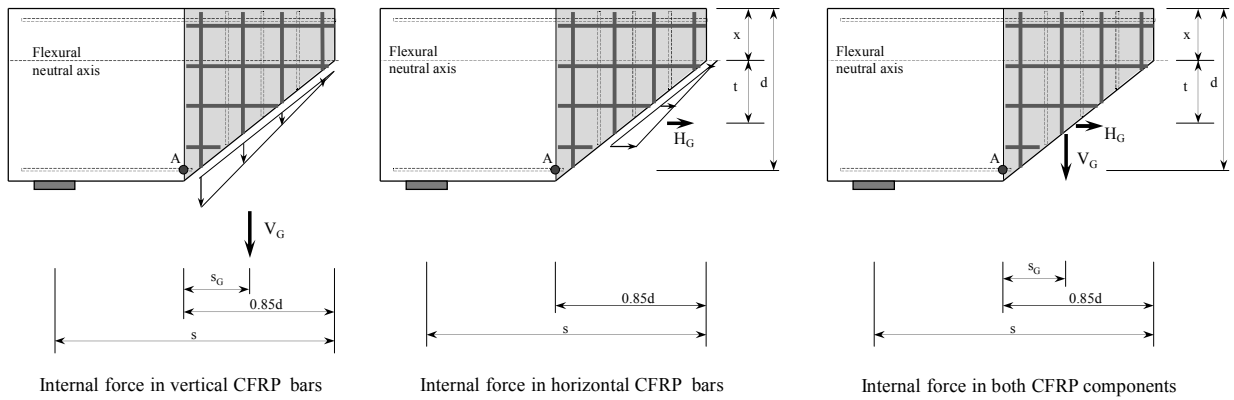
Figure 6-11: Internal force of CFRP: horizontal and vertical bar

The linear distribution of stresses in CFRP vertical bars crossing the critical shear crack is illustrated in Fig. 6-12 as below:
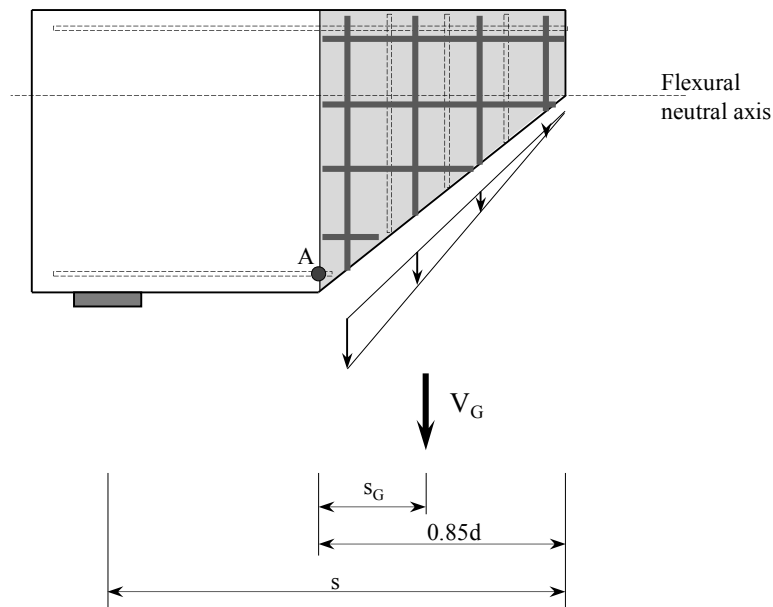
Figure 6-12: Contribution of CFRP grid vertical bar

The contribution of CFRP grid is calculated based on the triangular distribution of force. The non-dimensionless contribution of CFRP grid is defined as Eq.30.

$$v_G = \frac{V_G}{f_{ct}.b.d} = \frac{1}{f_{ct}.b.d}\left(\frac{1}{2}f_G \cdot A_G \cdot 0.85 \cdot d\right) \tag{30}$$

where

$$\mathrm{v}_G = 0.425 \cdot \frac{f_G}{f_{ct}} \cdot \rho_G \tag{31}$$

$$\rho_G = \frac{A_G}{b} \tag{32}$$

A_G: area per unit length of CFRP grid for the vertical bar only

ρ_G: reinforcement ratio of CFRP grid

f_G: tensile strength of CFRP grid
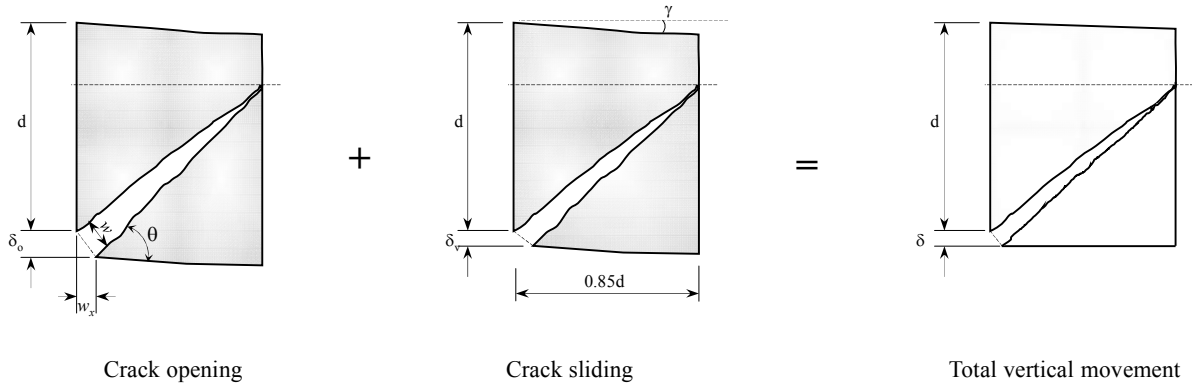
Figure 6-13: Movement components of the crack surface

In order to assess shear force, it is considered in this work that the longitudinal bars are double fixed at the two stirrups adjacent to the crack initiation, and subjected to bending due to a relative imposed displacement between their ends. In this manner, the relative displacement between the two crack surfaces is smeared along the stirrups spacing.

The relative vertical displacement between the crack surfaces is considered as the sum of two components:
-   one due to the crack opening δ_o (see Fig 6-13)
-   one due to the crack sliding δ_v.

6.3.5.   Contribution of the un-cracked concrete chord

The contribution of the compression concrete zone to the shear strength can be calculated by the formulas adapted by (Marí et al. 2015) for RC beams with and without stirrups, which was adapted for the case of FRP RC beams without stirrups (Marí et al. 2014). A concise summary of the model is expressed as follow.

Define the normal stress, shear stress of un-cracked concrete zone. See Fig. 6-14.
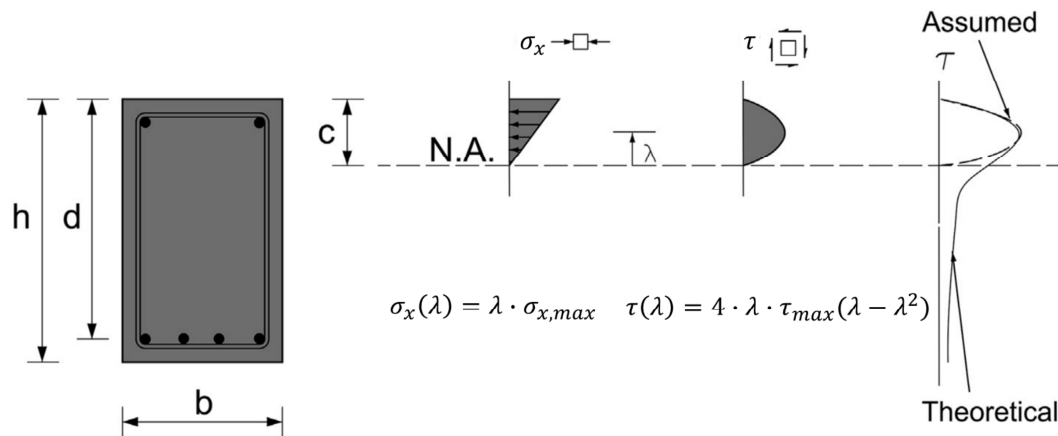
Figure 6-14: Considered distribution of stresses at the un-cracked concrete chord. Adapted from (Marí et al. 2015)
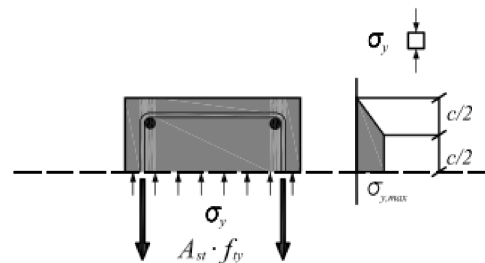
Figure 6-15: Compression stress caused by the stirrups in the un-cracked concrete zone.

Normal stress in y-direction is the compression stress of the longitudinal fiber of concrete material interact with each other. Normal stress in y-direction is illustrated in Fig. 6-15.

It causes by the confinement effect of stirrups. Stirrup often is made from deformed bars, and shaped into a full frame. Thus it provides a good adherence with concrete. Cross-section of CFRP bars is a rectangle. Therefore, a CFRP bar could be considered as a rough bar. The frictional force between vertical CFRP bars is small. In (Wang 2016), it is supposed that the vertical bars of CFRP grid need an adequate length to perform the fictional bondging strength with mortar. In general, the vertical bars contribute ahaft strength to the tensile strength. Moreover, the result revealed in chapter 3, with a limited height of the compresive concrete chord, the bonding lenght between mortar and concrete is not enought to support the full capacity of CFRP tensile strength. Consequently, the confining effect caused by CFRP is much smaller than by stirrups. Then, in this calculation, ignore the confining effect caused by CFRP grid.

Principle stress at any point in concrete chord base on normal stress in x,y direction and the shear stress.

$$\sigma_{1,2} = \frac{\sigma_x + \sigma_y}{2} \pm \sqrt{\left(\frac{\sigma_x - \sigma_y}{2}\right)^2 + \tau^2} \tag{38}$$

By mathematical transformation we obtain Eq. 39.

$$\tau = \sigma_1 \sqrt{1 - \frac{\sigma_x + \sigma_y}{\sigma_1} + \frac{\sigma_x \cdot \sigma_y}{\sigma_1^2}} \tag{39}$$

$$\tau(y) = f(y) \tag{40}$$

      The shear strength contributed by the un-cracked concrete chord when the principal tensile stress reaches the concrete tensile strength is obtained by integrating the shear stressed along the concrete surface, as below:

$$V_c = \int_0^x \tau(\gamma) \cdot b \cdot dy = \frac{\tau_\lambda \cdot b \cdot x}{6 \cdot \lambda \cdot (1-\lambda)} \tag{41}$$

$$V_C = K_\lambda \cdot b. x. \sigma_1 \sqrt{1 - \frac{\sigma_x + \sigma_y}{\sigma_1} + \frac{\sigma_x \cdot \sigma_y}{\sigma_1^2}} \tag{42}$$

where

$$K_\lambda = \frac{1}{6 \cdot \lambda \cdot (1-\lambda)} \tag{43}$$

and

$$\xi = \frac{x}{d} \quad : \text{dimensionless neutral axis depth}$$

where;

      x :   is the neutral axis depth calculated according to Eq. 47

      σ_x :   is the concrete normal stress

      τ_λ :   is the shear stresses at the failure point, placed at a distance $y = \lambda.c$ from the neutral axis

The value of the neutral axis depth, x, is:

$$\xi = \frac{x}{d} = \alpha_e \cdot \rho \cdot \left(-1 + \sqrt{1 + \frac{2}{\alpha_e \cdot \rho}}\right) \tag{44}$$

where;

      $\alpha_e = E_s/E_c$: is the modular ratio between;

      E_s :is the reinforcement longitudinal modulus;

      E_c :is the Young modulus of concrete;

      $\rho = A_s/(b.d)$: is the longitudinal reinforcement ratio;

      b : the section width.

Failure follows the Kupfer's biaxial failure envelop

$$\frac{\sigma_1}{f_{ct}} + 0.8. \frac{\sigma_2}{f_{cc}} = 1 \tag{45}$$

Place

$$R_t = \frac{\sigma_1}{f_{ct}} = 1 - 0.8. \frac{\sigma_2}{f_{cc}} \tag{46}$$

R_t is the ratio between the principal tensile stress σ_I and the tensile strength f_{ct} at the critical point. R_t is a reduction factor of tensile strength due to the multiaxial stress stage.

Non-dimensionless shear strength contributed by the un-crack concrete zone can be defined by this following equation:

$$v_C = K_\lambda \cdot R_t \cdot \xi \cdot \sqrt{1 - \frac{\sigma_x + \sigma_y}{\sigma_1} + \frac{\sigma_x \cdot \sigma_y}{\sigma_1^2}} \tag{47}$$

Critical point inside the un-crack concrete chord
with the coordinate of

$$y = 0.425 \cdot x \tag{48}$$

$$\lambda_{critical\ point} = 0.425 \tag{49}$$

The critical section is not a flat plane, it is formed due to the propagation of the critical crack. Normally, it starts from the bottom of the cross section where the moment reaches the cracking moment of the section. This unflat section is difined by the two bracnch of the critical crack. At the ultimate loading stage it crosses the neutral surface and turns toward the loading point.

The starting point of the critical section is defined by a distance s_{cr} from the support, as follow:

$$S_{cr} = \frac{M_{cr}}{V_u} \tag{50}$$

The intersection between critical section and the neutral surface sets the surface of the concrete chord. See Fig. 6-6. This ending point is located by a distance s from the support, s (see Fig. 6-6) is calculated as follow:

$$s = s_{cr} + 0.85d = s_{cr} + \frac{M_{cr}}{V_u} \tag{51}$$

Fig. 6-6 illustrates the critical section and the distances; s and s_{cr}. Equilibrium of moment is taken with respect to the point A, point A is the intersection of the critical crack and the longitudinal reinforcement. See Fig. 6-6.

$$C = T + H_G + V_w \cdot tan\ \theta \tag{52}$$

$$V = V_c + V_w + V_s + V_G + V_l \tag{53}$$

$$0 = M - C.z + V_c \cdot 0.85 \cdot d + V_w \cdot \frac{(0.85 \cdot d - 0.5 \cdot x_w \cdot \cot\theta)}{\cos^2\theta} + V_s \cdot \frac{0.85}{2} \cdot d + V_G \cdot \frac{0.85}{3} \cdot d + H_G \cdot \frac{d-x}{3} \tag{54}$$

where

$$z = d - \frac{x}{3} \tag{55}$$

$$C = b \cdot \frac{1}{2} \cdot \sigma_{x,max} \cdot x \tag{56}$$

$$\Rightarrow \ \sigma_{x,max} = \frac{2C}{b \cdot x} \tag{57}$$

The strain of horizontal CFRP bar is restrained due to the longitudinal movement of the tensile reinforcement bars. Consequently, Moment by CFRP horizontal force H_G is small compared with other forces. So HG is conservatively ignored.

At any point at concrete chord, see Fig. 6-14, the normal stress of x-direction is defined by a linear dependence as below:

$$\sigma_x(\lambda) = \lambda \cdot \sigma_{x,max}, = \lambda \cdot \frac{2 \cdot C}{b \cdot x} \tag{58}$$

From equilibrium equation Eq.54, it can be rewritten as Eq. as follow.

$$C = \frac{1}{d - \frac{x}{3}} \cdot \left(M + V_c \cdot 0.85 \cdot d + V_w \cdot \frac{(0.85 \cdot d - 0.5 \cdot x_w \cdot \cot\theta)}{\cos^2\theta} + V_s \cdot \frac{0.85}{2} \cdot d + V_G \cdot \frac{0.85}{3} \cdot d \right) \tag{59}$$

Substitute Eq. 59 to Eq. 58, we have

$$\sigma_x = \frac{2 \cdot \lambda}{b \cdot x \cdot \left(d - \frac{x}{3}\right)} \cdot \left(M + V_c \cdot 0.85 \cdot d + V_w \cdot \frac{(0.85 \cdot d - 0.5 \cdot x_w \cdot \cot\theta)}{\cos^2\theta} + V_s \cdot \frac{0.85}{2} \cdot d + V_G \cdot \frac{0.85}{3} \cdot d \right)$$

$$\tag{60}$$

Replace with:

$$\frac{M}{f_{ct} \cdot b \cdot d^2} = \mu \ \text{dimensionless bending moment} \tag{61}$$

$$\frac{x}{d} = \xi$$

$$d_w = \frac{(0.85 \cdot d - 0.5 \cdot x_w \cdot \cot\theta)}{d \cdot \cos^2\theta} \tag{62}$$

then $d_w.d$ = level arm of force V_w with respect to the point A

The relationship between the joint contributions of the transverse reinforcement crossing the diagonal critical shear crack V_s and of the CFRP vertical bars V_S
From which Eq. 31 and

$$\frac{v_G}{v_s} = \frac{0.425 \cdot f_G \cdot \rho_G}{0.85 \cdot f_{yw} \cdot \rho_w} = \frac{1}{2} \cdot \frac{f_G}{f_{yw}} \frac{\rho_G}{\rho_w} \tag{63}$$

Consider the average tensile strength of transverse reinforcement (steel) is 400 Mpa while the tensile strength of CFRP grid is 1400 Mpa.

And with a normal shear strengthening purpose for RC beam, the ratio between the transverse reinforcement of CFRP grid and stirrup is 2:

$$\frac{f_G}{f_{yw}} = \frac{1400}{400} = 3.5 \tag{64}$$

Then

$$\frac{v_G}{v_s} = 3.5 \tag{65}$$

Substitute into Eq. 60

$$\sigma_x = \frac{f_{ct} \cdot \lambda}{\xi \cdot \left(1 - \frac{\xi}{3}\right)} \cdot (\mu + 1.7 \cdot v_c + 2 \cdot d_w \cdot v_w + 2.831 \cdot v_s) \tag{66}$$

$$\sigma_y = f_{ct} \cdot \frac{A_{sw} \cdot f_{yw}}{f_{ct} \cdot b} = \frac{f_{ct} \cdot V_s}{0.85 \cdot f_{ct} \cdot b \cdot d} = \frac{f_{ct} \cdot v_s}{0.85} \tag{67}$$

Substitute Eq. 66, 67 to Eq. 47, considering the rule of negative or positive of stress.

$$v_c = \frac{V_c}{f_{ct} \cdot b \cdot d} = R_t \cdot K_\lambda \cdot \xi \cdot \sqrt{1 + \frac{\lambda}{\xi \cdot (1 - \frac{\xi}{3}) \cdot R_t} \frac{(2 \cdot \mu + 1.7 \cdot v_c + 2 \cdot d_w \cdot v_w + 2.831 \cdot v_s)}{} \cdot \left(\frac{v_s}{0.85 \cdot R_t} + 1\right) + \frac{v_s}{0.85 \cdot R_t}}$$

$$\tag{68}$$

μ is the dimensionless moment at the cross-section that contains the starting point of the critical crack. See Fig. 6-6. The critical crack initiates when the moment of this cross-section reach the cracking moment, M_{cr}, which in non-dimensional terms:

$$\mu_{cr} = \frac{M_{cr}}{f_{ct} \cdot b \cdot d^2} = \frac{b \cdot h^2 \cdot f_{ct}}{6 \cdot f_{ct} \cdot b \cdot d^2} = \frac{1}{6} \cdot \left(\frac{h}{d}\right)^2 \approx 0.2 \tag{69}$$

In an actual experiment that reports in (Oller et al. 2015), the value of v_c higher much more than v_w, the average of v_w equal to 0.15 can be adopted.

Because the contribution of vw is small compared to the other type of contribution, the lever arm, d_w, of v_w with respect to the point A could be conservatively adopted a value of 0.425. This is consistent with (Oller et al. 2015) and (Marí et al. 2016).

R_t is determined by the principle stress, then depends on the normal stress and the shear stress also. v_c is calculated by the value of normal stress Eq.66 and shear stress Eq.67. And Rt, consequently influenced by the shear force v_c

To solve the Eq. 68, the iterative method needs to be applied. Value of R_t can be initially chosen equal to 1. As v_c is calculated, normal stress, shear stress, and principle stress are also determined. R_t is recalculated by Eq. 46.
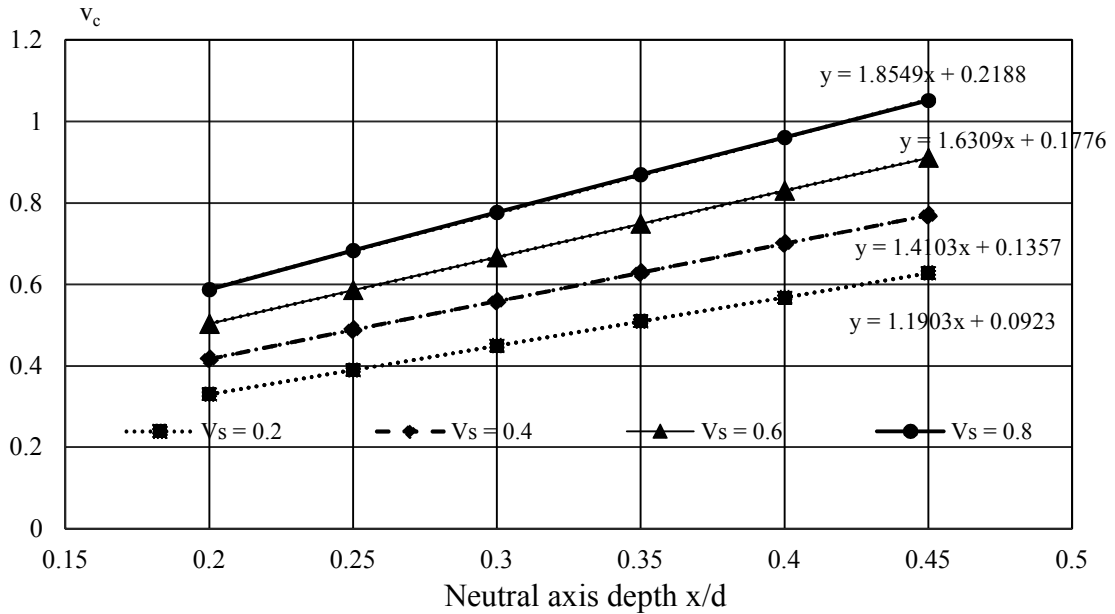
Figure 6-16: Non-dimensionless shear strength by the un-cracked concrete chord

Fig. 6-16 shows the result of equation Eq. 68 for different value of neutral axis depth and the transverse reinforcement contribution v_s.

From the Fig. 6-15, it is indicated that the relationship between the shear contribution of the un-cracked concrete zone and the neutral axis depth is linear. This result is consistent with earlier studies, (Marí et al. 2014; Oller et al. 2015; Tureyen and Frosch 2003).

The solution of Eq. 68 can be modified and expressed in a linear function of neutral axis depth, x/d.

$$v_c = (1.0829 \cdot v_s + 0.968) \cdot \xi + 0.2172 \cdot v_s + 0.0508 \qquad (70)$$

To obtain a more simple form of the practical equation, the term of *0.2172×v_t* is included inside the parenthesis, an average value of *ξ = 0.25* is assumed (Oller et al. 2015). The Eq. 70 turns into Eq. 71

$$v_c = (1.95 \cdot v_s + 0.968) \cdot \xi + 0.05 \qquad (71)$$

Influence of size effect (Zararis and Papadakis 2001) suggested a reduction factor due to the size effect of the experimental specimen.

$$\zeta = 1.2 - 0.2a \qquad (72)$$

where

a: shear span, in meter

Taking to account the reduction factor of size influence, the Eq.71 can be guessed by following:

$$v_c = \zeta \cdot \left((1.95 \cdot v_s + 0.968) \cdot \xi + 0.05 \right) \qquad (73)$$

115

Equation Eq. 73 is solved in case of transverse reinforcement of CFRP grid and stirrup is $\frac{\rho_G}{\rho_w} = 2$. With other demand of reinforcement, the Eq. 68 need to be resolved. The calculating process is accomplished similarly; the list of results is displayed as follow:

with $\frac{\rho_G}{\rho_w} = 0.5 \implies v_c = \zeta \cdot \left((1.4 \cdot v_s + 0.974) \cdot \xi + 0.046\right)$

(74)

with $\frac{\rho_G}{\rho_w} = 1.0 \implies v_c = \zeta \cdot \left((1.6071 \cdot v_s + 0.9749) \cdot \xi + 0.046\right)$

with $\frac{\rho_G}{\rho_w} = 1.5 \implies v_c = \zeta \cdot \left((1.7867 \cdot v_s + 0.9644) \cdot \xi + 0.0507\right)$

with $\frac{\rho_G}{\rho_w} = 2.5 \implies v_c = \zeta \cdot \left((2.119 \cdot v_s + 0.9641) \cdot \xi + 0.0542\right)$

with $\frac{\rho_G}{\rho_w} = 3.0 \implies v_c = \zeta \cdot \left((2.2728 \cdot v_s + 0.9663) \cdot \xi + 0.0552\right)$

After modified, the general form of these equations can be expressed without depending on $\frac{\rho_G}{\rho_w}$ as below:

$$\implies v_c = \zeta \cdot \left((0.198 \cdot v_G + 1.2496 \cdot v_s + 0.969) \cdot \xi + 0.05\right) \qquad (75)$$

6.3.6. For the beam have no stirrup, only transverse reinforcement by CFRP grid.

Without the appearance of stirrups, the shear strength of beams is the sum of contributions of the un-crack concrete chord, the longitudinal reinforcement, the residual tensile stress of the inclined crack and the CFRP grid, Eq. 2 can be expressed as follow:

$$v = v_c + v_l + v_w + v_G \tag{76}$$

the analysis for v_l, v_w, v_G is same as the previous calculation.

The non-dimensional terms of longitudinal reinforcing bars, the residual tensile stress of the critical crack is similarly calculated as in the case of with stirrups. Difference between two cases of beams, is the stage of stress of the un-crack concrete chord. With the beam that has the stirrup, the confined effect cause the normal compressive stress in the y-direction. Without the appearance of stirrups, the longitudinal fiber of beam is assumed that no longer interact each others. Then, the normal stress in y-direction is equal to zero.

$$\sigma_y = 0 \tag{77}$$

The Eq. 47 turns into Eq. 78

$$v_C = K_\lambda \cdot R_t \cdot \xi \cdot \sqrt{1 - \frac{\sigma_x}{\sigma_1}} \tag{78}$$

The normal stress

$$\sigma_x = \frac{2 \cdot \lambda}{b \cdot x \cdot \left(d - \frac{x}{3}\right)} \cdot \left(M + V_c \cdot 0.85 \cdot d + V_w \cdot \frac{(0.85 \cdot d - 0.5 \cdot x_w \cdot \cot\theta)}{\cos^2\theta} + V_G \cdot \frac{0.85}{3} \cdot d\right) \tag{79}$$

$$\sigma_x = \frac{2 \cdot f_{ct} \cdot \lambda}{\xi \cdot \left(1 - \frac{\xi}{3}\right)} \cdot (\mu + 0.85 \cdot v_c + d_w \cdot v_w + 0.283 \cdot v_G) \tag{80}$$

Assume

$\mu = 2$

$v_w = 0.15$

$d_w = 0.425$

$$\sigma_x = \frac{f_{ct} \cdot \lambda}{\xi \cdot \left(1 - \frac{\xi}{3}\right)} \cdot (0.52375 + 1.7 \cdot v_c + 0.566 \cdot v_G) \tag{81}$$

Substitute to Eq. 78

$$v_c = \frac{V_c}{f_{ct} \cdot b \cdot d} = R_t \cdot K_\lambda \cdot \xi \cdot \sqrt{1 + \frac{\lambda}{\xi \cdot (1 - \frac{\xi}{3}) \cdot R_t} (0.52375 + 1.7 \cdot v_c + 0.566 \cdot v_G)} \tag{82}$$

The solution for Eq. 82 is shown in Fig. 6-17.
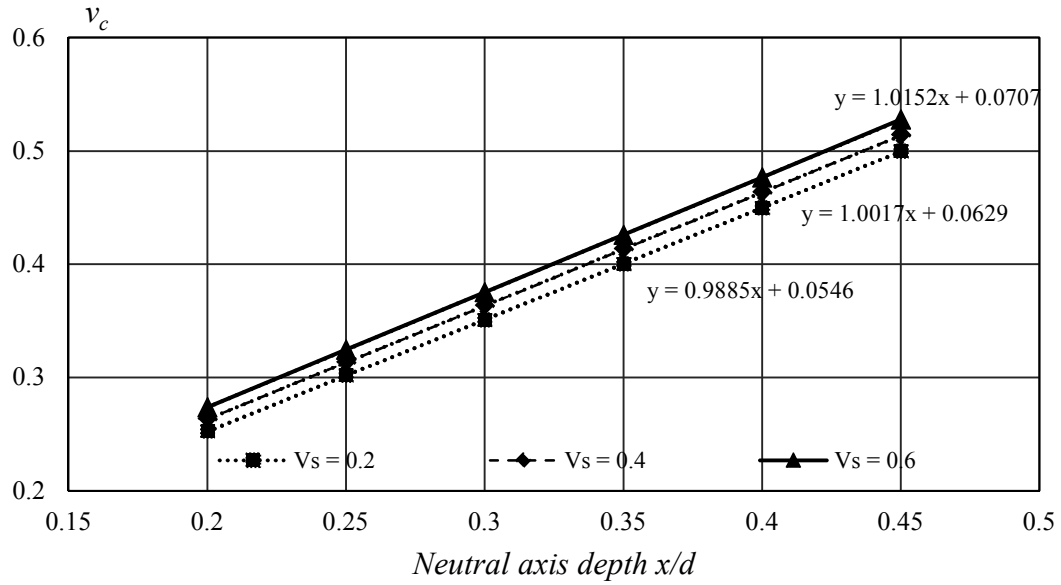
Figure 6-17: Non-dimensionless shear strength by the un-cracked concrete chord

$$v_c = (0.0667 \cdot v_G + 0.9751) \cdot \xi + 0.0402 \cdot v_G + 0.0466 \tag{83}$$

Assume that:

$\xi = 0.25$

$$v_c = (0.2275 \cdot v_G + 0.975) \cdot \xi + 0.05 \tag{84}$$

Considering the size effect

$$v_c = \zeta \cdot \big((0.2275 \cdot v_G + 0.975) \cdot \xi + 0.05\big) \tag{85}$$

Table 6-1: The summary of the solution for shear strength in 3 cases of transverse reinforcement

	Beam with stirrup Adopted from Marí et al. 2014	Beam with stirrup and CFRP grid Given by Author	Beam with CFRP grid, without Stirrups Given by Author
v_l	$v_l = 0.25.\xi - 0.05$	$v_l = 0.25.\xi - 0.05$	$v_l = 0.25.\xi - 0.05$
v_w	$v_w = 167.\dfrac{f_{ct}}{E_c}.\left(1 + \dfrac{2.E_c.G_f}{f_{ct}^2.d}\right)$	$v_w = 167.\dfrac{f_{ct}}{E_c}.\left(1 + \dfrac{2.E_c.G_f}{f_{ct}^2.d}\right)$	$v_w = 167.\dfrac{f_{ct}}{E_c}.\left(1 + \dfrac{2.E_c.G_f}{f_{ct}^2.d}\right)$
v_s	$v_s = 0.85.\rho_w.\dfrac{f_{yw}}{f_{ct}}$	$v_s = 0.85.\rho_w.\dfrac{f_{yw}}{f_{ct}}$	-
v_G	-	$v_G = 0.425.\dfrac{f_G}{f_{ct}}.\rho_G$	$v_G = 0.425.\dfrac{f_G}{f_{ct}}.\rho_G$
v_c	$v_c = \zeta.\left((0.77 \cdot v_s + 0.88) \cdot \xi + 0.02\right)$	$v_c = \zeta.\left((0.198 \cdot v_G + 1.2496 \cdot v_s + 0.969)\right.$ $\left. \cdot \xi + 0.05\right)$	$v_c = \zeta.\left((0.2275 \cdot v_G + 0.975) \cdot \xi + 0.05\right)$
$\Sigma =$	$v = v_l + v_w + v_s + v_c$	$v = v_l + v_w + v_s + v_G + v_c$	$v = v_l + v_w + v_G + v_c$

v_c dimensionless contribution to the shear strength of the un-cracked concrete chord

v_l dimensionless contribution to the shear strength of the longitudinal reinforcement

v_s dimensionless contribution to the shear strength of the transverse reinforcement

v_w dimensionless contribution to the shear strength of the critical crack

v_G dimensionless contribution to the shear strength of the CFRP grid

6.3.7. Application Example

Apply the formula in the previous part to calculate the shear strength of three sample RC beams. In chapter 4 of this thesis, the detail of reinforcing scheme of beams have been disclosed.

6.3.7.1. RC beam 1

The beam has the dimensions of 0.2 m × 0.5 m × 2.75 m, and the effective depth was *d = 423* mm. Neutral axis depth *x = 263* mm. The span length was *2.35* m, and a shear span of *1.1* m. The shear span-to-depth ratio *a/d* was 2.6. It was made by the concrete of the compressive strength *f_{cc}= 34.1* MPa, the tensile strength *f_{ct}= 2.92* MPa, Young's modulus *E_c= 31,900* MPa. RC beam 1 was reinforced with 6D32 longitudinal rebars at the bottom and 2D10 longitudinal rebars on the top. In RC beam 1, D10 bar was used for stirrups, section square of D10 is *71.33* mm². The stirrup spacing was 0.2 m.. The yield strength of the stirrup steel was *f_{yw} = 413* MPa. Strengthening scheme of RC beam 1 is shown in Fig. 6-18.
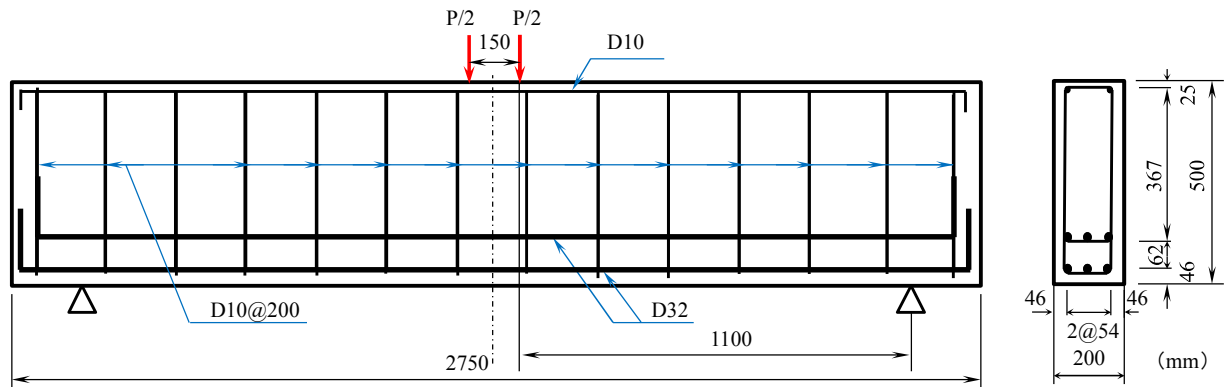
Figure 6-18: Strengthening scheme of RC beam 1

The contribution to shear strength transferred along the crack:

$$v_w = 167.\frac{f_{ct}}{E_c}.\left(1 + \frac{2.E_c.G_f}{f_{ct}^2.d}\right)$$

where

f_{ct} = 2.92 Mpa; E_c = 31900 Mpa; d = 423 mm

$$G_f = G_{Fo} \cdot \left(\frac{f_{cm}}{f_{cmo}}\right)^{0.18}$$

G_{Fo} = 0.11 N/m; f_{cmo} = 10 MPa

$\Rightarrow$ *v_w = 0.0524*

The contribution of the longitudinal reinforcement

$$v_l = 0.25.\xi - 0.05$$

where

$$\xi = \frac{x}{d} = \frac{263}{423} = 0.62$$

$\Rightarrow$ *v_l = 0.105*

The contribution of transverse reinforcement crossing the diagonal critical shear crack:

$$v_s = 0.85.\rho_w.\frac{f_{yw}}{f_{ct}}$$

where

f_{yw} = 413 MPa; f_{ct} = 2.92 MPa

$$\rho_w = \frac{A_{sw}}{b} = 2 \cdot \frac{71.33}{S_t \cdot b} = 2 \cdot \frac{71.33}{200 \cdot 200}$$

$\Rightarrow$ $v_s = 0.4163$

Contribution of the un-cracked concrete zone

$$v_c = \zeta \cdot \big((0.77 \cdot v_s + 0.88) \cdot \xi + 0.02\big)$$

where

$\xi = 1.2 - 0.2a = 1.2 - 0.2 \times 1.1 = 0.98$ is the reduction factor due to size effect

$a = 1.1$ m : shear span in meter

$\Rightarrow$ $v_c = 0.749$

The non-dimensionless of shear strength

$$v = v_c + v_l + v_w + v_s = 0.749 + 0.105 + 0.0524 + 0.4163 = 1.323$$

Shear strength of RC beam 1.

$$V = v. f_{ct}. b. d = 1.323 \cdot 2.92 \cdot 200 \cdot 423 = 326823N \approx 327kN$$

6.3.7.2.   RC beam 2

The beam has the dimensions of 0.2 m × 0.5 m × 2.75 m, and the effective depth was $d = 423$ mm. Neutral axis depth $x = 220$ mm. The span length was 2.35 m, and a shear span of 1.1 m. The shear span-to-depth ratio a/d was 2.6. It was made by the concrete of the compressive strength $f_{cc}= 34.1$ MPa, the tensile strength $f_{ct}= 2.92$ MPa, Young's modulus $E_c= 31,900$ MPa. RC beam 1 was reinforced with 6D32 longitudinal rebars at the bottom and 2D10 longitudinal rebars on the top. The D6 bar was used for stirrups, with section square of 31.67 mm^2. The stirrup spacing was 0.2 m. The yield strength of the stirrup steel was $f_{yw} = 417$ MPa. RC beam 2 was shear strengthened by CFRP grid and mortar.   The beam width after strengthened is 240 mm. CFRP grid used in the experiment was CFRP-CR8 with a grid spacing of 100 mm x 100 mm. The tensile strength of CFRP grid $f_G = 1400$ Mpa. The strengthening scheme of RC beam 2 is shown in Fig. 6-19.
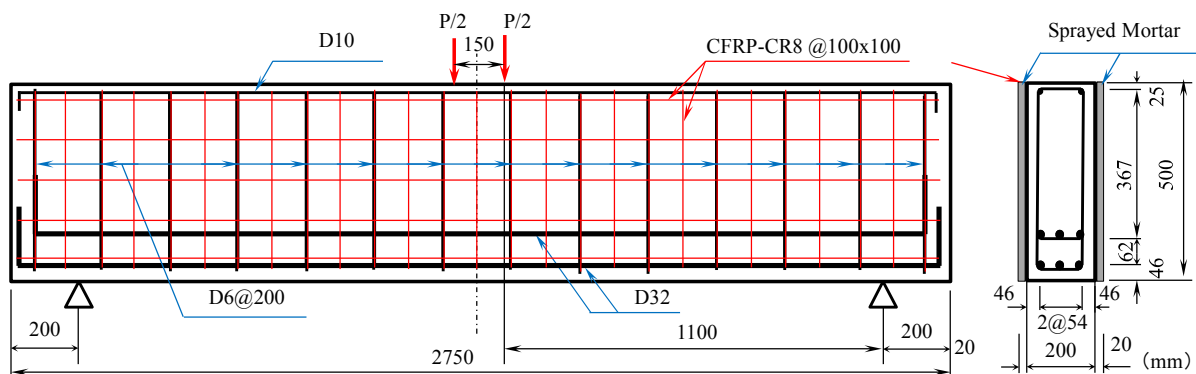
Figure 6-19: Strengthening scheme of RC beam 2

The contribution to shear strength transferred along the crack:

122

$$v_w = 167.\frac{f_{ct}}{E_c}.\left(1 + \frac{2.E_c.G_f}{f_{ct}^2.d}\right)$$

$\Rightarrow$ v_w = 0.0524 (same as RC beam 1)

The contribution of the longitudinal reinforcement

$$v_l = 0.25.\xi - 0.05$$

where

$$\xi = \frac{x}{d} = \frac{220}{423} = 0.52$$

v_l = 0.125

The contribution of transverse reinforcement crossing the diagonal critical shear crack:

$$v_s = 0.85.\rho_w.\frac{f_{yw}}{f_{ct}}$$

where

$$f_{yw} = 417\ MPa;\ f_{ct} = 2.92\ MPa$$
$$\rho_w = \frac{A_{sw}}{b} = 2 \cdot \frac{31.67}{S_t \cdot b} = 2 \cdot \frac{31.67}{200 \cdot 240}$$

$\Rightarrow$ v_s = 0.1587

Contribution of CFRP grid

$$v_G = 0.425 \cdot \frac{f_G}{f_{ct}} \cdot \rho_G$$

where

$$f_G = 1400\ MPa;\ f_{ct} = 2.92\ MPa$$
$$\rho_G = \frac{A_G}{b} = 2 \cdot \frac{26.5}{S_t \cdot b} = 2 \cdot \frac{26.5}{100 \cdot 240}$$

$\Rightarrow$ v_G = 0.448

Contribution of the un-cracked concrete zone

$\Rightarrow$

$$v_c = \zeta \cdot \left((0.198 \cdot v_G + 1.2496 \cdot v_s + 0.969) \cdot \xi + 0.05\right)$$

where

$\xi = 1.2 - 0.2a = 1.2 - 0.2 \times 1.1 = 0.98$ is the reduction factor due to size effect

$a = 1.1$ m : shear span in meter

$\Rightarrow$ v_c = 0.609

The non-dimensionless of shear strength

$8v = v_c + v_l + v_w + v_s + v_G$ = 0.609 + 0.125 + 0.0524 + 0.1587 + 0.448 = 1.39

Shear strength of RC beam 2.

$$V = v.f_{ct}.b.d = 1.39 \cdot 2.92 \cdot 240 \cdot 423 = 412{,}049N \approx 412kN$$

6.3.7.3.   RC beam 3

The beam has the original dimensions of 0.2 m × 0.5 m × 2.75 m, and the effective depth was *d = 423* mm. Neutral axis depth *x = 220* mm. The span length was *2.35* m, and a shear span of *1.1* m. The shear span-to-depth ratio *a/d* was 2.6. It was made by the concrete of the

compressive strength f_{cc}= *34.1* MPa, the tensile strength f_{ct}= *2.92* MPa, Young's modulus E_c= *31,900* MPa. RC beam 1 was reinforced with 6D32 longitudinal rebars at the bottom and 2D10 longitudinal rebars on the top. There is no stirrup in RC beam 3. Then it was shear strengthened by CFRP grid and mortar. The beam width after strengthened is *240* mm. CFRP grid used in the experiment was CFRP-CR8 with a grid spacing of 100 mm x 100 mm. The tensile strength of CFRP grid f_G = *1400* Mpa. The strengthening scheme of RC beam 3 is shown in Fig. 6-20.
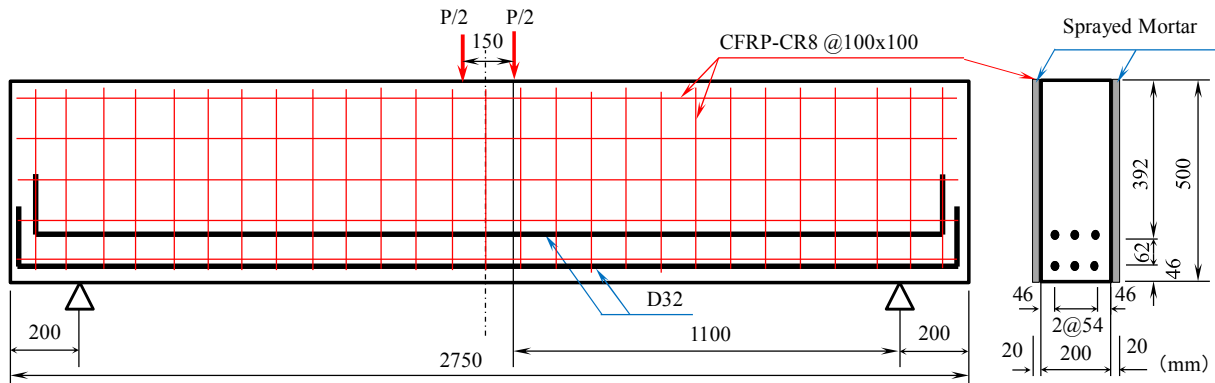
Figure 6-20: Strengthening scheme of RC beam 3

The contribution to shear strength transferred along the crack:

$$v_w = 167 \cdot \frac{f_{ct}}{E_c} \cdot \left(1 + \frac{2.E_c.G_f}{f_{ct}^2.d}\right)$$

⇨ v_w = *0.0524* (same as RC beam 1)

The contribution of the longitudinal reinforcement

$$v_l = 0.25 \cdot \xi - 0.05$$

v_l = *0.125* (same as RC beam 2)

Contribution of CFRP grid

$$v_G = 0.425 \cdot \frac{f_G}{f_{ct}} \cdot \rho_G$$

⇨ v_G = *0.448* (same like RC beam 2)

Contribution of the un-cracked concrete zone

$$v_c = \zeta \cdot \left((0.2275 \cdot v_G + 0.975) \cdot \xi + 0.05\right)$$

where

ξ = *1.2 – 0.2a = 1.2 – 0.2 x 1.1 = 0.98* is the reduction factor due to size effect

a = *1.1* m: shear span in meter

⇨ v_c = *0.505*

The non-dimensionless of shear strength

$$v = v_c + v_l + v_w + v_G = 0.505 + 0.105 + 0.0524 + 0.4483 = 1.11$$

Shear strength of RC beam 2.

$$V = v \cdot f_{ct} \cdot b \cdot d = 1.11 \cdot 2.92 \cdot 240 \cdot 423 = 329,046N \approx 329kN$$

6.3.7.4. *Comparison of the results*

Table 6-2: Summary of Shear strength contribution for the three beams

	v	v_l	v_l/v	v_w	v_w/v	v_s	v_s/v	v_G	v_G/v	v_c	v_c/v
RC beam 1	1.323	0.105	8%	0.0524	4%	0.4163	31%			0.749	57%
RC beam 2	1.39	0.125	8%	0.0524	4%	0.1587	11%	0.4483	30%	0.609	48%
RC beam 3	1.11	0.125	10%	0.0524	4%			0.4483	37%	0.505	49%

Table 6-2 exhibits the summary of shear strength contribution of each part. With two beams applied CFRP grid, the un-crack concrete chord plays an essential role for the shear strength. It contributes nearly 50% in the specific sample case. From this study, the shear strength of the compression concrete zone, V_c, increases as the amount of the transverse reinforcement ratio increases, both Stirrup or CFRP grid. Contribution for shear strength of the residual tensile stresses along the crack is less than 5%, and of longitudinal rebar is less than 10%.

Table 6-3: Comparison of results

	Designed JSCE kN	Maximum load kN	Estimated load	Comparison	
	(1)	(2)	(3)	$\dfrac{(2)}{(1)}$	$\dfrac{(2)}{(3)}$
RC beam 1	354	690	654	195%	106%
RC beam 2	697	757	824	109%	92%
RC beam 3	656	617	658	94%	94%

Table 6-3 shows the comparison of designed value, maximum load, and estimated load. The designed load is calculated by using the equations in (JSCE et al. 1996), detail of the calculation is described in chapter 4. The maximum load of the three beams is taken from the experiment data. Fig. 6-21, 6-22, 6-23 shows the ultimate load of RC beam 1, 2, 3. The estimated load is determined by applying the proposed formula in this dissertation. These estimated loads are calculated base on the estimated shear strength of beams.

The estimated load is calculated as follow:

$$v_c = \frac{P}{2} \quad => P_{estimated} = 2 \times v_c$$

v_c: shear strength of the three beams, calculated in section **6.3.7.1** to **6.3.7.3** in this chapter. Ultimate load (assumed) is the value of load that corresponds to the stage of the stirrup (being yielded) or CFRP (being fracture). RC beam 1. RC beam 2. RC beam 3.

According to Table 6-3, there is a big difference between the result obtained by applying the JSCE formula to calculate the shear strength of RC beams strengthened by CFRP grid. The Safety ratio for applying JSCE is nearly 2.0 (actually 195%) with RC beam 1 but almost 1.0 (actually 109% and 94%) with RC beam 2 and 3. A more detail explanation was disclosed in chapter 4 already.

The estimated values for load provide a consistent result with the data from the experiment in chapter 4, all approximately equal to 1.0 (106%, 92% and 94% correspondent to RC beam 1, 2 and 3, respectively). The formula used for RC beam 1 is derived from Marí 2015. This formula has been checked by Marí with 892 beams without stirrup and 239 beams with stirrup and shows a resonable result. 892 beams had the ratio of shear span to the effective depth a/d higher or equal than 2.5, with a rectangular cross-section and tested under one or two points load (Collins et al. 2008). For 239 beams with stirrups, the databases have been published by (Cladera and Marí, 2007; Yu and Bazant, 2011), a study on slender simply supported beams. According to the above comments, it is supposed that the result of applying the proposed formulas in this study is moderately accurate and could be reliable. And It is feasible to calculate the shear strength of the RC beams strengthened with CFRP grid.
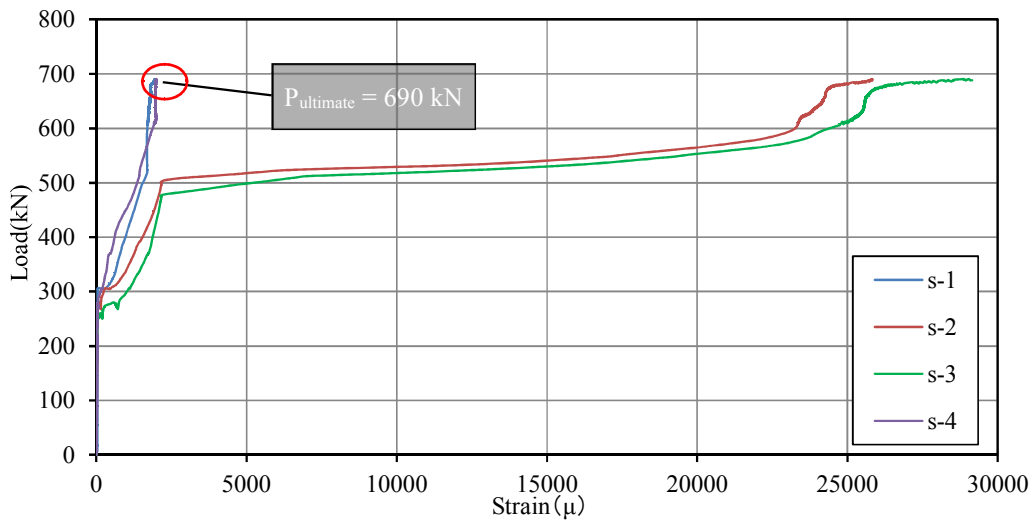
Figure 6-21: Load-strain curves of stirrups at the ultimate load of RC beam 1
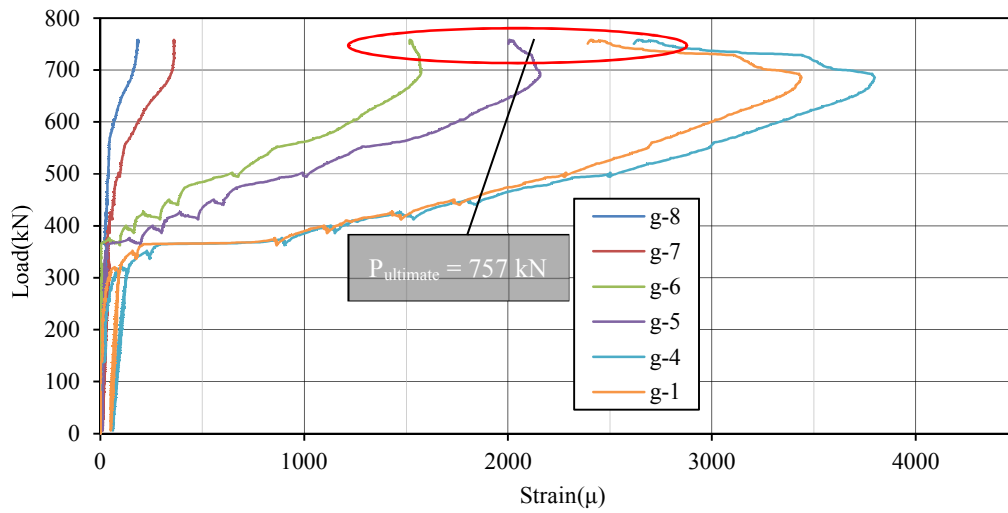
Figure 6-22: Load-strain curves of CFRP vertical bar at the ultimate load of RC beam 2
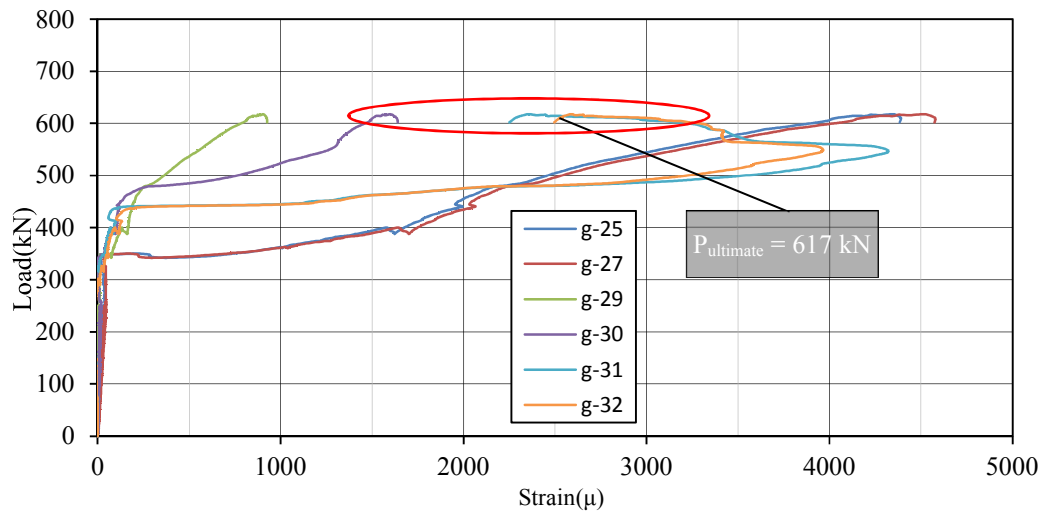
Figure 6-23: Load-strain curves of the ultimate load of RC beam 3

6.4.   CONCLUSIONS

Basing on the mechanical model of shear strength contribution, a simplified formula for prediction of the shear strength of slender reinforced concrete beams in combination with CFRP grid and sprayed mortar. The problems are solved in two cases, RC beam transverse strengthened with CFRP grid and stirrups, and RC beam transverse strengthened with CFRP grid and without stirrup.

The contribution to the shear strength of RC beam is assumed to be the sum of the shear transferred by un-crack concrete compression zone, by stirrups, by CFRP grid, by residual tensile and frictional stresses of the crack. The un-crack concrete chord is supposed to fail due to the principle stress reach the boundary of Kupfer's biaxial failure envelope.

The estimated load of RC beam shear-strengthened by CFRP is calculated until the ultimate stage of beams. At the ultimate stage, the hypothesis is imposed that the CFRP vertical bar of the critical crack cross the CFRP grid closest to the support is equal to the tensile strength of the CFRP grid. From above analysis, the bellow conclusions could be drawn:

- Mechanical-based formulations have been generated in both cases of shear-strengthening using either CFRP grid alone or combining with stirrups. The equations have also been shortened in an uncomplicated form for applying easily to the real concrete structure. These equations have been checked with some cases of RC beams.

- In both cases of applying CFRP grid the un-crack concrete chord plays a vital role for the shear strength. It contributes nearly 50% in the specific sample case. From this study the shear strength of the compression concrete zone, V_c, increases as the amount of the transverse reinforcement ratio increases, both Stirrup or CFRP grid. Contribution for shear strength of inclined crack is less than 5%, and of longitudinal rebar is less than 10%.

- With the assumption that the initiation of the critical crack start from the section where the bending moment diagram at failure reaches the cracking moment. This inclined crack propagates toward the neutral axis, and then the loading point at the ultimate stage. The horizontal projection of the critical crack is approximate to *0.85d*. Such assumed model has found to consist with the observed experimental crack pattern.

- The estimated shear strength of strengthened RC beam is consistent with the experiment results and the available shear strength formulation for RC beams (of Mari) also.

- The proposed equation for the shear strength estimation is really useful for design and assessment purposes. This formulation derived from the mechanical principles then calibrated by the experiment results. This model is analysis for rectangular RC beam, and It can be extended to other geometry structure and different kind of transverse reinforcement also.

Chapter 7:

CONCLUSIONS & FURTHER RESEARCH

7.1. DISSERTATION SUMMARY

In this dissertation, the author has investigated of the capability of four materials: concrete, steel, CFRP grid, and mortar, acting together in a strengthened structure. In the experiment, three concrete prisms are reinforced by different schemes of steel bars and/or CFRP grid in the axial direction. Specimen 1, the control one, with a square section of concrete, axially reinforced by rebars. Specimen 2 is reinforced by CFRP grid, and Specimen 3 is reinforced by both rebars and CFRP grid. The strengthened specimen 2 and 3 have the same dimensions as specimen 1, they were applied the axial tensile force until failure. According to the test results, good combination of four materials has been proved. Both strengthened specimens perform the very high bearing capacity comparing to the specimen 1. The behavior of reinforcing materials and the capability of CFRP grid strongly influenced by the bonding interface between concrete and mortar. In this study, although the bonding surfaces are repaired by an common method such as sandblasting (the roughness of surface after sandblasting is 0.16 mm) and epoxy primer applying. In both specimens, the fracture still occurs at the bonding surface (the average shear stresses is 1.1 MPa), and CFRP grid only performs 76% of tensile strength. It is considered that, a better condition of surface roughness of more than 0.3 mm is necessary to make use the full capacity of the CFRP grid.

The experiment program also shows the effectiveness of CFRP grid in enhancing the shear capacity of RC beams under four-point bending test. Three large beams (200 x 500 x 2750 mm) were fabricated, which are the same in the longitudinal reinforcement but different in transverse reinforcement. RC beam 1, the reference one, shear-strengthened by stirrup D10, RC beam 2 has stirrup D6 and CFRP CR8, and RC beam 3 has CFRP CR8 only. The cross-sectional area of reinforcing materials in RC beam 2 and RC beam 3 is equivalent to 120% and 75%, respectively, compared with the cross-sectional area of stirrups in RC beam 1. The result shows that CFRP grid and sprayed mortar could significantly improve the shear strengthening. RC beam 2 and RC beam 3 attains 10% higher and 10% lower of ultimate load comparing to RC beam 1. In general, the stiffness, ductility characteristic, and the cracking load of the strengthened RC beams are upgraded. When the load increased, variations of the stirrup strains and the CFRP grid strains at the same position in a strengthened RC beam have similar tendencies. After stirrups yielded and cracks developed, the behavior of CFRP grid and stirrups was considerably affected. In this application, CFRP grid didn't work at full capacity. The maximum stress of CFRP grid was 85% of the tensile

strength. When calculating the shear strength of RC beam, the material factor for CFRP sheet in JSCE's guideline is 1.3, but for CFRP grid, this factor of 1.5 is proposed.

Additionally, this thesis also studies the crack propagation of strengthened beams using CFRP grid. Acoustic emission (AE) sensors were attached on the two beams to monitor the development of cracks from the starting point till the ultimate state. The actual observed fact is combined with AE result to conclude the better understanding of the formation and propagation of diagonal cracks. According to the test data, micro-cracks occur and develop so early, even when the load is low and in the compressed area also. Chapter 5 also discusses the contribution of the horizontal and vertical bar of CFRP grid to the shear strength. The analysis indicates that the vertical component of the CFRP grid plays the key role for shear strength contribution when compared with the horizontal part. And horizontal CFRP bars work as anchors supporting the vertical movement between CFRP grid and spray mortar, especially, at the tip of the critical crack.

In the final part of the thesis, the author presents the simplified formula to estimate the shear strength of strengthened RC beams based on the mechanical model. The problems are solved in two cases, RC beam shear-strengthened by CFRP grid and/without stirrups. The contribution to the shear strength is assumed to be the sum of the shear transferred by un-crack concrete compression zone, by stirrups, by CFRP grid, by residual tensile and frictional stresses of the critical crack. Applying the input data from the chapter 4, the shear strength of RC beams can be calculated. These calculating values are consistent with the ultimate load from the test. Therefore, these formulas are applicable for estimating the shear strength of RC beams strengthened with CFRP grid. Additionally, in both cases of applying the CFRP grid, the un-crack concrete chord plays a vital role in the shear strength contribution (nearly 50%).

7.2.   SUMMARY OF CONCLUSIONS

From all above results of this dissertation, the general conclusions can be drawn as follow:

(1)   The reinforcing effect of CFRP grid material is demonstrated in a simple experiment. Specimen 2 and specimen 3 strengthened by CFRP grid exhibited a good combination of 4 materials: concrete, steel, mortar and CFRP grid. Both strengthened specimens perform the very high bearing capacity comparing to the control one – specimen 1. Comparing between specimen 3 and specimen 1, the maximum load of SP3 is 212% higher than that of SP1 when the cross-sectional area of reinforcement is only 184% higher.

(2)   As reinforced with CFRP grid material, the strengthened structures perform the high stiffness and less brittle. The deformation occurs smoothly due to the good adhesion between materials; concrete and mortar.

The interface bonding plays an important role in the reinforcing effect. In this study, although the bonding surfaces are repaired by an appropriate method such as sandblasting, epoxy primer applying, both specimens the fracture still occurs at the bonding surface, CFRP –CR5 did not show the full capacity. To take advantage of CFRP grid and to enhance the effect of strengthening work, a better condition of surface roughness and an adequate length of bonding interface is necessary.

(3)   CFRP grid and sprayed mortar could be significantly effective in shear strengthening. In this experiment, RC beams strengthened with CFRP CR8 and sprayed mortar (RC beam 2 and RC beam 3) attained 110.7% and 89.4% of shear capacity compared with the ultimate load of the control beam (RC beam 1). The cross-sectional area of reinforcing materials in RC beam 2 and RC beam 3 were equivalent to 118.7% and 74.3%, respectively, of the cross-sectional area of stirrups in RC beam 1. In general, the stiffness, ductility characteristic, and the cracking load of the strengthened RC beams (RC beam 2 and RC beam 3) using CFRP grid and spayed mortar were improved.

(4)   The behavior between the CFRP grid and the stirrups reflects the bonding between concrete and sprayed mortar. It is one of the most important factors that influence the reinforcement effectiveness. According to experimental results, when the load increased, variations of the stirrup strains and the CFRP grid strains at the same position in a strengthened RC beam had similar tendencies. After the stirrups yielded and the cracks

developed in a strengthened RC beam, the bonding between concrete and sprayed mortar was considerably affected.

(5)　　In an application of CFRP grid and sprayed mortar, CFRP grid could not work at 100% of the tensile strength. Ref　(JSCE et al. 1996) reports the material factor of 1.3 for calculating CFRP sheet capacity, but the maximum stress of the CFRP grid was 85.3% of the tensile strength in our experiments. Therefore, a material factor of 1.5 is proposed for the CFRP grid when applying the formula in Ref (Japan Society of Civil Engineers 2007) to calculate the shear strength of a RC beam strengthened with CFRP grid and sprayed mortar. Using a coefficient of 1.5 means the CFRP grid works at 66.7% of its capacity.

It is concluded that the shear-strengthening of RC beams by CFRP grid and sprayed mortar is effective. CFRP grid and sprayed mortar are useful in strengthening and retrofitting of concrete structures. CFRP grid can support or replace stirrups in RC beams in providing shear strength. The availability of CFRP grid and sprayed mortar should be more intensively investigated and widely applied in concrete structures in the future.

(6)　　In order to study the crack propagation, the combination of results from the two methods; actual observed fact and AE technique, the more distinct and detail understanding about the formation and development of the crack has been found. Especially, the micro-crack cannot be identified from outside of the beam, but the location and magnitude can be detected accurately by the AE sensor method. In this experimental program, with two beams, the micro-crack appears in beams since the load still low (0-100 kN) in both the tension zone and the compression zone also.

(7)　　Comparing the number of cracks in RC beam 1 and RC beam 2, it is supposed that the number of cracks in the shear-strengthened beam (RC beam 2) is significantly smaller than the control beams (RC beam 1). It also shows the effect of reinforcing concrete beams with CFRP grid not only increases the strength of the structure but also contributes to the reduction of cracks and the brittleness of the structure. The reduction of the number of crack sounds is recorded up to 51% at the level of load that most cracks occur (load of 300-400kN in this test).

(8)   By the above analysis, two following conclusions about the effect of CFRP grid in shear-strengthening and behavior between horizontal and vertical components have been drawn. The contribution for shear strength of both components depends on the location of the CFRP grid in RC beam. With the CFRP node at the neutral axis, the roles of them are equal while at the remain positions, the vertical component is the important part for the shear strength. In general, vertical bar plays a much more important role compared with the horizontal component. It provides more efficiency for control the shear failure. Furthermore, the horizontal component is also an anchor for the good adhesion between the vertical component and the mortar. The attitude of applying load, the appearance and the development of cracks also affect the contribution of vertical and horizontal CFRP bar.

(9)   Basing on the mechanical model of shear strength contribution, a simplified formula for prediction of the shear strength of slender reinforced concrete beams in combination with CFRP grid and sprayed mortar. The problems are solved in two cases, RC beam transverse strengthened with CFRP grid and stirrups, and RC beam transverse strengthened with CFRP grid and without stirrup. The contribution to the shear strength of RC beam is assumed to be the sum of the shear transferred by un-crack concrete compression zone, by stirrups, by CFRP grid, by residual tensile and frictional stresses of the crack. The un-crack concrete chord is supposed to fail due to the principle stress reach the boundary of Kupfer's biaxial failure envelope. The estimated load of RC beam shear-strengthened by CFRP is calculated until the ultimate stage of beams. At the ultimate stage, the hypothesis is imposed that the CFRP vertical bar of the critical crack cross the CFRP grid closest to the support is equal to the tensile strength of the CFRP grid. Mechanical-based formulations have been generated in both cases of shear-strengthening using CFRP grid; CFRP grid combining with and without stirrups. The Equations have also been shortened in an uncomplicated form for applying easily to the real concrete structure. These equations have been checked with some cases of RC beams.

(10)   In both cases of applying CFRP grid, the un-crack concrete chord plays a vital role for the shear strength. It contributes nearly 50% in the specific sample case. From this study, the shear strength of the compression concrete zone, V_c, increases as the amount of the transverse reinforcement ratio increases, both Stirrup or CFRP grid. Contribution for shear strength of inclined crack is less than 5%, and of longitudinal rebar is less than 10%.

(11)   With the assumption that the initiation of the critical crack start from the section where the bending moment diagram at failure reaches the cracking moment. This

inclined crack propagates toward the neutral axis, and then the loading point at the ultimate stage. The horizontal projection of the critical crack is approximate to *0.85d*. Such assumed model has found to consistent with the observed experimental crack pattern.

(12)   The estimated shear strength of strengthened RC beam is consistent with the experiment results and the available shear strength formulation for RC beams (of Mari) also.

(13)   The proposed equation for the shear strength estimation is really useful for design and assessment purposes. This formulation derived from the mechanical principles then calibrated by the experiment results. This model is analysis for rectangular RC beam, and It can be extended to other geometry structure and different kind of transverse reinforcement also.

7.3. FURTHER RESEARCH

It is impossible to test on all types of CFRP grid and in all cases of strengthening due to constraints of consuming time and cost. However, more research relating to the research contained in this thesis should be done in the future to enrich the awareness about the work of CFRP grid. The following suggestions for future research are offered:

- The crack occurs and propagates in RC beams due to the shear force is the inclined crack. This appearance influences the behavior of stirrups and CFRP grid also. To conduct an experimental program on the behavior of stirrups and CFRP grid due to the critical crack will be a promising direction for the study.

- Distribution of shear stresses on the bonding surface between concrete and mortar. The shear stress at the location near the critical crack significantly different from that of the further locations. Other research on the distribution of the shear stress on the bonding interface of between two materials under the concentrated load. The problem can be approached under the combination of two methods; experiment and FEM software.

- Adequate length of the bonding interface between mortar and concrete is a critical factor to make use of the capacity of CFRP grid. More extensive researches on the sufficient onding length between two materials needs to be implemented in the future to clarify this problem.

REFERENCES

ACI. 2015. *Guide for the Design and Construction of Structural Concrete Reinforced with FRP Bars*.

Adebar, Perry and Joost Van Leeuwen. 1999. "Side-Face Reinforcement for Flexural and Diagonal Cracking in Large Concrete Beams." *ACI Structural Journal* 96(5):693–704.

Advisory Committee on Technical Recommendations for Construction. 2006. "Guidelines for the Design, Construction and Production Control of Fiber Reinforced Concrete Structures." *Cnr-Dt 203/2006* (June).

Ahmed, Ehab A., Ehab F. El-Salakawy, and Brahim Benmokrane. 2010. "Shear Performance of RC Bridge Girders Reinforced with Carbon FRP Stirrups." *Journal of Bridge Engineering* 15(1):44–54. Retrieved (http://ascelibrary.org/doi/10.1061/%28ASCE%29BE.1943-5592.0000035).

Anon. n.d. "CFRP Repair and Reinforcement Method Technology Research Association." *Dec. 5, 2016*. Retrieved December 5, 2016 (http://tampoken.com/04.html).

Association for Advanced composite Technology on Construction. 2018. "The Continuous Fiber Reinforcing Materials." *Association for Advanced Composite Technology on Construction Field*. Retrieved (http://acc-club.jp/english/1.html).

Austin, Simon, Peter Robins, and Youguang Pan. 1999. "Shear Bond Testing of Concrete Repairs." *Cement and Concrete Research* 29(7):1067–76.

Bairan Garcia, Jesus Miguel and Antonio R. Mari. 2006. "Coupled Model for the Nonlinear Analysis of Sections Made of Anisotropic Materials, Subjected to General 3D Loading. Part 2: Implementation and Validation." *Computers and Structures* 84(31–32):2264–76.

Bank, Lawrence C., Thomas I. Campbell, and Charles W. Dolan. 2006. "Guide for the Design and Construction of Concrete Reinforced with FRP Bars Reported by ACI Committee 440." *Concrete* 1–42.

Banthia, Nemkumar. 2002. "Fiber Reinforced Polymers in Concrete Construction and Advanced Repair Technologies."

Bukhari, I. A., R. L. Vollum, S. Ahmad, and J. Sagaseta. 2010. "Shear Strengthening of Reinforced Concrete Beams with CFRP." *Magazine of Concrete Research* 62(1):65–77. Retrieved (http://www.icevirtuallibrary.com/doi/10.1680/macr.2008.62.1.65).

Campana, Stefano, Miguel Fernández Ruiz, Andrea Anastasi, and Aurelio Muttoni. 2013. "Analysis of Shear-Transfer Actions on One-Way RC Members Based on Measured Cracking Pattern and Failure Kinematics." *Magazine of Concrete Research* 65(6):386–404. Retrieved (http://www.icevirtuallibrary.com/doi/10.1680/macr.12.00142).

Can/Csa. 2012. *CAN/CSA-S806-12. Design and Construction of Building Structures with Fibre-Reinforced Polymers*.

Canadian Standards Association. 2014. *CSA S6-14 Canadian Highway Bridge Design Code*.

Chen, J. F. and J. G. Teng. 2003. "Shear Capacity of FRP-Strengthened RC Beams: FRP Debonding." *Construction and Building Materials* 17(1):27–41.

Cladera, Antoni et al. 2016. "The Compression Chord Capacity Model for the Shear Design and Assessment of Reinforced and Prestressed Concrete Beams." *Structural Concrete* 17(6):1017–32.

Cladera, Antoni and Antonio R. Marí. 2005. "Experimental Study on High-Strength Concrete Beams Failing in Shear." *Engineering Structures* 27(10):1519–27.

Cladera, Antoni, Antonio Marí, Carlos Ribas, Jesús Bairán, and Eva Oller. 2015. "Predicting the Shear-Flexural Strength of Slender Reinforced Concrete T and I Shaped Beams." *Engineering Structures* 101:386–98. Retrieved (http://dx.doi.org/10.1016/j.engstruct.2015.07.025).

Ding, L., G. Wu, and Z. S. Wu. 2010. "Bond Mechanism of Carbon Fiber Reinforced Polymer Grid to Concrete." *Proceeding of the 5th International Conference on FRP Composites in Civil Engineering, Beijing, China* 27–30.

Ferreira, Denise, Jesús Bairán, and Antonio Marí. 2013. "Numerical Simulation of Shear-Strengthened RC Beams." *Engineering Structures* 46:359–74.

FIB- Bulletin 42. 2013. *Model Code 2010*.

Grace, Nabil, Tsuyoshi Enomoto, Prince Baah, and Mena Bebawy. 2012. "Flexural Behavior of CFRP Precast Prestressed Decked Bulb *T* -Beams." *Journal of Composites for Construction* 16(3):225–34. Retrieved (http://ascelibrary.org/doi/10.1061/%28ASCE%29CC.1943-5614.0000266).

Guo, Rui, Kohei Yamaguchi, Shinichi Hino, and Nobuhiro Miyano. 2014. "Shearing Capacity and Adhesive Properties of Reinforced Interface for RC Beam with Haunch Retrofitted by CFRP Grid with Spraying PCM Shotcrete." 74(2).

H. Nilson, Arthur. 2018. "Design of Prestressed Concrete / A.H. Nilson."

HASSAN, Hussein Mokhtar, Sabry A. FARGHALY, and Tamon UEDA. 1991. "Displacements at Shear Crack in Beams with Shear Reinforcement under Static and Fatigue Loadings." *Doboku Gakkai Ronbunshu* 1991(433):215–22.

Japan Society of Civil Engineers. 2007. *Standard Specifications for Concrete Structures*. Retrieved (http://conc.civil.okayama-u.ac.jp/~tayano7/JSCE/publication.html).

JSCE et al. 1996. "RECOMMENDATION FOR DESIGN AND CONSTRUCTION OF CONCRETE STRUCTURES USING CONTINUOUS FIBER REINFORCING MATERIALS." (1):59–80.

Júlio, Eduardo N. B. S., Fernando A. B. Branco, and Vítor D. Silva. 2004. "Concrete-to-Concrete Bond Strength. Influence of the Roughness of the Substrate Surface." *Construction and Building Materials* 18(9):675–81.

Karayannis, Chris G. and Constantin E. Chalioris. 2013. "Shear Tests of Reinforced Concrete Beams with Continuous Rectangular Spiral Reinforcement." *Construction and Building Materials* 46:86–97.

Kupfer, Helmut B. and Kurt H. Gerstle. 1973. "Behavior of Concrete Under Biaxial Stress." *Journal of the Engineering Mechanics Division, ASCE* 99(4):853–66.

Marí, A., J. M. Bairán, A. Cladera, and E. Oller. 2016. "Shear Design and Assessment of Reinforced and Prestressed Concrete Beams Based on a Mechanical Model." *Journal of Structural Engineering (United States)* 142(10).

Marí, Antonio, Jesús Bairán, Antoni Cladera, Eva Oller, and Carlos Ribas. 2015. "Shear-Flexural Strength Mechanical Model for the Design and Assessment of Reinforced Concrete Beams." *Structure and Infrastructure Engineering* 11(11):1399–1419.

Marí, Antonio, Antoni Cladera, Eva Oller, and Jesús Bairán. 2014. "Shear Design of FRP Reinforced Concrete Beams without Transverse Reinforcement." *Composites Part B: Engineering* 57:228–41.

MLIT - Ministry of Land Infrastructure Transport and Tourism in Japan. 2013. "White Paper on Land, Infrastructure, Transport and Tourism in Japan, 2012." 289.

Mohr, Steffen, Jesús M. Bairán, and Antonio R. Marí. 2010. "A Frame Element Model for the Analysis of Reinforced Concrete Structures under Shear and Bending." *Engineering Structures* 32(12):3936–54.

Oller, Eva, Antonio Marí, Jesús Miguel Bairán, and Antoni Cladera. 2015. "Shear Design of Reinforced Concrete Beams with FRP Longitudinal and Transverse Reinforcement." *Composites Part B: Engineering* 74:104–22.

Piyamahant, Songkram and Hiroshi Shima. 2008. "Shear Behavior of Reinforced Concrete Beams Strengthened with CFRP Strips." *Journal of the Korea Concrete Institute* 20(3):299–305.

S6-09-Addeendum, CSA and Michel BRUNEAU. 2018. "Seismic Design Provisions - the Canadian Highway Bridge Design Code."

Santos, Dinis S., Pedro M. D. Santos, and Daniel Dias-Da-Costa. 2012. "Effect of Surface Preparation and Bonding Agent on the Concrete-to-Concrete Interface Strength." *Construction and Building Materials* 37:102–10. Retrieved (http://dx.doi.org/10.1016/j.conbuildmat.2012.07.028).

Saravanakumar, P. and A. Govindaraj. 2016. "Influence of Vertical and Inclined Shear Reinforcement on Shear Cracking Behaviour in Reinforced Concrete Beams." *International Journal of Civil Engineering and Technology* 7(6):602–10.

De Silva, Sudhira, Hiroshi Mutsuyoshi, Eakarat Witchukreangkrai, and Tatsuya Uramatsu. 2018. *ANALYSIS OF SHEAR CRACKING BEHAVIOR IN PARTIALLY PRESTRESSED CONCRETE BEAMS*.

Sumikin, Nippon Steel &. n.d. *Price Quotation of Nippon Steel & Sumikin Materials Co., LTD*.

Tamon, Ueda. 2005. "FRP for Construction In Japan." *Joint Seminar on Concrete Engineering* (March):54–68. Retrieved (https://www.researchgate.net/profile/Tamon_Ueda/publication/237784282_FRP_FOR_CONSTRUCTION_IN_JAPAN/links/56e811d108aea51e7f3b0f9c.pdf%0Ahttp://www.jsce.or.jp/committee/concrete/e/newsletter/newsletter02/newsletter02f/5-Mongolia (Ueda).pdf).

TRAN Vu Dung. 2016. "Numerical Analysis of the Shear Behavior of Reinforced Concrete Beam Strengthened with CFRP and Sprayed Mortar."

Tureyen, a K. and R. J. Frosch. 2003. "Concrete Shear Strength: Another Perspective." *ACI Structural Journal* 100(5):609–15.

Ueda, M., A. Hiraga, and T. Nishimura. 2011. "Compressive Strength of a Carbon Fiber in Matrix." *ICCM International Conferences on Composite Materials* (3):2–7.

Vecchio, Frank J. and Michael P. Collins. 1986. "The Modified Compression Field Theory for Reinforced Concrete Elements Subjected to Shear." *ACI Structural Journal* 83:925–33.

Wang, Bo. 2016. "Study on Tensile Behavior and Failure Mechnism of CFRP Grid-Sprayed Mortar in Strengthened Concrete Structures."

Ward, John, Mitch Magee, Carin L. Roberts-Wollmann, and Thomas E. Cousins. 2018. "Carbon Fiber Reinforced Polymer Grids for Shear and End Zone Reinforcement in Bridge Beams." Final Repo.

Wee, T. H., S. Swaddiwudhipong, and H. R. Lu. 2000. "Tensile Strain Capacity of Concrete under Various States of Stress." *Magazine of Concrete Research* 52(3):185–93. Retrieved (http://www.icevirtuallibrary.com/content/article/10.1680/macr.2000.52.3.185).

Yi, Ding, Chen Xiaobing, and Chen Wenyong. 2011. "The Flexural Behavior of Beams Strengthened with FRP Grid and ECC." (33):2–4.

Zakaria, Mohamed, Tamon Ueda, Zhimin Wu, and Liang Meng. 2009. "Experimental Investigation on Shear Cracking Behavior in Reinforced Concrete Beams with Shear Reinforcement." *Journal of Advanced Concrete Technology* 7(1):79–96.

Zararis, Prodromos D. and George Ch. Papadakis. 2001. "Diagonal Shear Failure and Size Effect in RC Beams without Web Reinforcement." *Journal of Structural Engineering* 127(7):733–42. Retrieved (http://ascelibrary.org/doi/10.1061/%28ASCE%290733-9445%282001%29127%3A7%28733%29).

Zhang, Burong, Radhouane Masmoudi, and Brahim Benmokrane. 2004. "Behaviour of One-Way Concrete Slabs Reinforced with CFRP Grid Reinforcements." *Construction and Building Materials* 18(8):625–35.